MULTI-SCALE IMPACT RESILIENT SMART COMPOSITES (MIRACS) FOR HAZARD MITIGATION

by

MAHADI MASUD

(Under the Direction of Mi Geum Chorzepa, PhD)

ABSTRACT

There is an increasing need to engineer structures resilient to multiple hazards, especially extreme dynamic loading such as impact, blast, and seismic loads. Material innovations in composites play an important role to meet this need. A two-phase experimental program has been developed, and it focuses on the discovery of Multi-scale Impact Resilient smArt Composites (MIRAC) while: (1) optimizing the impact toughness and fiber volume fraction; and (2) providing valuable experimental data on MIRACs. The Phase-I experimental program determines the compressive, tensile, and flexural strength of 15 specimen groups, as well as the impact toughness of MIRACs including carbon nanofibers. Based on a small-scale repeated impact test performed, the multi-scale fiber reinforced composites lead to increased impact resilience by tenfold. The Phase-II experimental program includes a drop-weight impact test of ten half-scale fiber reinforced composite beams. A steel impactor weighing 227 kg is dropped freely from a height of 6.1 m with an estimated velocity of 10.93 m/s. The results from the Phase-II test indicate that providing multi-scale (macro, micro, and nano) fiber reinforcement is essential to achieve a significant increase in impact resilience of cementitious composites as they effectively bridge different scale cracks and prevent coalescence of cracks.

INDEX WORDS: cementitious composites; ECC; multi scale fiber; FRC, impact resilience; toughness; CNFs, nano fiber; steel; PVA; PP

MULTI-SCALE IMPACT RESILIENT SMART COMPOSITES (MIRACS) FOR HAZARD MITIGATION

by

MAHADI MASUD

BSc in Civil Engineering, Bangladesh University of Engineering and Technology, Bangladesh, 2012

A Thesis Submitted to the Graduate Faculty of the University of Georgia in Partial Fulfillment of the Requirements for the Degree

MASTER OF SCIENCE

ATHENS, GEORGIA

2015

MULTI-SCALE IMPACT RESILIENT SMART COMPOSITES (MIRACS) FOR HAZARD MITIGATION

by

MAHADI MASUD

Major Professor:	Mi Geum Chorzepa
Committee:	Stephan A. Durham
	Ramana M. Pidaparti

Electronic Version Approved:

Julie Coffield
Interim Dean of the Graduate School
The University of Georgia
May 2015

DEDICATION

I dedicate my thesis work to my family and my advisor, Dr. Chorzepa, for their support, caring, belief, and patience. This journey would not have been possible without the support and guidance of my thesis committee, Dr. Chorzepa, Dr. Durham, and Dr. Pidaparti. I would like to give special thanks to my thesis committee.

ACKNOWLEDGEMENTS

I am grateful for the support from the College of Engineering at the University of Georgia and the University of Georgia Research Foundation. Special thanks to undergraduate and Young Dawgs student assistants including Reed Blevins, Jason Wright, Catherine Johnson, Rashaan Fowles, and Gustavo Cortina, and to Forta, Boral, Bekaert, Argos, Grace, and BASF for generous material donations. The opinions, findings, and conclusions do not reflect the views of the funding institutions or other individuals.

TABLE OF CONTENTS

LIST OF TABLES

LIST OF FIGURES

CHAPTER 1

INTRODUCTION

The behavior of reinforced concrete (RC) structures under extreme loads such as impact loading has been extensively studied by many researchers [1-7]. In the United States alone, due to the increased levels of terrorism and natural hazards around the world, a significant effort has been put towards the research in the field of impact loading. The impact hazards include, but are not limited to:

Severe weather events: tornado (150-300 mph wind) borne debris or storm launched debris (e.g., electric poles) impacting civil structures.

Accidents: vehicle/airplane crash, vessel collision against bridge piers, offshore structures exposed to passing ships.

Malevolent attacks: vehicle/airplane crash, missile impact, a military attack with projectile weapons.

Fig. 1.1 – Damage from impact loading [8].

The natural and man-made impact hazards against civil structures can result in a loss of structural integrity and spalling of high speed debris (or structural elements) as shown in Fig. 1.1, and thus cause serious injury to building occupants and civilians in the vicinity. Therefore, it is critical to understand the structural response and damage from impact loadings, to discover more resilient materials or composite systems, and engineer structures for impact hazards. Impact problems, particularly in regard to those structures involving concrete, have become the focus of recent research [1-7] with numerous reinforced concrete members being tested under impact loading over the past three decades. Physical phenomena involving concrete structures under impact loading include complex material response that makes obtaining an accurate analytical solution difficult. The nature of concrete material response presents particular complexities and challenges, especially under extreme dynamic loads over short durations. Available experimental results are observed to be inconsistent due to the nature of concrete heterogeneity and a host of other variables [9].

One of the most used and effective materials for impact resilient cement-based composite structures is fiber reinforcement. Steel, polymeric, glass, and carbon based fibers were developed in the 1960s, 70s, 80s, and 90s, respectively [10]. The fiber size varies: macro-, micro-, and nano-scales. The most popular choices include hooked macro steel fibers, synthetic macro/micro fibers, polyvinyl alcohol (PVA) fibers, carbon nano fibers (CNF), and carbon nano tubes (CNT) although nano-fiber reinforced composites are still considered to be associated with academic research on account of their high cost. However, it is noted that cost of industrial CNF/CNT was $27,000/lb in 1992, $550/lb in 2006, $120/lb in 2011, and may soon be just $0.5/lb [11] if mass produced, making the use of nano-materials practical in the construction industry.

Carbon nano fibers (CNFs) exhibit extraordinary mechanical properties including a predicted Young's modulus of over 1 Tera-Pascal and a tensile strength of 200 Giga Pascal (29,000 ksi) [12]. Furthermore, CNFs are referred to as "smart materials" because they have the ability to "sense" damage, specifically they conduct electricity and their electrical conductivity changes the DC electrical resistivity [13] of composites in response to damage. Thus, CNF employed in engineered composite structural components like MIRAC not only improve a component's ductility and toughness but also provide quantitative information for a damage assessment.

Chapter 2 of this thesis contains a literature review which provides a brief summary of the research that has been done in the field of fiber reinforced composites, especially their structural response under impact loads. Chapter 3 analyzes the shortcomings of available research. Chapter 4 states the objectives as well as significance of this research. Chapters 5 through 8 present a two-phase experimental program and results from the two programs. Chapter 9 presents the conclusions from the two-phase experimental program and include recommendations for future work.

CHAPTER 2

LITERATURE REVIEW

2.1 Material response of fiber reinforced concrete (FRC)

2.1.1 Steel FRC (SFRC)

Williamson et al. [14] reported that steel fibers improved the compressive strength of concrete as much as 23% for concrete containing 2% vol. of steel fibers. Yazıcı et al. [15] also reported 4-19% increase of compressive strength by steel fibers having different aspect ratio and volume fraction. Steel fibers at low volume fraction e.g. 0.35% by vol. reduced compressive strength of FRC mixes but high volume fraction e.g. 0.5% and 1% by vol. increased compressive strength of FRCs [16]. Modulus of rupture of these steel fiber mixes were increased irrespective of the fiber volume fraction in the FRC mixes [16]. Steel FRC with 2.5% by vol. of steel fibers showed high flexural strength and low deflection capacity due to its high modulus [17]. Soulioti et al. [18] reported increase in first-peak strength, the peak strength, the residual strength and especially the flexural toughness with increased volume fraction of steel fibers. Hooked-end steel bars were seen to be more effective in improving flexural properties of concrete than other type of steel fibers [18]. Again, Uygunoğlu et al. [19] showed that the flexural strength of SFRCs could be significantly improved with increasing aspect ratio and volume fraction of steel fibers.

2.1.2 PVA FRC

PVA FRC with 2.5% by vol. of PVA fibers showed lower flexural strength but higher deflection capacity than steel fiber FRC due to its low stiffness [17]. SU et al. [20] studied bending performance of PVA FRC and observed that PVA fibers can improve initial cracking load and the ultimate bearing capacity. Yang et al. [9] showed that PVA fiber reinforced composites containing 2% volume fraction of PVA fibers improved strain-hardening behavior when these composites were subjected to strain rate ranging from 10^{-5} (quasi-static loading) to 10^{-1} s^{-1} (low speed impact). This study showed that the rate sensitivity of concrete which exhibits high strength accompanied by high brittleness with higher loading rate could be solved by introducing micro-fibers like PVA fibers [9].

Ayub et al. [21] reported that the 3% PVA fiber was the optimum fiber volume to improve the mechanical properties of PVA FRC.

2.1.3 Steel-PVA FRC

Flexural strength of steel-PVA FRC (SPFRC) were found to lay between flexural strength of individual fiber mixes of steel or PVA [17]. Ahmed et al. [17] showed that the flexural strength of SPFRC hybrid mix was higher than PVA FRC but the deflection capacity was higher than steel FRC as high modulus of steel fibers and low stiffness of PVA fibers came into play simultaneously. But in this study, PVA fibers were seen to be ruptured with crack development due to its high bond strength and low tensile strength unlike steel fibers. Again, toughness indices of all steel-PVA fiber mixes were seen to be increased with increasing steel fiber content. Again, high volume of fly ash used in the SPFRC mix was attributed to the further improvement of deflection capacity while reducing flexural strength. For a very high fiber volume content e.g. as much as 2.5%, 50% replacement of cement by fly ash was found to be an optimum content. But fly ash % beyond 50% was observed to increase porosity in the mix and thus reduction of flexural strength was observed. Again, HyFRC containing steel and PVA fibers showed greater first crack deflection for the same flexural toughness [22].

Yanggeunhyeok et al. [23] reported that SPFRC with 0.51% by vol. of steel fibers and 0.14% by vol. of PVA fibers showed higher toughness compared to SPFRC with 0.51% by vol. of steel fibers and 0.07% by vol. of PVA fibers.

The compressive strength of SPFRC with 0.50% by vol. of steel fibers and 0.07% by vol. of PVA fibers were seen to be increased by as much as 31% compared to non-reinforced concrete [23]. Yanggeunhyeok et al. [23] also reported that shorter the length of PVA fibers greater the increase in compressive strength.

2.1.4 Polypropylene FRC (PPFRC)

Hsie et al. [24] showed that the compressive strength improvement of polypropylene hybrid (PP) fiber reinforced concrete (FRC) ranged from 14.60% to 17.31% [24]. In this investigation, monofilament PP and staple PP fibers were mixed together to get the hybrid mix. This study showed that the PP hybrid FRC has better compressive strength increase that steel-polypropylene hybrid FRC as monofilament PP fibers used in this study had high young's modulus and stiffness for the rough shape and high content of these fibers can resist more compression. Bayasi et al. [25] investigated PPFRC with two different fiber lengths- ½" and ¾ ". PPFRC with ½" PP fibers showed increased compressive strength whereas mixes with ¾" fibers showed no obvious effect on compressive strength of concrete. Alhozaimy et al. [26] reported that fiber volume fraction of upto 0.30% did not show any significant effects on compressive strength at 95% level of confidence.

Splitting tensile strength has been reported to be increased by 8.88-13.35% by the addition of PP fibers. Although, hybrid PP (monofilament + staple) mixes showed more improvement in splitting tensile strength than a single PP FRC which contains either monofilament or staple PP fibers[24].

Hybrid PPFRC showed increased modulus of rupture by 8.99-24.60% as compared to plain concrete due to its high elastic modulus and stiffness [24]. Hsie et al. [24] reported that majority of PP fibers were pulled out during flexure test. According to Bayasi [25], significant flexural post-peak resistance of PP fiber concrete mixes were observed for ½" fibrillated PP fibers at a volume of 0.5%. Alhozaimy [26], on the other hand, reported that PP fibers at 0.3% volume fraction did not affect the flexural strength of concrete but the flexural toughness were increased upto 386% due to the addition of fibers at 0.3% vol. fraction. Hsie et al. [24] reported that the addition of PP fibers significantly improved toughness of concrete mixes. With increasing fiber content, PPFRC was seen to increase toughness indexes [24].

When macro PP fibers were used in the concrete mix, they exhibited a decrease in both flexural strength and compressive strength at low volume fraction (e.g. 0.5%) but exhibited an increase in flexural strength at high fiber volume fraction (e.g. 1.0%) [15].

In case of impact strength, Bayasi [25] reported dramatic improvement of impact strength in case of ½" fibrillated PP fibers. No. of Blows to first crack jumped from 5 to 186 and no. of blows to failure jumped from 5 to 201 as 0.3%, ½" PP fibers were added to the control mix. Alhozaimy [26] reported large variations in impact test results. No. of Blows to first crack and failure were both significantly increased in this study.

2.1.5 PP-Carbon (micro) FRC

Hybrid mixes of Macro PP fibers in combination with micro mesophase-pitch-based carbon fibers were seen to exhibit lower compressive strength than the plain concrete mix while increasing modulus of rupture [16].

2.1.6 Carbon (micro) FRC

Concrete mixes containing micro carbon fibers showed a decrease in compressive strength while increasing flexural strength [16].

2.1.7 Carbon (macro) –steel FRC

Hybrid mixes containing 0.2% carbon and 0.3% steel fibers exhibited high compressive strength, splitting tensile strength and modulus of rupture than the plain mix [27]. This mix also showed high flexural toughness by bridging across macro-cracks and reducing its opening.

2.1.8 Carbon (nano) FRC (CNF-FRC)

Carbon nanofiber's (CNFs) use in cement composites has been quite limited as considerable research effort has been concentrated on CNFs in polymer composites [29]. In the recent years, only a few noticeable researches [28-30] have been done which dealt with the effect of CNFs in improving the mechanical properties of FRC e.g. compressive strength, splitting tensile strength, impact strength etc.

Sanchez et al. [28] studied microstructural, physical and mechanical properties of hybrid CNF/SF cement composites. The role of silica flume (SF) was also studied in case of SF's ability to increase CNF dispersion and concomitant problems such as SF agglomeration and dispersion. This study reported that at a concentration of 2 wt% CNFs in the composite along with SF, a much rougher fracture service was observed indicating an inhomogeneous microstructure within the composite. The addition of SF improved the dispersion of CNFs compared to composites without SF because SF disrupted Van der Walls forces acting between fibers and subsequently reduced fiber clump formation. As fly ash contains particles finer than Portland cement particles-one pound of fly ash contains approximately 33% more fines than a pound of Portland cement. So, as silica flume improved dispersion of CNFs due to its small sized particles compared to the cement particles allowing SF to separate CNFs during dry mixing. Similar trend could be expected from fly ash as fly ash is finer than cement particles. Gao et al. [31] reported that CNF-self consolidating concrete (SCC) containing heat treated (highly conductive) CNF at 1.0% by vol. of binder showed 21.4% improvement in case of compressive strength compared to plain SCC. Several other mixes containing higher and lower % CNF were studied [10] and 1.0% CNF was found to be the threshold volume. Higher ductility was also observed for CNF-SCC compared to plain SCC. This study also showed that while well-dispersed CNF improved strength and stiffness of concrete, higher concentration of CNF caused poor dispersion and subsequent clump of CNF inside cement matrix. Again, this study showed that when less conductive CNF at 0.16% was used with plain concrete, compressive strength increased by 42.7% compared to plain concrete. But similar improvement did not happen in case of other concentrations. This study reported strength variation as 0.16% > 0.31% > 0.78% > 0% > 1.55%. It was evident that the strength of concrete decreased beyond 0.16% CNF concentration.

Xie et al. [32] reported that effective dispersion is the key to obtain a CNF/cement composite with improved performance. CNFs and CNTs showed an inclination towards agglomeration, formation of bundles and slippage [22] which prevented the CNFs from improving the physical properties of composites. In order to obtain very good dispersion, chemical functionalization was proved to be the best possible method.

2.2 Structural response of RC and FRC structures

Civil engineering structures are susceptible to dynamic loading conditions in the form of impact loadings, blast loadings and earthquakes. Impact loads may result from the crashing of comparatively rigid heavy objects at low velocities, such as falling rocks in mountain areas, falling heavy loads dealt with in factories and warehouses due to accidents, falling heavy loads from higher floors during construction, vehicle crash impact on transportation structures, projectile or aircraft impact on protective structures, marine and offshore structures exposed to ice impact, and, structures sustaining shock and impact loads during explosions [1-4]. In order to develop a performance-based impact resistant design approach, a thorough experimental investigation for the structural safety of RC and PT structures subjected to impact loadings has become essential these days.

To simulate the behavior of Reinforced Concrete (RC) structures under low velocity impact loads, an extensive amount of drop-weight tests and analytical evaluation has been done [1-7, 33, 34]. But very little research has been done on the effects of impact loads on FRC structures. Again, it is evident from the previous article that in recent years, innovative materials are also being introduced for impact resistance of RC and post-tensioned (PT) structures [5]. Hence, it has become increasingly important to undertake an investigation in order to observe structural response of FRC structures. In the following sections, a review of the research works which has been done in order to determine the behavior of civil engineering structures under impact loadings is presented.

2.2.1 Effects on RC structures

Yang et al. [9] illustrated the behavior of RC structures under impact loadings. Tensile stresses generated in reinforced and prestressed concrete structures due to dynamic loading are reported to occur in two steps: Firstly, the compressive stress wave is generated on the loading side of the structure by impact loading and secondly, the compressive stress wave hits the free boundary on the distal side of the structural element and then reflected as a tensile stress [9]. Hence, tensile properties of concrete are one of the most critical criteria under impact loading and to eliminate this problem, fiber reinforced ductile concrete has been proposed and used in recent years.

Fujikake et al. [4] reported that the behavior of a structural component under impact loading consisted of two response phases, as shown in Fig. 2.1: Firstly, the local response which is caused by the stress wave that occurs at the loading point during a very short period after the impact; and the overall response caused by the elastic-plastic deformation that occurs over a long period in the whole structural member after impact.

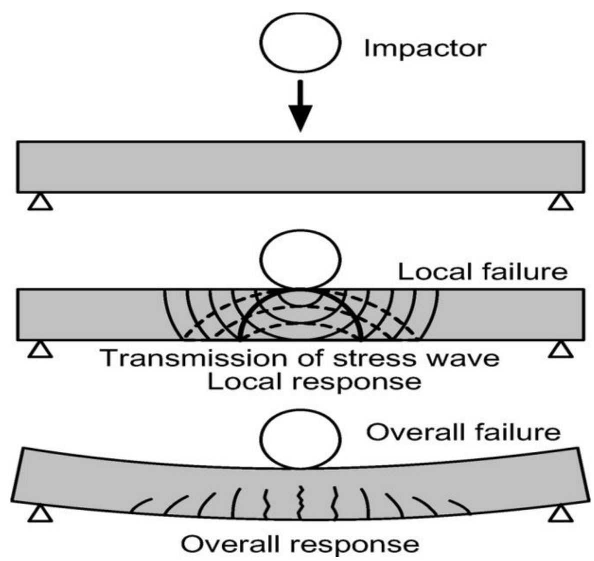

Fig. 2.1 - Impact responses of a RC member [4].

Investigations on the influence of drop height and the effect of the amount of longitudinal steel reinforcement to the response of RC beams were made [4]. It has been shown that in order to properly investigate the structural safety of RC beams, both its flexural capacity and its maximum deformation response has to be estimated [23]. Overall flexural failure was given priority [4] just like other researchers [7, 33-34] which was the critical condition for beams. It was ensured that the RC beams were weaker in flexure by varying shear resistance from 50-155% larger than its bending resistance [4]. On the other hand, Saatci et al. [3] reported that methods developed to predict the response of reinforced concrete under impact loads must consider shear mechanisms for accurate analytical modeling.

According to Fujikake [4], increasing the amount of tensile reinforcement in a RC beam with an under-reinforced section could cause local failure near the impact loading point. Again, increasing the amount of longitudinal compressive reinforcement could affect the degree of failure. Larger local failures were also observed in a RC beam with lesser amount of compressive reinforcement than the RC beam which had higher amount of compressive reinforcement.

Impact responses such as the maximum impact load, the impulse, the duration of impact load, the maximum midspan deflection, and the time taken for the maximum midspan deflection were reported to be increased as the drop height was increased [4]. It was noteworthy that at the same drop height, different RC beams with different tensile and compressive reinforcement showed very similar impact force. Again, an impact force of 112400 lbf (500 KN) was reported at a drop height of 94.5 in. (2.4 m) where the drop weight was 881.85 lbs (400 kg); thus, the acceleration of the drop weight would be around 127g (Gravitative acceleration, g =9.8ms^{-2}).

Saatci et al. [3] studied effects of shear mechanisms on the impact behavior of RC beams where the drop height was 128.3 in. (3.26 m) and the drop weights were 465 lbs (211 kg) and 1323 lbs (600 kg). Saatci et al. [3] reported that during impact testing all specimens developed severe diagonal cracks with an angle of approximately 45 degrees by forming shear-plugs. Again, diagonal cracks parallel to the major shear-plug cracks along with some vertical flexural cracks at the midspan and at the supports were also reported. According to Saatci [3], failure modes are determined mainly by the static behavior of the specimens; in the flexure-critical specimens, shear-plugs developed faster than did the support shear cracks. Just like Fujikake [4], Saatci [3] observed that specimens with higher shear capacity could sustain higher impacts and absorb more energy whereas the ones with lower shear capacity suffered extensive damage under the same or smaller impact loads. So, shear mechanisms are extremely important to predict the response of RC beams under impact loadings [3]. In this study, a maximum impact force of 168600 lbf (750 KN) and a maximum acceleration of 800g were observed throughout the test.

Chen et al. [1] investigated drop weight impact on beam specimens with a cross section of 4” x 8” (101. 6mm width x 203.2 mm Depth) and longitudinal tensile reinforcement of 0.4 in^2(258 mm^2). All tests were conducted under a drop-weight of 218 lbs (98.7 kg) with an impact velocity of 287.5 in/sec (7.3 m/s). This study reported that the impact force is dependent on the span of a beam but not on the end conditions. Again, the plywood surface which was used as a load distributor, distributed the force or impact load in a similar form to a flat impactor [9]. This investigation was unable to correlate concrete strength and peak load of impact.

The crack patterns reported by Chen et al. [1] include diagonal shear cracks (at the maximum impact load) and vertical flexural cracks as well as formation of horizontal cracks which result in scabbing of concrete. A short period of separation between the impactor and beam is reported [9] as the beam deformed at a faster rate than the impactor. Three types of post-test failure modes have also been reported by Chen [1]. Firstly, a predominantly flexural failure with considerable crushing beneath the impactor and some shear cracking in the impact zone and vertical cracks starting from the top of a beam along the beam section away from the impact zone. These failure modes were observed for a beam with a compressive strength of 7136 psi and an impact interface of 12 mm (0.47 in) plywood. Secondly, a mainly localized failure at the impact zone with extensive concrete crushing below the impactor, and yielding of the tension steel bars were observed for a beam with a compressive strength of 7136 psi and a direct impact interface with hemispherical impactor. Lastly, this failure was accompanied by loss of the concrete cover to the tension steel reinforcement at the bottom of a beam owing to scabbing.

Habel et al. [35] studied impact response on a 142 in. (3600 mm) long reinforced concrete slab strips with a cross section of 10” x 6.7” (254 mm width x 170.2 mm depth) and longitudinal tensile reinforcement of 0.465 in^2 (303.2 mm^2). This study reported that impact forces calculated from the accelerations obtained from accelerometers mounted on the drop weights (measured) and from deflections and accelerations of the specimens (calculated) were generally in good agreement. But the initial peak of drop weight force was significantly higher for calculated values than the measured values. This study proved that drop weight force could be well derived from acceleration measurements of the drop weight by Newton’s second law. From the drop weight test results, it was evident that the RC member underwent a concentrated deformation (localization) at mid span which is consistent with the test results of Fujikake [4].

A summary of drop weight, drop height, impact load, acceleration and other parameters observed in previous research works are shown in Table 2.1.

Table 2.1 - Summary of previous drop-weight impact tests

Ref.	Tensile reinforce-ment (in^2)	Drop weight (lb)	Drop height (in)	Maximum Impact load (lbf)	Maximum Acceleration (in terms of g)	Impact velocity (in/sec)	Sampling rate, (kHz)	Impactor interface
[23]	1.2	882	94.5	112404	N/A	N/A	100	Hemispherical
[22]	2.18	465, 1323	128.3	168600	800	315	2.4, 19.2	Flat
[9]	0.4	218	107.1	147025	450	287.5	500	Flat/Hemispherical
[28]	0.465	465	128.4	92172	N/A	315	2.4	Flat

2.2.2 Impact resistance and Engineered composites

2.2.2.1 Engineered Cementitious Composites (ECC)

Yang et al. [9] studied damage characteristics, load and energy dissipation capacities and response to repeated loads by performing low speed drop weight tower test on Reinforced ECC (R/ECC) panels and beams. This study was focused on the investigation of the tensile dynamic response of ductile concrete. Engineered Cementitious Composites (ECC) were used which showed high ductility and damage tolerance under tensile and shear loading [5]. In this study, it was observed that an ECC square shaped panel with no steel reinforcement only showed micro-cracks on the distal side of the panel only after the test was performed three times whereas a specimen with 0.5% steel reinforcement (without ECC) failed by brittle failure after the first impact. Again, in a separate test, it was seen that the load capacity of the R/ECC beam was increased by 32% from that of the R/C beam, but the energy capacity was increased by 500%. So, the addition of steel reinforcing bars for enhancing structural load and energy capacities is more efficient in R/ECC than in R/C due to the high tensile ductility of ECC so that a compatible deformation between steel reinforcement and ECC was achieved during impact. This compatible deformation was obtained by engaging a longer segment of steel to undergo plastic yielding. Hence, these tests clearly demonstrate the potential for R/ECC elements to sustain multiple impact loads and to maintain damage tolerance.

2.2.2.2 Ultra High Performance Fiber Reinforced Concrete (UHPFRC)

Habel et al. [35] studied the impact response of reinforced and posttensioned concrete members with ultrahigh-performance fiber-reinforced concrete (UHPFRC) overlay. Parameters considered for the tests were the reinforcement configuration of the concrete substrate, the addition of reinforcing bars in the UHPFRC layer, and the static system. It was observed in the study that the UHPFRC had a load distributing function. This function helped to reduce crack widths in the substrate and lower member deflections. The objective of this study was to determine the benefits of using UHPFRC for rehabilitation and strengthening of structures subjected to low velocity impact-type loading [35]. For this, drop weight tests were performed in both three-point bending and cantilever configurations, with the drop weight impacting the UHPFRC overlay. They reported that more force was transferred in the slab strips with the UHPFRC overlay than in the corresponding reference specimens due to the initial stiffness of the slab strips and the effect of posttensioning. The addition of UHPFRC layer significantly changed the crack pattern of the specimens. Crack widths were also smaller than normal reinforced and posttensioned concrete specimens and shear cones occurred only in the concrete layer demonstrating less wider cracks. Again, it was observed that no bond failure occurred at the interface between UHPFRC and the conventional concrete indicating the monolithic structural behaviors. The addition of UHPFRC improved the resistance of the slab strip to impact loading. This improvement was verified by less damage compared to specimens with UHPFRC with increasing static height and also due to the absence of spalling and crushing in the zone of the impact. UHPFRC overlays showed reduced deflections by a factor of 2 for the reinforced configuration and by a factor of 3 for the prestressed configuration.

2.2.2.3 High Performance Fiber Reinforced Concrete (HPFRC)

Farnam et al. [36] studied the behavior of High Performance Fiber Reinforced Concrete specimens (Slabs and cylinders) by undergoing impact tests and mechanical properties tests.

Several HPFRC slab specimens were constructed using 2% vol. of steel fibers, metakaolin as a pozzolanic material (17.6% of cement volume) for this study. For the impact tests, crack propagation, failure patterns and crack width in various sides of specimens were observed. Plain concrete specimens failed in the first strike whereas HPFRC specimens showed radial flexural micro-cracks in the first strike. Before failure, punching failure was observed which were enlarged with the effect of circular microcracks. Finally, the specimens failed due to shear punching failure in the shape of a truncated cone shape.

2.3 Spring-mass models for impact loads

Global response of structural members which are subjected to impact and impulsive loading had been analyzed with mass-spring models by various researchers [37-39]. Daudeville et al. [37] studied impact results from the collision of two bodies, one with an initial speed and the other one at rest. This problem could be modeled as two colliding masses, m_1 and m_2, a contact spring with a stiffness k_1, in between the two masses to simulate the force after contact, and another spring with a stiffness k_2 which represents the deformation and resisting force of the structure [Fig. 2.2]. Both springs was modeled as having nonlinear force-deformation relationships.

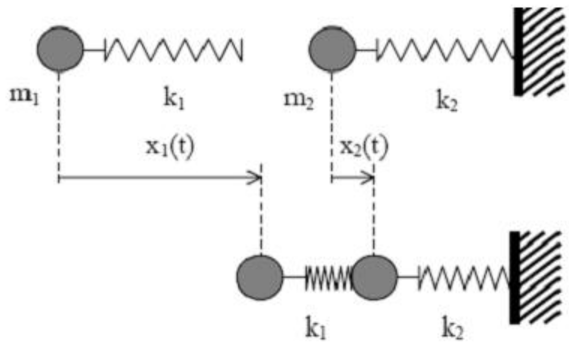

Fig. 2.2 - Simple mechanical model of an impact by means of two-mass system [37].

According to Daudeville, the two-mass system is governed by the following differential equations:

$m_1\ddot{x}_1\,(t) +\ k_1[x_1(t) - x_2(t)] = 0$……… (1)

$m_2\ddot{x}_2\,(t) - k_1[x_1(t) - x_2(t)] +\ k_2 x_2(t) = 0$……… (2)

In case where x_1>>x_2, i.e. the deformation of the projectile is much greater than the deformation of the impacted structure, then with $F(t)=k_1x_1(t)$,

$m_1\ddot{x}_1\,(t) +\ k_1[x_1(t)] = 0$…….. (3)

$m_2\ddot{x}_2\,(t) +\ k_2 x_2(t) = F(t)$…….. (4)

The first equation [Eq. (3)] is an independent equation to determine F(t), while the second [Eq. (4)] gives the deformation of the structure under an independently acting force F(t).

This case, where the resisting structure remains un-deformed, so that the kinetic energy of the striking body is completely transferred into deformation ($x(t)=x_1(t)$ and $V(t)= V(x_1)$ of the striking body, is called soft impact .

The limiting counterpart ($x_1(t) << x_2(t)$) is called hard impact and occurs when the striking body is rigid and the kinetic energy of the striker is completely (the residual velocity V(t)=0) or partially (the residual velocity V(t)≠0) absorbed by deformation of the struck structure [37].

Habel et al. [38] described an impact event as a single degree of freedom one mass-spring model [Fig. 2.3].

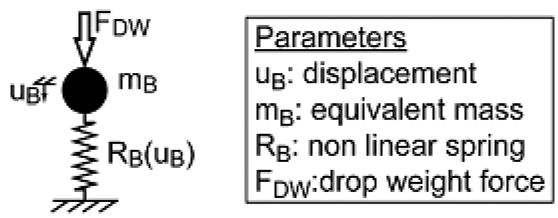

Fig. 2.3 - Mass spring model: Model definition [38].

In this model, the slab strip or beam was modeled as mass m_B and F_{DW} is the drop weight force applied on the slab strip or beam. F_{DW} can be obtained by experimental study where measurement of the acceleration (a_{DW}) of the drop-weight is necessary $F_{DW} = m_{DW}*a_{DW}$. The nonlinear spring R_B in this model can be represented by the structural response of the beam or slab strip in the form of an equivalent force vs. mid span deflection curve. Finally, *Mathematical formulation provided by Habel et al. [38]:*

$$m_B.\frac{d^2u_B}{dt^2} + R_B(u_B,t) - F_{DW}(t) = 0$$

Where the mass m_B corresponds to the equivalent slab strip or beam mass as per CEB-FIP [39] as

$$m_B = \int_0^L \overline{m}\,.\varphi^2\,.dx$$

Where,

m_B = concentrated slab strip/beam mass

$\overline{m}$ = mass per unit length of the specimen

φ = shape function (based on the deflected shape of the specimen)

L = span length

Again, the non-linear spring R_B can be obtained from the static load vs. deflection curves and F_{DW} can be measured directly from the acceleration value of the impact event. This model doesn't consider damping effects of the impact event which is the shortcoming of this model. But it can accurately simulate the first deflection rise.

2.4 Impact force and deflection calculation by analytical methods

Two types of deformation or damage in the concrete beams were observed under impact loading; local and global deformations where local damage is caused by the contact force between the impactor and the beam in the vicinity of the impact zone and global damage is induced by the impact force and vibration of beam [7].

2.4.1 Impact force calculation

Several spring-mass models are available to calculate impact force and deflections. Tang and Saadatmanesh (2005) [7] had successfully used a spring-mass model proposed by Abrate (1998) [40]. In this current study, the spring-mass model [40] has been used to calculate impact forces. This model represents two degrees of freedom. From force equilibrium of the free-body diagram, the equations of motion can be developed

$$m_1 \frac{d^2 y_1}{dt^2} + F = 0 \ldots\ldots (5)$$

$$m_2 \frac{d^2 y_2}{dt^2} + K_{bs} y_2 + K_m {y_2}^3 - F = 0 \ldots\ldots\ldots\ldots (6)$$

Where, m_1 and m_2 are the masses of impactor and beam respectively; y_1 and y_2 are the displacements of impactor and beam respectively; F is the impact force on the beam due to the impact; K_{bs} is the linear stiffness of the beam obtained from static test results; and K_m is membrane stiffness. The initial conditions are expressed at t= 0 (just before contact occurs).

$\frac{dy_1}{dt}(0) = V; y_1(0) = y_2(0) = 0$…… (7)

Where, V is the initial velocity of the impactor just before contact occurs.

Considering the geometrical nonlinearity and the indentation negligible, the model was significantly simplified to a single degree of freedom system (Tang and Saadatmanesh 2005) with the equation of motion as

$m_1 \frac{d^2 y}{dt^2} + K_{bs} y = 0$…….. (8)

To further simplify the equation, Tang and Saadatmanesh (2005) neglected the effective mass of the structure as the structure and the impactor move together as soon as contact is made, that is $y_1 = y_2 = y$. Using the initial conditions at t = 0, the general solution of Eq. (8) is

$y = \frac{V}{\omega} \sin \omega t$……. (9)

Where, $\omega = \sqrt{\frac{K_{bs}}{m_1}}$

As the impact force F is equal to the force in the linear spring K_{bs}, the contact force history can be expressed as

$F = K_{bs} y = V(K_{bs} m_1)^{1/2} \sin\omega t$ ………. (10)

Eq. (10) is derived by Tang and Saadatmanesh (2005) based on the assumption that the beam stiffness remains constant during the impact. Actually, the stiffness of concrete beam decreases as beam cracks. Based on the test results, Eq. (10) is modified with a constant γ to incorporate the effects of reduced stiffness. Equation (10) is then expressed as

$F = K_{bs}y = \frac{V(K_{bs}m_1)^{1/2}}{\gamma}\sin\omega t$.......... (11)

Where, γ was determined from the test results. In this study, γ was calculated as the average ratio of the measured first impact force for the test beams and the impact force calculated from Eq. (10).

2.4.2 Deflection calculations

Tang and Saadatmanesh (2005) proposed an equation [Eq. (12)] which was developed based on a flexural wave theory proposed by Graff (1975) [41].

Displacement, $y(x,t) = \frac{2P}{\rho Al}\sum_{n=1,3,5}^{\infty}\frac{(-1)^{(n-1)/2}\sin\beta_n x_0 \sin\omega_n t}{w_n}$ .... (12)

Where, l is the length of the beam, $\beta_n = \frac{n\pi}{l}$, $\beta_n x_0 = \frac{n\pi}{2}$, $a = \frac{EI}{A\rho}$, $\omega_n = a{\beta_n}^2$, EI is the bending stiffness of the beams, density of beam ρ, Area of beam, A.

Now, in Eq. (12), the value of P is obtained from Eq. (11) for each beam. In the calculation of maximum deflection using Eq. (12), a total of five terms were used for summary, that is, n= 1, 3, 5, 7, and 9.

CHAPTER 3

PROBLEM STATEMENT

The shortcomings of current research and research needs are identified as follows:

(1) Better data is needed. Available impact test results are limited and thus may not be an adequate measure for model accuracy. For instance, displacements are reported at limited locations and are not reliable in some cases (due to concrete delamination at the distal side of the impactor, as shown in Fig. 3.1, and noise in LVDT data).

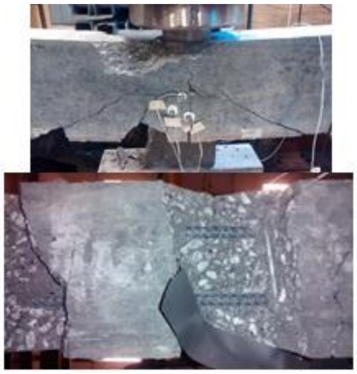

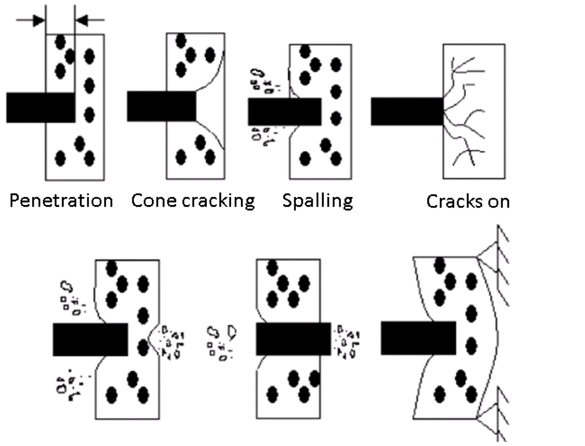

Fig. 3. 2 - Effects of impact on concrete [43].

Fig. 3. 1 - Concrete scabbing on the distal side of the impactor.

(2) Composites are needed. In addition to the need to assess conventional civil structures, there is a strong need to engineer impact resilient cementitious composite structures (e.g., tornado shelters, critical bridge components, and other public safety critical structures).

(3) Ability to predict and understand the physically visible effects of impact loading is needed. Fig. 3.2 shows the effects of impact loadings on a concrete target which includes material damage, erosion or fragmentation resulting from penetration, scabbing, perforation, etc. Indeed, various empirical procedures have been developed for determining penetration depth, perforation thickness, and scabbing thickness [43] for conventional concrete targets subjected to missile impact. Nonetheless, there is a strong need to predict the damage patterns of engineered composite structures under impact loading.

(4) Full or half-scale testing is needed. Despite the innovations in micro/nano materials, scaling up the nano-technology (i.e. nano-scale materials used in large structures) in the construction industry appears not only financially burdensome (due to large scale validation required) but also challenging to validate multi-scale analytical models for design. Reliable data from a large-scale experimental program is essential.

(5) Previous studies indicate that a fiber with a hydrophobic surface and/or a matrix with higher fly ash content can be used to compensate the rate sensitivity of the material components that limits the tensile ductility at higher loading rates [9]. Furthermore, hybrid fiber systems (e.g., micro and nano fibers) enhance mechanical properties (e.g., tension) under impact loading [11].

(6) Engineered cementitious composites (ECCs) enhance energy dissipation and thus increases impact resilience; however, previous impact studies are mostly limited to plain or single fiber reinforced concrete beams and thus do not include engineered cementitious composites reinforced with multi-scale hybrid fibers.

(7) Understanding of ancillary effects of impact is needed. Fiber reinforced composites have the potential to withstand high velocity projectiles. However, a high velocity impact may generate temperatures and pressures which could compromise the structural integrity of engineered composites. Polypropylene fibers melt at relatively low temperature and thus relieve the pressure build-up by creating a network of escape routes for the gas phases (e.g., water vapor/CO_2) [44]. The effectiveness of polypropylene fibers in ECCs has not been fully explored.

CHAPTER 4

RESEARCH OBJECTIVES AND PLANS

4.1 Research Objectives

There are three specific objectives of the proposed study:

Objective 1: Identify the most efficient (i.e. increased ductility and toughness) macro/micro/nanofiber types and volume fractions for design of MIRACs.

Objective 2: Achieve a uniform dispersion of CNFs in cementitious composites.

Objective 3: Study the performance of MIRACs in a large scale impact test.

4.2 Specific Plans to Meet the Objectives

Plan 1: Design a small-scale impact test to identify the most effective fibers types and volume fractions for MIRACs.

Plan 2: A uniform mix of nano-fibers has been achieved with a combination of chemical admixture/mixing sequence/batch volume & by a trial-error method. Scanning Electron Microscope (SEM) images need to be produced to ensure a uniform dispersion of carbon nano fibers as the clumps weaken macro-scale properties.

Plan 3: Design and develop a large-scale low-velocity drop weight impact test to study the performance of composite RC beams and report the performance of MIRACs.

In the following chapters, the above three specific plans are incorporated in a two-phase experimental program:

Phase I Small-scale impact test – Plans 1 and 2 (Chapters 5 and 6)

Phase II Large-scale impact test – Plan 3 (Chapters 7 and 8).

CHAPTER 5

EXPERIMENTAL PROGRAM: PHASE I

This chapter presents the first phase experimental investigation which includes a small-scale impact test to identify the most effective fibers types and volume fractions for MIRACs and achieved a uniform dispersion of carbon nanofibers in cementitious composites. Two specimen groups are developed for Phase I: (1) Group 1: Fiber reinforced composites consisting of macro-scale steel, micro-scale PVA, and nano-scale CNFs (2) Group 2: Fiber reinforced composites consisting of macro-scale PP, micro-scale PVA, and nano-scale CNFs. The following sections discuss fiber volume fractions, materials, mixing procedures and test methods of the experimental program.

5.1 Group 1 - Fiber reinforced composites consisting of steel, PVA and CNFs

In total, 10 concrete-fiber mix proportions are investigated in this study. Table 5.1 presents the test groups: 1 control group without any fiber reinforcement; 4 sample groups with single fiber reinforcement – carbon nano fibers (CNFs), polyvinyl alcohol (PVA) fibers, and steel fibers; 4 sample groups consisting of 50/50 or 40/60 steel/PVA mixing ratios for total fiber volume fractions of 1% and 0.75%; and finally 1 sample group simultaneously including multi-scale fibers (steel, PVA, and CNFs) with a fiber volume fraction of 1%.

Table 5.1 - Ten test groups and fiber mix proportions (GROUP -1)

Specimen Designation Fiber type Mixing ratio – Total fiber volume fraction (%)	Fiber type	CNF weight / Cement weight (%)	Macro vs. micro fiber mixing ratio (%)		Total fiber vol. (%)	Fiber scale
			Steel	PVA		
Control	No fiber	0	n/a*	n/a	0	No Fiber
S-0.75%	Steel	0	n/a	n/a	0.75	Single Macro
S-1%	Steel	0	n/a	n/a	1	Single Macro
P-0.75%	PVA	0	n/a	n/a	0.75	Single Micro
N	CNF	1	n/a	n/a	n/a	Single Nano
SP50/50-0.75%	Steel+PVA	0	50	50	0.75	Macro + Micro
SP40/60-0.75%	Steel+PVA	0	40	60	0.75	Macro + Micro
SP50/50-1%	Steel+PVA	0	50	50	1	Macro + Micro
SP40/60-1%	Steel+PVA	0	40	60	1	Macro + Micro
MIRAC-1%	Steel+PVA+CNF	1	50	50	1	Macro + Micro + Nano

* n/a: not applicable.

5.2 Group 2 - Fiber reinforced composites consisting of PP, PVA and CNFs

In total, 10 concrete-fiber mix proportions are investigated in this study. Table 5.2 presents the test groups: 1 control group without any fiber reinforcement; 4 sample groups with single fiber reinforcement – carbon nano fibers (CNFs), polyvinyl alcohol (PVA) fibers, and PP fibers; 4

sample groups consisting of 50/50 or 40/60 PP/PVA mixing ratios for total fiber volume fractions of 1% and 0.75%; and finally 1 sample group simultaneously including multi-scale fibers (PP, PVA, and CNFs) with a fiber volume fraction of 1%. To avoid confusion, 'mFRC' is used instead of 'MIRAC' in Table 5.2.

Table 5.2 - Ten test groups and fiber mix proportions (GROUP -2)

Specimen Designation Fiber type Mixing ratio – Total fiber volume fraction (%)	Fiber type	CNF weight / Cement weight (%)	Macro vs. micro fiber mixing ratio (%)		Total fiber vol. (%)	Fiber scale
			Steel	PVA		
Control	No fiber	0	n/a*	n/a	0	No Fiber
F-0.75%	PP	0	n/a	n/a	0.75	Single Macro
F-1%	PP	0	n/a	n/a	1	Single Macro
P-0.75%	PVA	0	n/a	n/a	0.75	Single Micro
N	CNF	1	n/a	n/a	n/a	Single Nano
FP50/50-0.75%	PP+PVA	0	50	50	0.75	Macro + Micro
FP40/60-0.75%	PP+PVA	0	40	60	0.75	Macro + Micro
FP50/50-1%	PP+PVA	0	50	50	1	Macro + Micro
FP40/60-1%	PP+PVA	0	40	60	1	Macro + Micro
mFRC-1%	PP+PVA+CNF	1	50	50	1	Macro + Micro + Nano

5.3 Materials

Crushed coarse gravel of size no. 67 is used according to Section 901, ACI 211 [45] with a maximum aggregate size of 19 mm and a specific gravity of 2.6. The ASTM Type III [46] cement is used. The fly ash used in this study corresponds to ASTM C 618 [47] Class F with a specific gravity of 2.3. The fine aggregate used is saturated surface-dry (SSD) clean river sand (fineness modulus = 2.6).

The superplasticizer used in this study is polycarboxylate-based high range water reducing admixture. It meets the ASTM C 494/C 494M [48] requirements for Type A, water-reducing, and Type F, high-range water-reducing, admixtures. The admixture is used to provide adequate workability. Figures 5.1 through 5.4 show four different types of multi-scale fiber reinforcement selected for this study. The properties of steel, PP and polyvinyl alcohol (PVA) fibers are shown in Table 5.3, and the properties of carbon nanofibers (CNFs) are presented in Table 5.4.

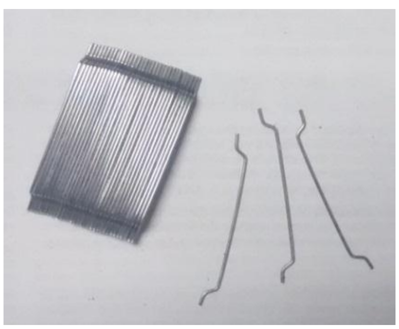

Fig. 5.1 - Macro-scale fiber reinforcement: steel fibers.

Fig. 5.2 - Macro-scale fiber reinforcement: PP fibers.

Fig. 5.3 - Micro-scale fiber reinforcement: Polyvinyl alcohol (PVA) fibers.

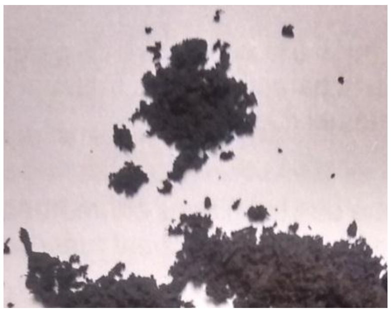

Fig. 5.4 - Nano-scale fiber reinforcement: Carbon nanofibers (CNFs).

Table 5.3 - Properties of steel, PP and PVA fibers

Criteria	Steel	PP	PVA
Length (mm)	30	54	8
Diameter (mm)	0.55	-	38×10^{-6}
Tensile Strength (MPa)	1345	570-660	1600
Young’s Modulus (GPa)	210	-	-
Geometry	Deformed End	Straight, Fibrillated	Straight
Specific Gravity	7.8	0.91	1.3
Flexural Strength (GPa)	-	-	40

Table 5.4 - Properties of carbon nano-fibers

Fiber diameter, nm (average):	100
CVD carbon overcoat present on fiber:	no
Surface area, m2/gm:	41
Dispersive surface energy, mJ/m2:	135
Moisture, wt%:	<5
Iron, ppm:	<100
Polyaromatic hydrocarbons, mg PAH/gm fiber:	<1

5.4 Mix proportions

Table 5.5 presents the concrete mix proportions selected for the control group. A water cement ratio of 0.48 is maintained for all specimens throughout the study. The workability of each mix is measured using the slump test prescribed by ASTM C143 [49].

Table 5.5 - Concrete mix proportions

Material	Quantity
Water (kg/m3)	202
Cement (kg/m3)	357
Fly Ash (kg/m3)	63
Coarse Aggregate (kg/m3)	1038
Fine Aggregate (kg/m3)	701
Superplasticizer (mL/lb of Cement)	0.88-1.70

Two fiber volume fractions (0.75% and 1.00%) are used in this study. For sample groups including carbon nano-fibers, the CNFs are provided by 1% weight of the cement binder (i.e., weight of cement and flyash) while maintaining the total volume fraction (0.75% or 1.00%) for macro and micro fibers.

5.5 Mixing procedures and specimen preparation

A small portion of the weighed water is used to keep the steel (or PP) and/or PVA fibers saturated to achieve a uniform dispersion of the fiber reinforcement. The remaining water, coarse aggregate, fine aggregate, cement and fly ash are mixed for 2.5 minutes. The remaining water and other materials are placed in the mixer and mixed for additional 1 minute. The batch is mixed for about 3 more minutes after PVA and/or steel (or PP) fibers are added to the mixer and additional 2.5 minutes after adding a superplasticizer. This mixing procedure is used to make the specimens that do not contain the CNFs.

For specimens including CNFs ('N' and 'MIRAC-1%' in Table 5.1 and 'N' and 'mFRC-1%' in Table 5.2), a dry-mixing procedure is employed. The carbon nano-fibers, fly ash, and cement are dry mixed for 5 minutes in a rotary concrete mixer while the mixer is fully enclosed such that the materials do not become air-borne and lost. This mixing method provides a uniform dispersion of the carbon nano-fibers within the cement matrix. This mixing procedure is verified by using a scanning electron microscope (SEM). It is used to view the surface of a small portion of the nano-fiber cement mixture as shown in Fig. 5.5. Six small specimens of 3-6mm in diameter are randomly extracted from each nano fiber mixture for SEM. The SEM image (Fig. 5.6) shows that the carbon nanofibers are well or uniformly dispersed in the concrete mixture.

Fig. 5.5 - Specimen preparation for Scanning Electron Microscope (SEM).

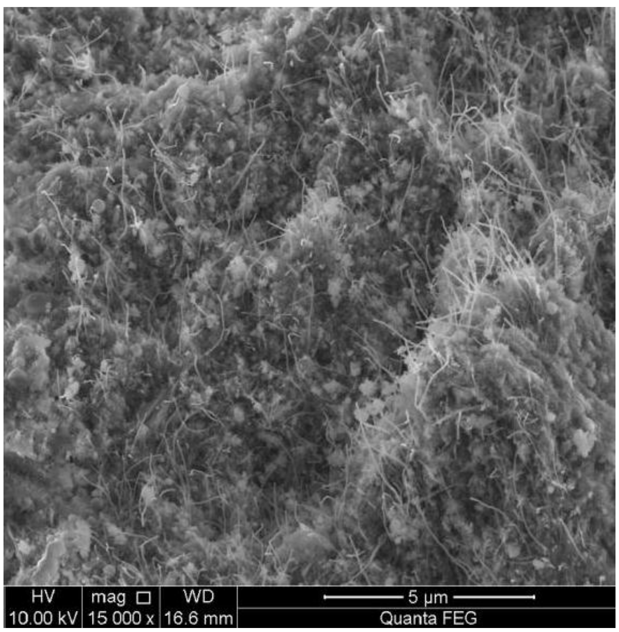

Fig. 5.6 - Typical SEM image of the specimens singly reinforced with CNFs.

Three different types of specimens are made for each mixture (or specimen group).

1. Six 100 x 200 mm (diameter x height) cylinders for compressive strength test and six 100 x 200 mm (diameter x height) cylinders for splitting tensile strength test;

2. Six 150 x 63.5 mm (diameter x height) cylindrical specimens (disks) for the impact strength test; and

3. Three 150 x 150 x 558 mm (width x depth x length) beams to determine the flexural strength (or Modulus of Rupture).

The electrical resistance of the above specimens including CNFs ranges between 40 kilo-ohms and 20 mega-ohms and highly depends on the surface areas of the specimen in contact with a digital multi-meter. For this reason, the electrical resistance of specimens is not monitored further. All specimens are prepared by placing the concrete-fiber mixture described above in greased molds. For the cylindrical specimens and disks, a vibrating table is used to obtain the required compaction accompanied by the use of a tamping rod, whereas a vibrator is used for the beam specimens for adequate compaction and removal of air bubbles. The specimens are demolded after 24 hours and then submerged in a storage tank for 28 days of curing. The water in the storage tank was saturated with calcium hydroxide to prevent leaching of calcium hydroxide from the specimens. Requirements of ASTM C511 [50] and ASTM C192 [51] are satisfied while preparing and curing of specimens.

5.6 Test methods

5.6.1 Static tests

The ASTM C39 [52] test method is used to determine the compressive strength of cylindrical specimens of the sample groups presented in Table 5.1 and Table 5.2. The test is performed on the cylindrical specimens with a loading rate of 0.24 MPa/sec which is maintained throughout the test. The splitting tensile strength of cylindrical specimens is determined by the ASTM C496 procedure [53]. The load is continuously increased at a rate of 0.0172 MPa/sec.

The ASTM C78 [54] procedure is used to determine the modulus of rupture (or flexural strength) under third-point loading. For specimens with 1% fiber volume fraction, a string potentiometer is used to obtain the mid-span displacement. Fig. 5.7 illustrates a schematic of the flexural test setup and span length. Equipment and Instruments used for Phase-I are presented in Appendix A.1.

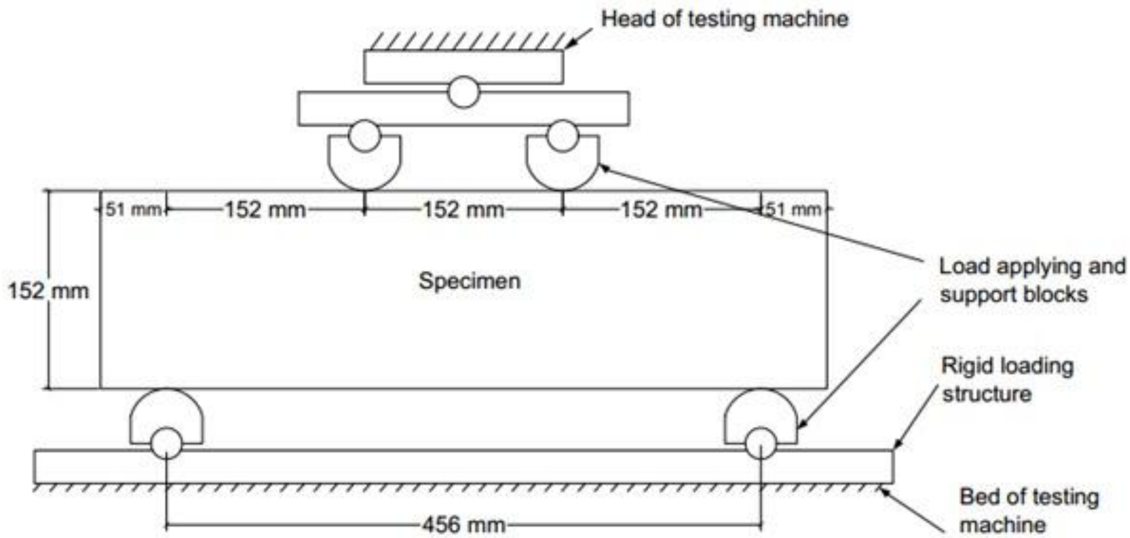

Fig. 5.7 - A schematic of MOR test setup (ASTM C78).

5.6.2 Impact tests

The “repeated impact” drop-weight test is performed as per the ACI 544.2R guide: Measurement of Properties of Fiber Reinforced Concrete [55] on the cylindrical (150 mm diameter and 63.5 mm height) specimens as shown in Fig. 5.8. This test provides the number of blows necessary to cause prescribed levels of distress in the test specimen which serves as a qualitative estimate of the energy absorbed by the specimen at the levels of distress specified [55]. In this test, a specimen is placed on a flat baseplate with a positioning bracket as shown in Fig. 8. A 63.5 mm diameter hardened steel ball is placed on top of specimen, and a manually operated 4.53 kg compaction hammer with a 456 mm drop [56] height is dropped repeatedly on the steel ball (Fig. 5.8). The number of drops or blows required to observe the first visible crack on the top surface and ultimate failure are both recorded, where ultimate failure is identified by the opening of cracks in a specimen sufficiently so that the pieces of concrete are touching three of the four positioning lugs on the baseplate [52].

Fig. 5.8 - Drop-weight impact test setup and specimen (Left: a plan view showing the steel ball without the drop hammer; Right: an elevation view).

CHAPTER 6

RESULTS FROM PHASE-I EXPERIMENT AND DISCUSSIONS

Results from Phase I for Group – 1 and Group – 2 test specimens are presented and discussed in the following sections.

6.1 Fiber reinforced composites consisting of steel, PVA and CNFs

The results from the experimental program are presented in Figures 6.1 through 6.6. The bar charts include the mean value of each specimen group, which is indicated by a solid bar, and the standard deviation displayed as two opposing bars with respect to the mean. The test data points are presented with unfilled dots.

6.1.1 Impact test results

“Repeated impact” drop-weight test was performed on cylindrical specimens described in Section 5.5 following guidelines of Section 5.6.2. Six specimens were tested for each mix group of Table 5.1. Fig. 6.12 presents impact tested specimens with no fiber, MIRAC specimen with steel fiber and MIRAC specimen with PP fiber.

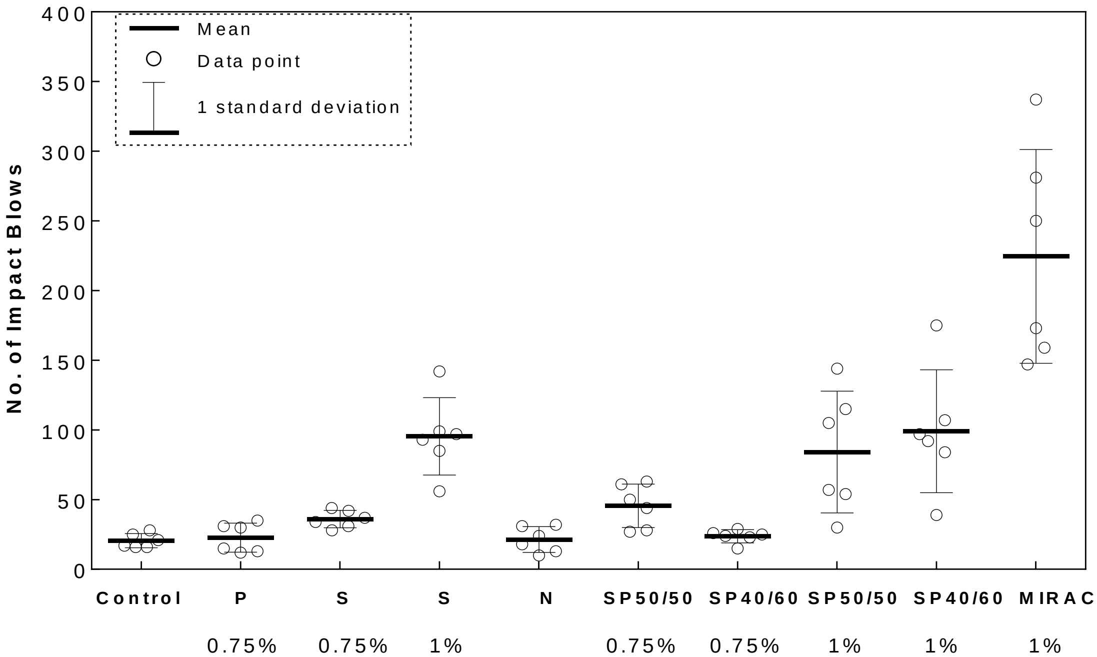

Fig. 6.1 - Impact toughness of 10 test groups of Table 5.1 based on the number of drops to observe the first visible crack.

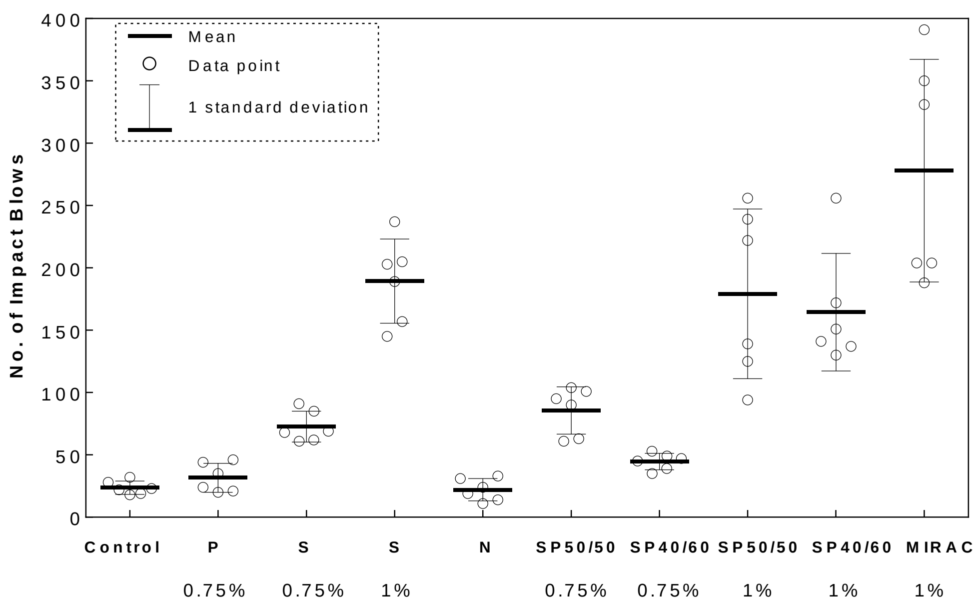

Fig. 6.2 - Impact toughness of 10 test groups of Table 5.1 based on the number of drops to observe the ultimate failure.

6.1.2 Compressive/tensile strength and MOR

Fig. 6.13 to Fig. 6.16 present compressive strength tested specimens with different fibers. Fig. 6.17 presents splitting tensile strength tested specimens with no fiber, MIRAC specimen with steel fiber and MIRAC specimen with PP fiber. Finally, Fig. 6.18 to Fig. 19 present fracture surface of MIRAC specimens after the flexural strength test.

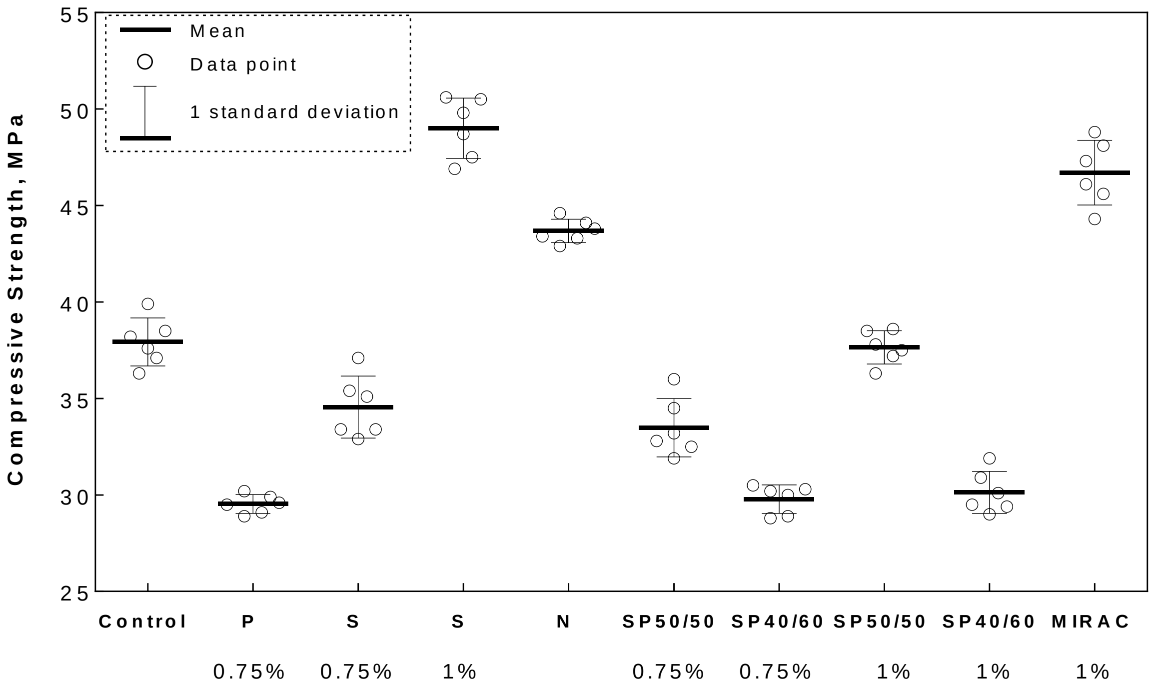

Fig. 6.3 - Compressive strength of 10 test groups of Table 5.1.

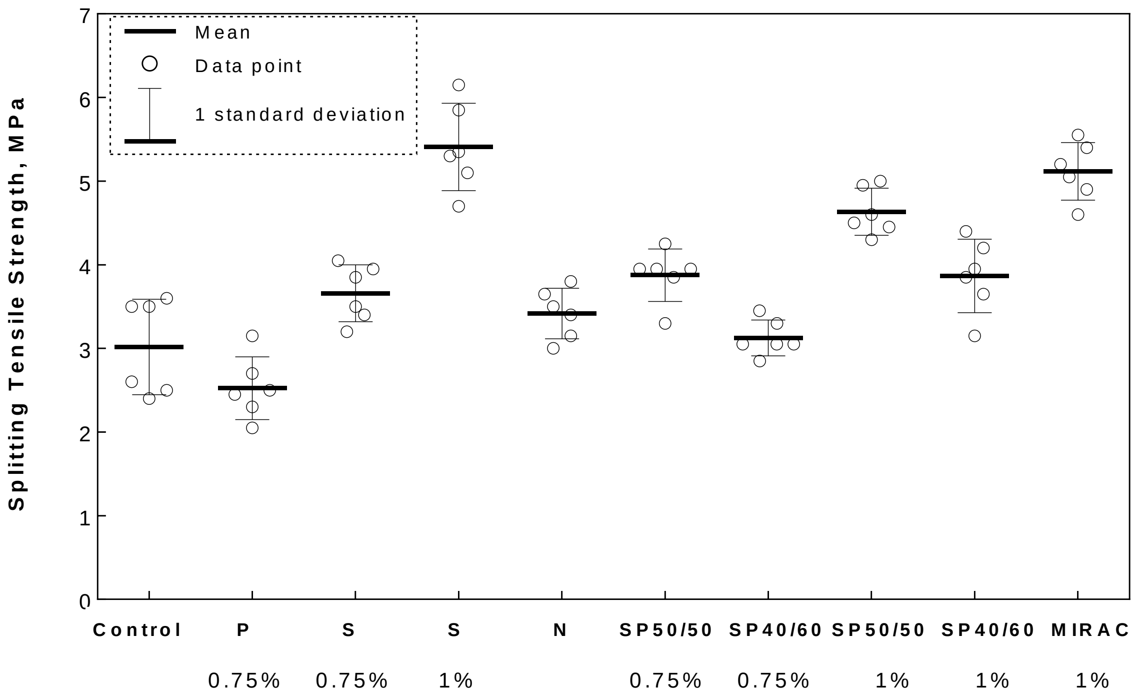

Fig. 6.4 - Splitting tensile strength of 10 test groups of Table 5.1.

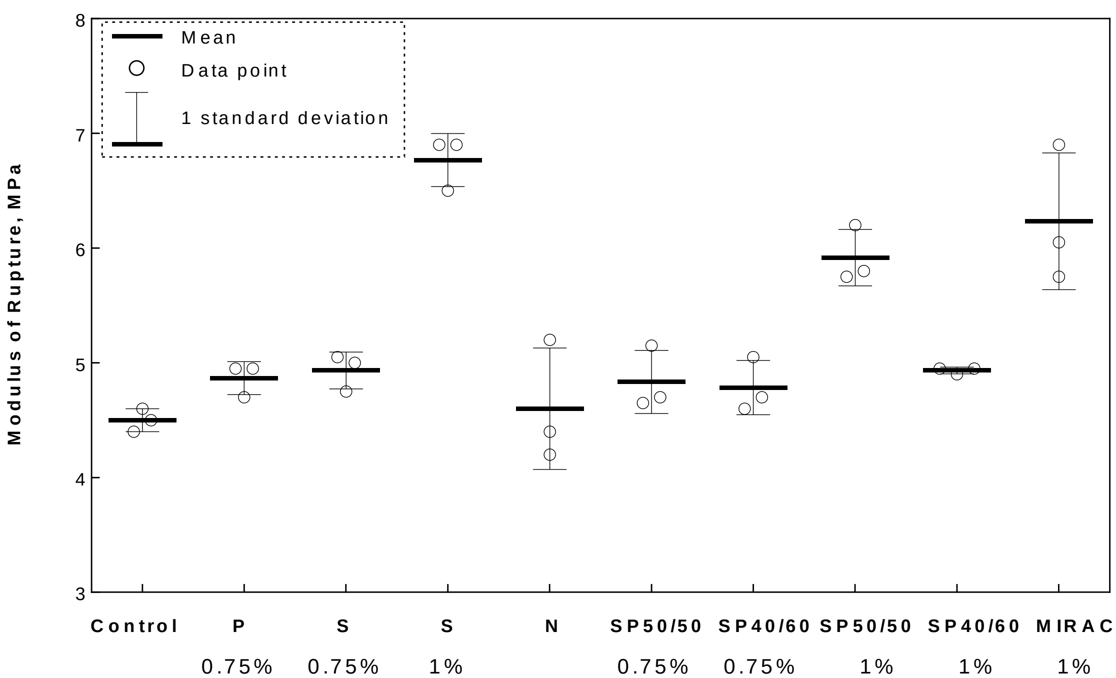

Fig. 6.5 - Modulus of rupture of 10 test groups of Table 5.1.

6.1.3 Load-deflection

For the beam specimens with a fiber volume fraction of 1%, the load versus deflection curve is presented in Fig. 6.6.

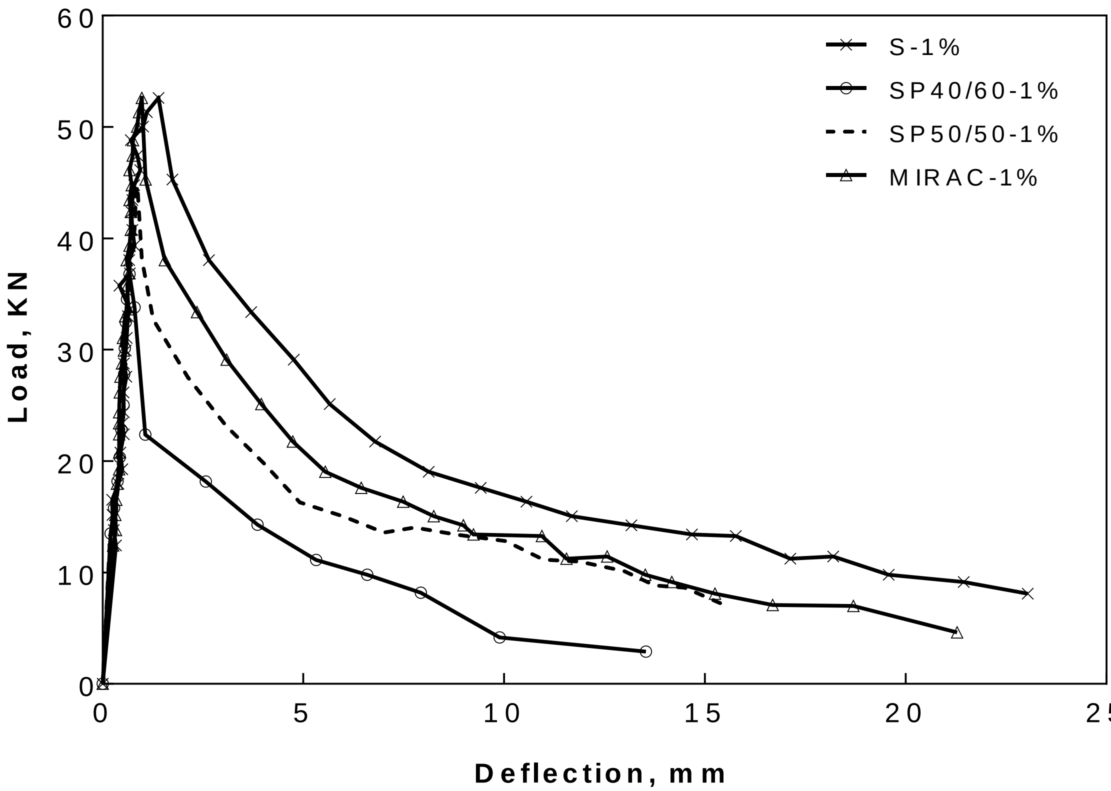

Fig. 6.6 - Load versus deflection response of beam specimens in Table 5.1 with 1% fiber volume fraction.

6.2 Fiber reinforced composites consisting of steel, PVA and CNFs

The results from the experimental program are presented in Figs. 6.7 through 6.11. The bar charts include the mean value of each specimen group, which is indicated by a solid bar, and the standard deviation displayed as two opposing bars with respect to the mean. The test data points are presented with unfilled dots. It is noted that the scatters in the data points are inherent due to the non-uniform distribution of synthetic polypropylene fibers as they are not observed in the Control case and other specimens made with steel fibers used in another study.

6.2.1 Impact test results

It is observed that the mFRC specimens, including the multi-scale fibers (PP, PVA, and CNF), significantly enhance the impact toughness as illustrated in Figs. 6.7 and 6.8.

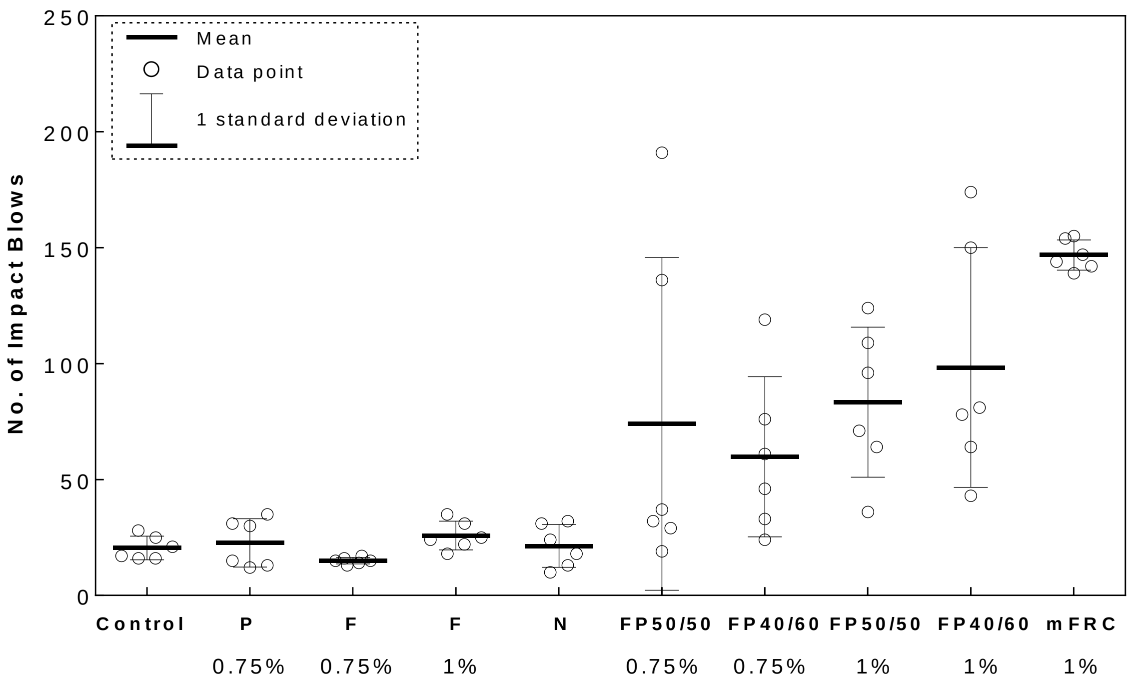

Fig. 6.7 - Impact toughness of 10 test groups of Table 5.2 based on the number of drops to observe the first visible crack.

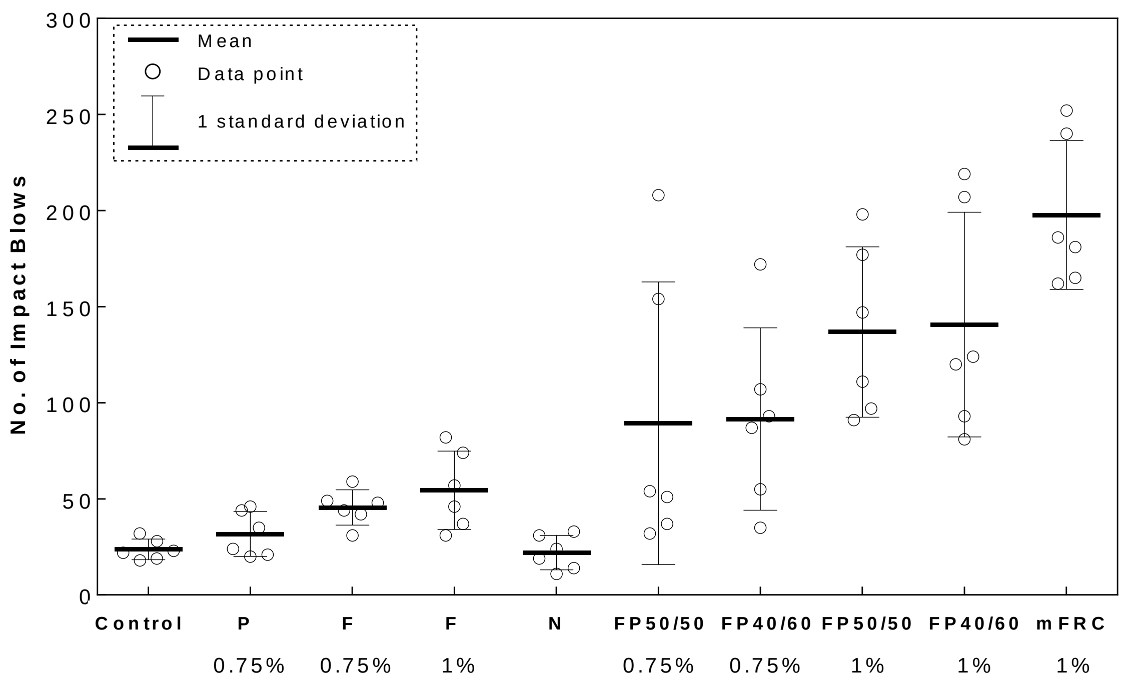

Fig. 6.8 - Impact toughness of 10 test groups of Table 5.2 based on the number of drops to ultimate failure.

6.2.2 Compressive/tensile strength and Modulus of rupture

Figs. 6.9 through 6.11 include the compressive/tensile strength and MOR for 10 sample groups of Table 5.2. The results show that the specimen size (i.e., 100 versus 150mm diameter cylinders) has negligible effect on the compressive and tensile strength. The average compressive strength obtained from the six 150mm diameter cylinders is 33 MPa and 31 MPa for the total volume fractions of 0.75% and 1%, respectively. The average tensile strength is 2.3 MPa and 3.1 MPa for the 0.75% and 1% fiber volume, respectively. These values obtained from the large cylinders are consistent with the values obtained from 100mm diameter cylinders (see Figs. 6.9 and 6.10). Therefore, the 100mm diameter cylinders are used for the other test specimen groups.

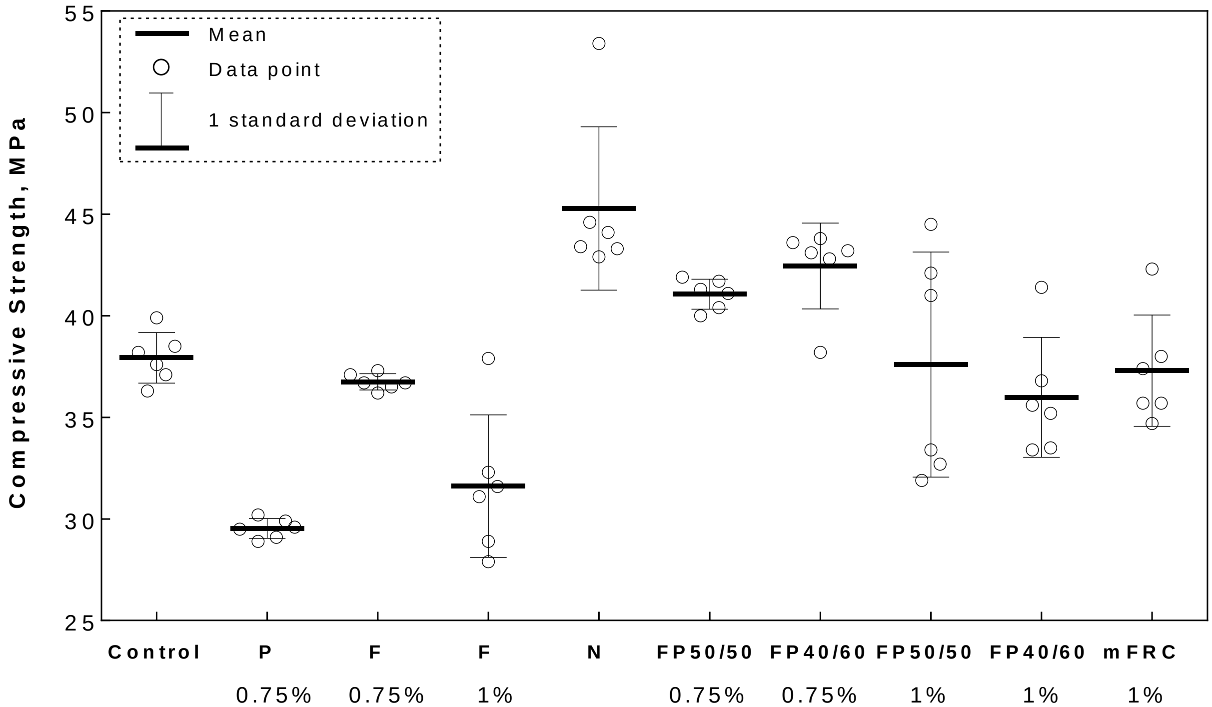

Fig. 6.9 - Compressive strength of 10 test groups of Table 5.2.

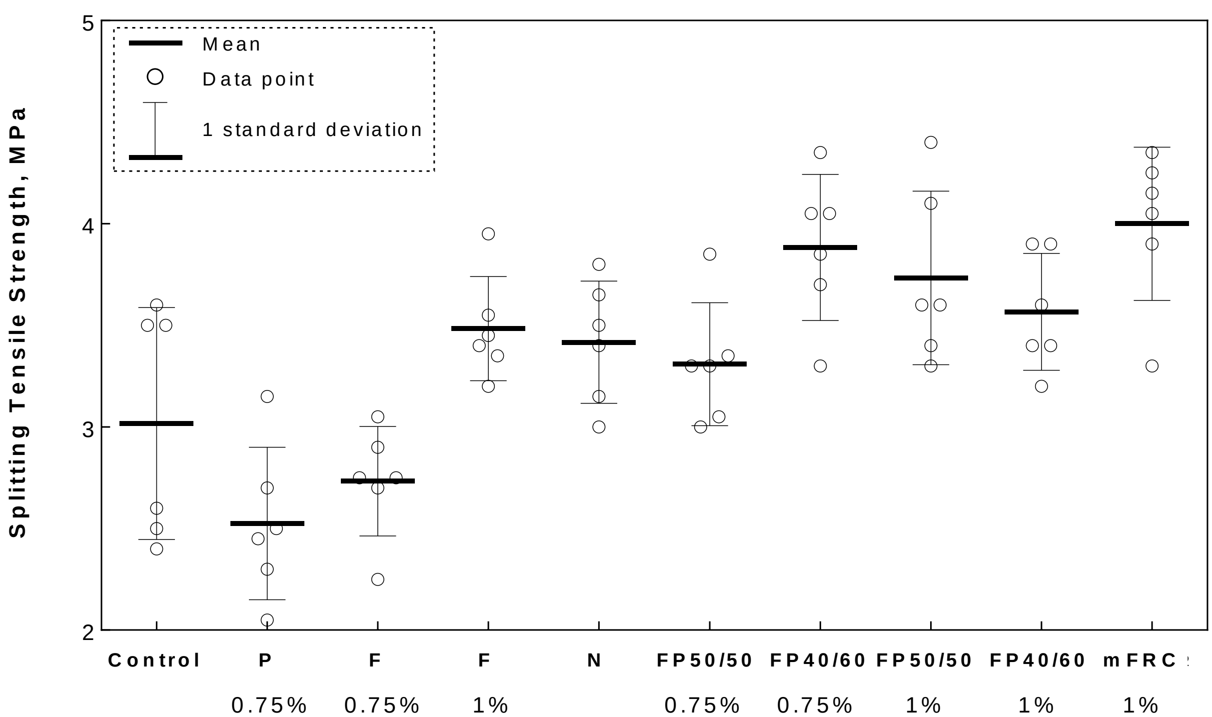

Fig. 6.10 - Splitting tensile strength of 10 test groups of Table 5.2.

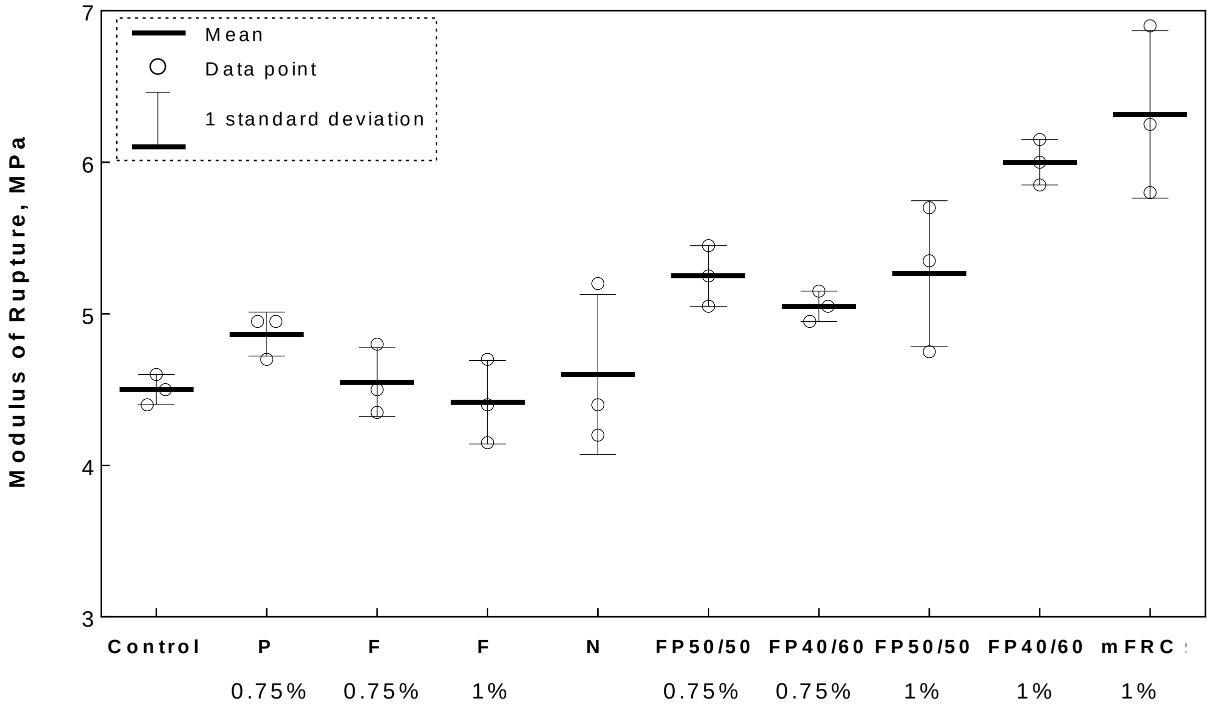

Fig. 6.11 - Modulus of Rupture of 10 test groups of Table 5.2.

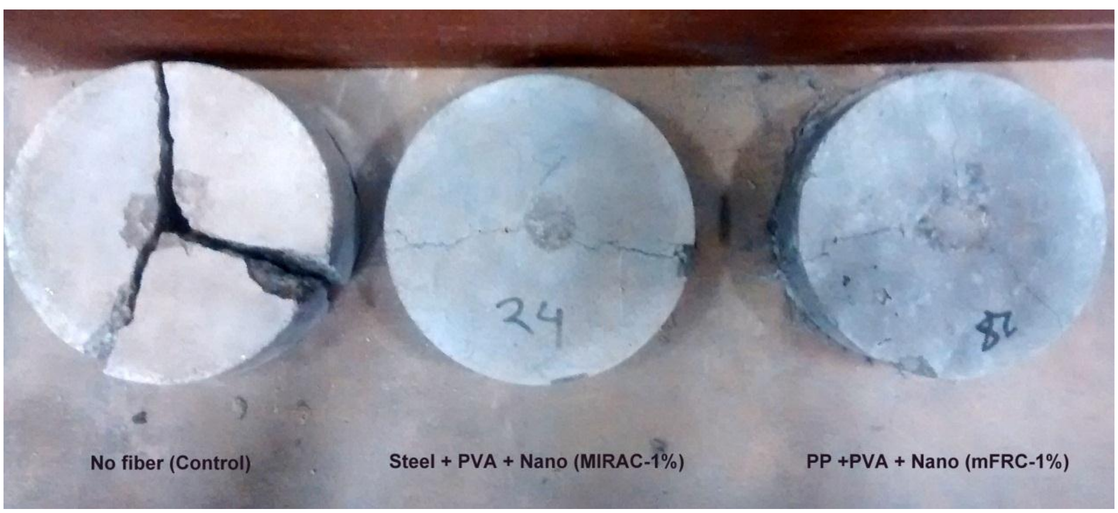

Fig. 6.12 - Impact tested specimens at ultimate failure.

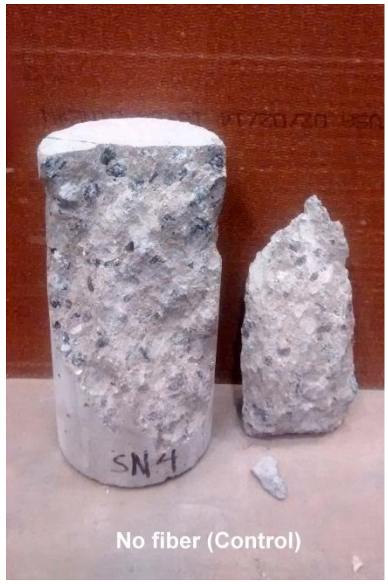

Fig. 6.13 - Compressive strength tested specimens with no fiber addition.

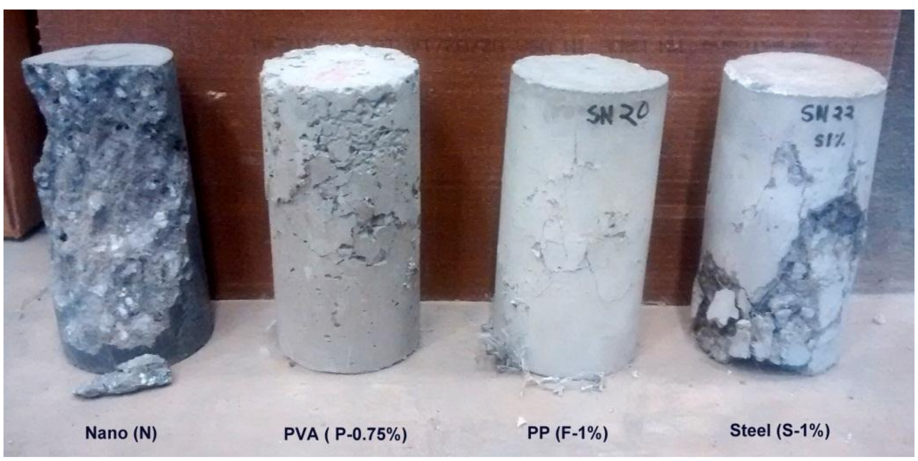

Fig. 6.14 - Compressive strength tested specimens with single fiber reinforcement.

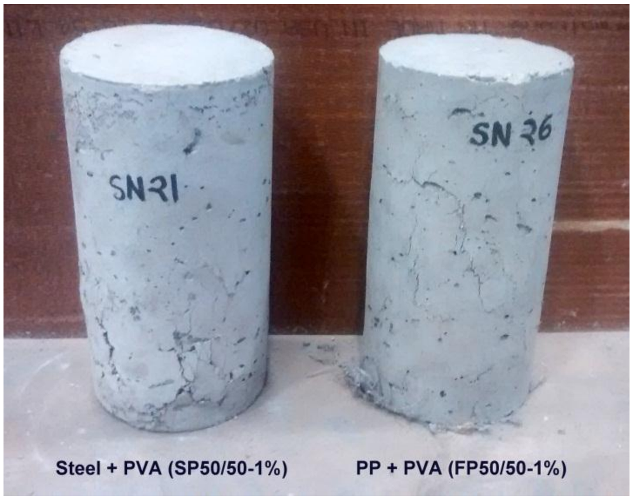

Fig. 6.15 - Compressive strength tested specimens with double fiber reinforcement.

Fig. 6.16 - Compressive strength tested specimens with triple fiber reinforcement.

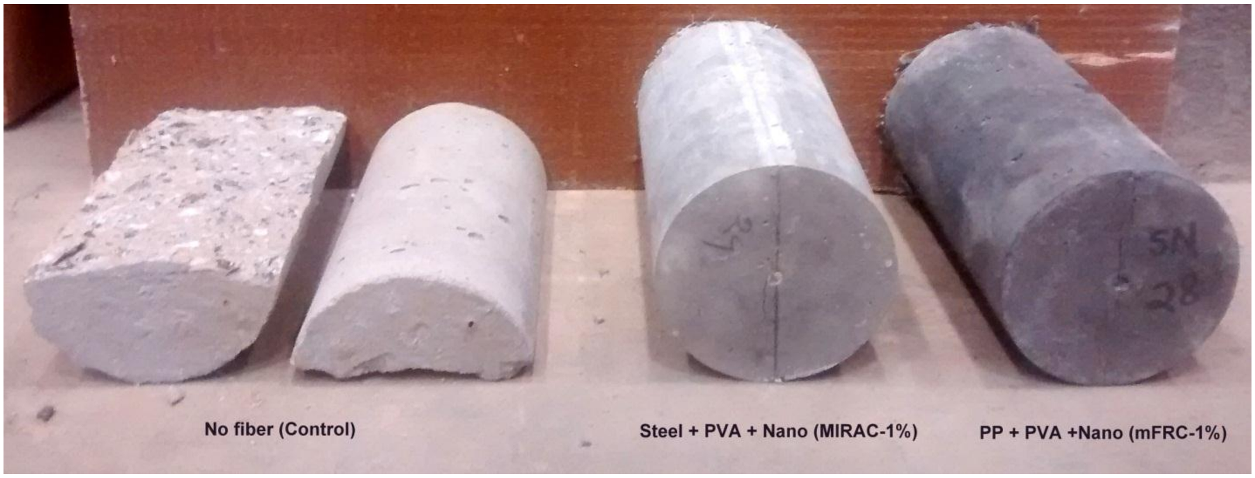

Fig. 6.17 - Splitting tensile strength tested specimens.

Fig. 6.18 - Fracture surface of MIRAC specimen with steel fibers (MIRAC-1% of Table 5.1).

Fig. 6.19 - Fracture surface of MIRAC specimen with PP fibers

(mFRC-1% of Table 5.2).

6.3 Discussion of results from Phase I

6.3.1 Fiber reinforced composites consisting of steel, PVA and CNFs

Table 6.1 presents the percentage improvement or reduction, indicated by positive and negative values, respectively, in mechanical properties and impact toughness over the control group based on the mean values determined from each group.

Table 6.1 - Percentage improvement and reduction over the control mix.

Specimen Designation: Fiber type Mixing ratio -Total fiber volume fraction (%)	Fiber type	Impact-first crack	Impact-ultimate failure	MOR	Tensile Strength	Compressive strength
		(%)	(%)	(%)	(%)	(%)
N	CNF	0	-8	2	14	15
P-0.75%	PVA	10	33	8	-16	-22
S-0.75%	Steel	71	204	9	22	-9
S-1%	Steel	352	688	50	81	29
SP50/50-0.75%	Steel+PVA	119	258	7	30	-12
SP50/50-1%	Steel+PVA	300	646	31	54	-1
SP40/60-0.75%	Steel+PVA	14	88	6	3	-22
SP40/60-1%	Steel+PVA	371	588	9	30	-21
MIRAC-1%	Steel+PVA+CNF	971	1058	38	71	23

6.3.1.1 Cementitious composites reinforced with nano fibers (CNFs)

In comparison with the control specimens, the specimens singly reinforced with CNFs (specimen designation, ‘N’) show improved mechanical properties. There is 15% and 14% improvement in compressive and splitting tensile strength, respectively. Although there is a slight increase (2%) in flexural strength (modulus of rupture), there is no significant advantage of CNFs when it comes to impact toughness. Therefore, cementitious composites reinforced with CNFs exhibit similar brittle behavior when subjected to impact loads.

6.3.1.2 Cementitious composites reinforced with micro fibers (PVA)

Concrete specimens singly reinforced with PVA fibers (0.75% by volume) have a negative effect on the mechanical properties with an exception of the flexural strength. When compared to the control specimen, the compressive and splitting tensile strength is reduced by 22% and 16%, respectively. However, the flexural strength improves by 8% over the control mix. Based on the number of impact blows counted to observe the first visible crack and ultimate failure, the improvement in impact toughness is 10% and 33%, respectively, due to the addition of PVA fibers.

6.3.1.3 Cementitious composites reinforced with macro fibers (steel)

Concrete specimens singly reinforced with the steel fibers (0.75% by volume) improve the impact toughness by 71% (first crack) and 204% (ultimate failure) over the control mix. Similarly, an improvement of 352% (first crack) and 688% (ultimate failure) is observed for specimens reinforced with 1% steel fibers by volume. In case of 0.75% steel addition, the compressive strength decreases by 9% and the tensile strength increases by 22%. When reinforced with 1% steel fibers, compressive and tensile strength increases by 29% and 81%, respectively. Finally, MOR values increase by 9% and 50% for the specimens with the two fibers volume fractions (0.75% and 1%, respectively).

6.3.1.4 Cementitious composites reinforced with macro and micro fibers (steel and PVA)

Steel and PVA fibers are mixed with a volume ratio of (1) 1:1 and (2) 1:1.5, shown as SP50/50 and SP40/60 in Table 5, while maintaining a total fiber volume fraction of 0.75% or 1%. Based on the obtained results, it is evident that cementitious composites including macro and micro fibers with a mixing ratio 1:1 and a total fiber volume fraction of 1% (SP50/50-1%) performs exceptionally well.

When a total fiber volume of 1% is used with the macro/micro fiber mixing ratio of 1:1 (SP50/50-1%), the impact toughness improves by 300% (first crack) and 646% (ultimate failure) relative to the control group. The average compressive strength does not change significantly as compared to the control mix, but the tensile strength increases by 54%. The average MOR value is also increased by 31%.

The cementitious composites reinforced with 0.75% fiber volume fraction show an improvement in toughness by 119% (first crack) and 258% (ultimate failure) over the control specimen, in case of using the macro/micro fiber mixing ratio of 1:1 (SP50/50-0.75%). The compressive strength is decreased by 12% while tensile strength is increased by 30%. The average MOR is also increased by 7%. The increased amount of PVA fibers (by 10% of the total fiber volume) improves the impact toughness by 105% and decreases by 71% for the total volume fraction of 1% and 0.75%, respectively, based on the observation of the first visible crack. However, the compressive/tensile/flexural strength is slightly increased regardless of the fiber volume fraction.

6.3.1.5 Cementitious composites reinforced with multi-scale fibers (steel, PVA, and CNFs)

In case of multi-scale fiber reinforced specimens (MIRAC-1%), the average impact toughness enhances by 971% and 1058% over the control case based on the first observed visible crack and ultimate failure, respectively, noting that the single steel fiber reinforced specimens (S-1%) increase the toughness by 300% (first crack) and 646% (ultimate failure) over the control specimens. The compressive strength is improved by 23% whereas the tensile strength is improved by 71% over the control mix, while the single steel fiber reinforced case improves compressive and tensile strength by 24% and 17%, respectively. A 38% improvement over the control mix is seen in the MOR values, which is 7% higher than steel fiber reinforced specimens (S-1%).

6.3.2 Fiber reinforced composites consisting of PP, PVA and CNFs

Table 6.2 presents the percentage improvement or reduction, indicated by positive and negative values, respectively, in impact toughness and mechanical properties over the Control group based on the mean values determined from each group.

Table 6.2 - Percentage improvement and reduction over the control mix.

Specimen Designation: Fiber type Mixing ratio - Total fiber volume fraction (%)	Fiber type	Impact toughness-first crack (%)	Impact toughness-ultimate failure (%)	MOR (%)	Tensile Strength (%)	Compressive strength (%)
N	CNF	0	-8	2	14	15
P-0.75%	PVA	10	33	8	-16	-22
F-0.75%	PP	-27	92	1	-9	-3
F-1%	PP	26	130	-2	16	-16
FP50/50-0.75%	PP+PVA	261	278	17	10	8
FP50/50-1%	PP+PVA	192	287	12	30	12
FP40/60-0.75%	PP+PVA	306	478	17	25	-1
FP40/60-1%	PP+PVA	380	494	33	20	-5
mFRC-1%	PP+PVA+CNF	616	735	40	33	-2

6.3.2.1 Effect of nano-scale fibers (CNFs)

The specimens singly reinforced with CNFs provide slightly improved mechanical properties in comparison with the Control group. The compressive and splitting tensile strength is improved by 15% and 14%, respectively. However, the nano-scale fibers provide no improvement in impact toughness. Therefore, engineered cementitious composites (ECCs) singly reinforced with CNFs exhibit similar brittle behavior observed in conventional unreinforced or plain concrete members when subjected to impact loads.

6.3.2.2 Effect of micro-scale fibers (PVA)

Concrete specimens singly reinforced with PVA fibers have an adverse effect on the mechanical properties although the flexural strength slightly increases. The compressive and splitting tensile strength is decreased by 22% and 16%, respectively, with respect to the Control case. The addition of PVA fibers improves the impact toughness by 10% and 33% based on the number of impact blows counted to observe the first visible crack and ultimate failure, respectively.

6.3.2.3 Effect of macro-scale fibers (Polypropylene)

FRC specimens singly reinforced with macro-scale polypropylene fibers (0.75% by volume) improve the impact toughness by 33% (ultimate failure) over the Control mix. However, the first crack is observed relatively earlier than the Control case. An improvement of 26% (first crack) and 130% (ultimate failure) is observed when the total fiber volume fraction is increased from 0.75% to 1%. In case of 0.75% polypropylene fiber addition, the compressive and tensile strength decreases by 3% and 9%, respectively. When more polypropylene fibers (0.25% by volume) are provided, the compressive strength is reduced by 16% whereas the tensile strength increases by 16% with respect to the Control case. Regardless of the two fiber volume fractions (0.75% and 1%), the average MOR values do not improve.

6.3.2.4 Effect of combined macro and micro fibers (Polypropylene and PVA)

As expected, FRC specimens including both macro and micro fibers improve the impact toughness as well as mechanical properties. Polypropylene and PVA fibers are mixed with a volume ratio of (1) 1:1 and (2) 1:1.5, designated as FP50/50 and FP40/60 in Table 5, while maintaining a total fiber volume fraction of 0.75% or 1%. It is noted that FRC composites including macro-scale polypropylene and micro-scale polyvinyl alcohol fibers with a mixing ratio 1:1.5 and a total fiber volume fraction of 1% (FP40/60-1%) perform exceptionally well relative to FP50/50-1%. On the contrary, the 10% increase in PVA fibers (FP40/60-1%) significantly reduces the workability of the concrete batch resulting in a slump of less than 25 mm. Although the slump may not be a good indicator of workability for FRC (ACI 544.2R 2009), the authors find it difficult to work with the batch. Therefore, a mixing ratio of 1:1 (FP50/50-1%) is selected to add CNFs for the multi-scale fiber reinforced concrete (mFRC) specimens yielding a slump of 40mm.

When a total fiber volume of 1% is used with the macro/micro fiber mixing ratio of 1:1 (FP50/50-1%), the impact toughness improves by 261% (first crack) and 278% (ultimate failure) relative to the Control group. The average compressive and tensile strength increases by 8 and 10%, respectively, over the Control mix. The average MOR value is also increased by 17%.

The increased amount of PVA fibers (10% by volume) improves the impact toughness by a factor of 2 (or 200%) based on the ultimate failure although the compressive strength is slightly reduced (see FP50/50-1% versus FP40/60-1%). The increased amount of the total fiber fraction (25% by volume) slightly increases the impact toughness by about 10% (see FP50/50-0.75% versus FP50/50-1%).

6.3.2.5 Effect of multi-scale fibers (PP, PVA, and CNFs)

The multi-scale (macro, micro, and nano) fiber reinforced specimens (mFRC-1%) include macro-scale polypropylene and micro-scale PVA fibers with a volume ratio of 1:1 (FP50/50-1%) and nano-scale CNFs by 1% cement binder weight. The mFRC specimens improve the average impact toughness by 616% and 735% over the Control group based on the first observed visible crack and ultimate failure, respectively. The ultimate impact resilience of ECCs can more than double by uniformly mixing a small amount (1% by cementitious binder weight) of carbon nanofibers in the macro and micro-scale fiber reinforced specimens (FP50/50-1%). The compressive strength is not improved by the multi-scale fiber reinforcement whereas the tensile strength is improved by 33% over the Control mix. A 40% improvement over the Control mix is seen in the MOR value.

6.4 Statistical analysis of impact results from Phase I

6.4.1 Fiber reinforced composites consisting of steel, PVA and CNFs

In this section, the effect of adding CNFs on the impact toughness of cementitious composites reinforced with steel/PVA fibers is studied by using the one-way analysis of variance technique (Christensen 1996). This method presents the test results in terms of confidence intervals. When another specimen is tested, it is likely to observe the first visible crack and ultimate failure when the impact drop number reaches between the intervals shown in Fig. 6.20. If so, the test results are statistically significant at the 95% confidence level.

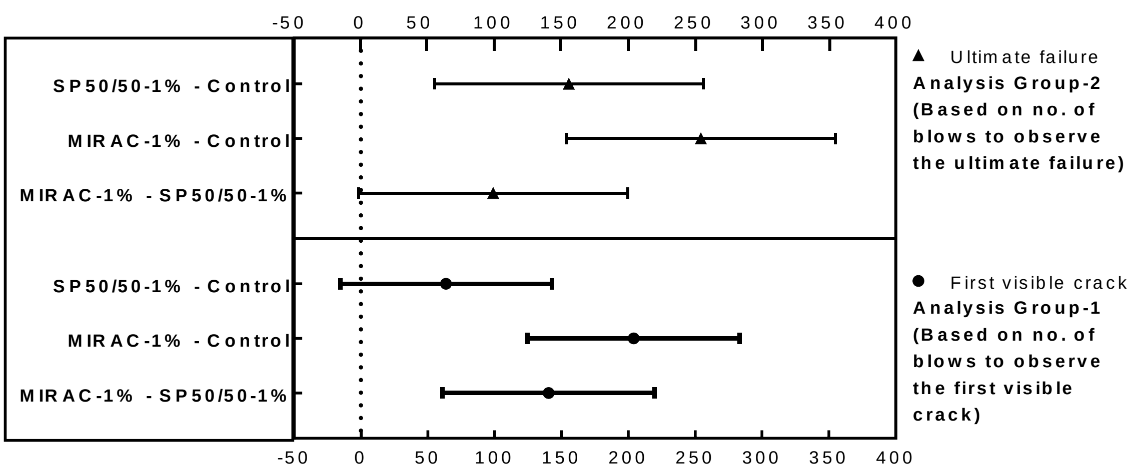

Fig. 6.20 - Analysis of impact test results - group means at 95% confidence interval.

Based on the number of blows counted to observe the first visible crack, Fig. 6.20 presents the mean difference produced by a statistical analysis of the impact test data obtained from Analysis Group 1 (Fig. 6.20). Reading the figure from the bottom up, the mean difference between MIRAC-1%and SP50/50-1% specimens is 140 impact drops and is depicted by the solid dot in the figure. At the 95% confidence interval, it can be said that the impact toughness is improved by 61 to 219 drops by adding CNFs to the macro/micro fiber reinforced composites. The mean difference between the MIRAC-1% and Control specimens is 204 weight drops, and impact toughness of MIRAC-1% is improved by 125 to 283 drops relative to the Control case. Finally, the mean difference between SP50/50-1% and Control case is 64 drops, and at the 95% confidence interval, it can be said that the toughness of concrete is increased by 142 drops by adding macro/micro fibers (SP50/50-1%) but it could also slightly reduce the toughness by 15 drops. Similar analysis can be performed based on the number of drops counted to observe the ultimate failure (see Analysis Group 2 in Fig. 6.20).

6.4.2 Fiber reinforced composites consisting of PP, PVA and CNFs

The effect of adding CNFs on the impact toughness of ECCs reinforced with PP and PVA fibers is analyzed by using the one-way analysis of variance technique (Christensen 1996). This method presents the test results in terms of confidence intervals. When another specimen is tested, the impact drop number is likely to range between the intervals to observe the first visible crack (Analysis Group 1) and ultimate failure (Analysis Group 2) as shown in Fig. 6.21. If the test data falls within the intervals, it is statistically significant at the 95% confidence level.

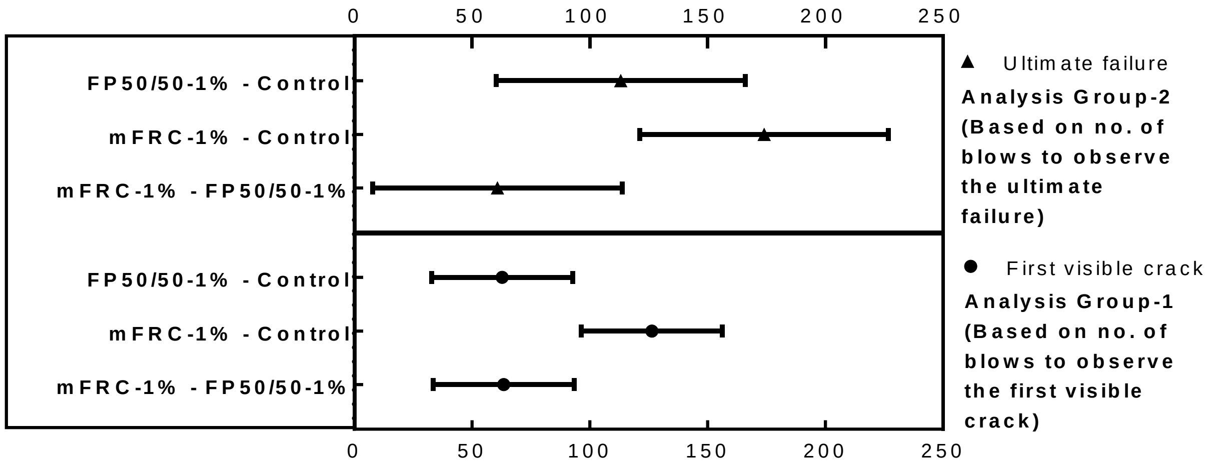

Fig. 6.21 - Analysis of impact test results - group means at 95% confidence interval.

Reading the figure (Fig. 6.21) from the bottom up, the mean difference between mFRC-1% and FP50/50-1% specimens in Analysis Group 1 is 140 impact drops and is depicted by the solid dot in the figure. At the 95% confidence interval, it can be said that the impact toughness is improved by 34 to 93 drops by adding CNFs to the macro/micro-scale fiber reinforced composites. The mean difference between the mFRC-1% and Control specimens is 126 weight drops, and the impact toughness of mFRC-1% is improved by 96 to 156 drops relative to the Control case. Finally, the mean difference between FP50/50-1% and Control case is 62 drops. At the 95% confidence interval, it can be said that the toughness of concrete is increased by 33 to 93 drops by adding macro/micro-scale fibers (FP50/50-1%). Similar statistical analysis can be made based on the number of drops counted to observe the ultimate failure (see Analysis Group 2 in Fig. 6.21).

CHAPTER 7

EXPERIMENTAL PROGRAM: PHASE II

This chapter includes the Phase-II experimental program. This phase aims to meet Objective 3, which is to design and develop a large-scale impact test to study the performance of composite RC beams, and study the performance of MIRAC beams by conducting dynamic and static beam tests. The following sections present specimen preparation, drop weight test setup, and test procedures of these two tests.

7.1 Impact tests

7.1.1 Specimen Preparation

Fifteen fiber reinforced concrete beams are constructed for the impact test, and three fiber reinforced concrete beams are made for static tests. All the specimens have a length of 7’ 6” (2286 mm), width of 6” (152.4 mm) and height of 10” (254 mm). All specimens are provided with a reinforcing ratio of 0.0081. Two bottom longitudinal bars are made using US standard #4 bars with a 0.20 in^2 (129 mm^2) area and a nominal diameter of ½ in. (12.7 mm). Two top longitudinal bars are made using US standard #3 bars with a 0.11 in^2 (71 mm^2) area and a nominal diameter of 0.375 in. (9.525 mm). Closed stirrups are made using US standard #2 bars with a 0.05 in^2 (32 mm^2) area and a nominal diameter of 0.25 in. (6.35 mm) and spaced at 4” (101.6 mm) on center such that the beam would not fail in shear. The ultimate tensile strength of the reinforcing bars is 60,000 psi (413 MPa) and the elastic modulus is 29×10^6 psi (200 GPa). A clear cover of 1.25” (31.75 mm) is provided at the top and bottom face, and 1” (25.4 mm) cover is used for the sides.

Fig. 7.1 and Fig. 7.2 show the longitudinal and cross sections of the beam specimens, respectively.

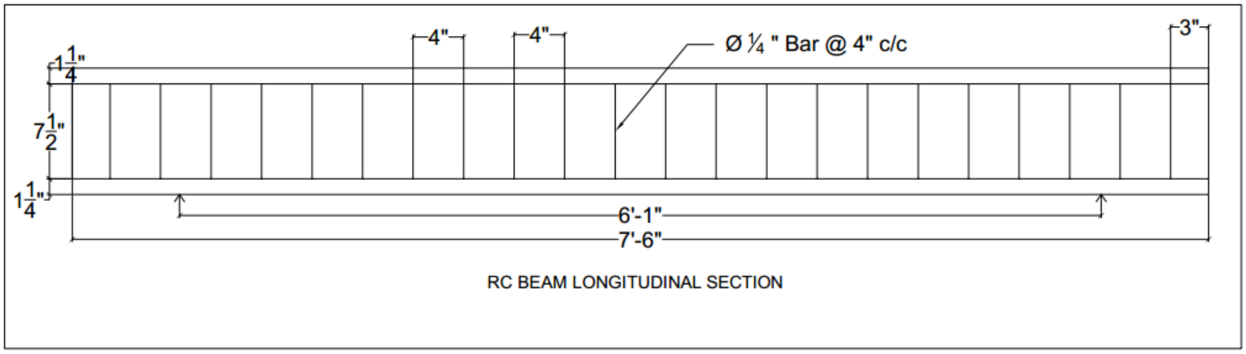

Fig. 7.1 - Longitudinal section of the test specimens

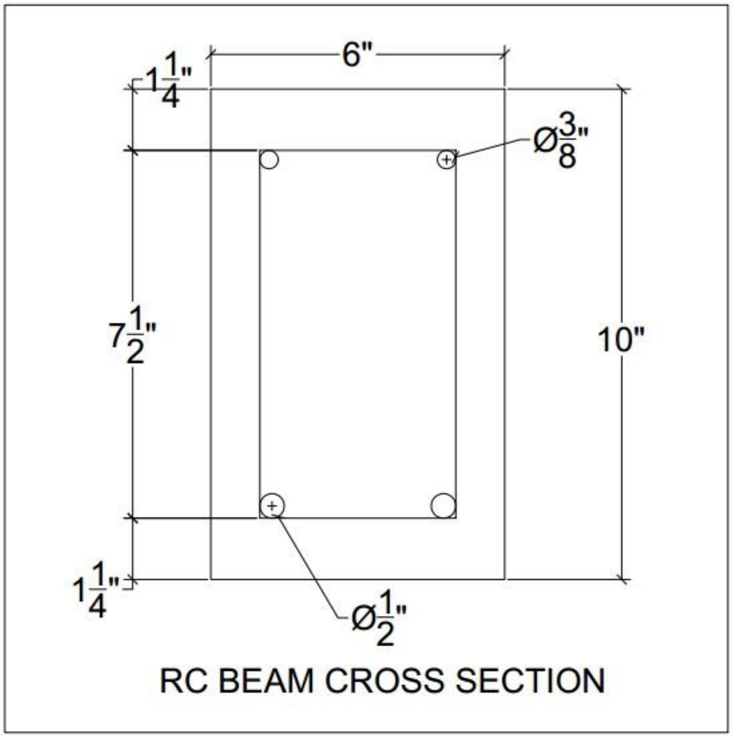

Fig. 7.2 - Cross section of the test specimens

Tables 7.1 and Table 7.2 summarize fiber volume fractions of the beam specimens in the two Groups (A and B).

Table 7.1 - Summary of FRC beam specimens for large-scale impact study (Test Group A)

Specimen Designation	Fiber type (Fiber mixing ratio %) - total fiber volume	Total Fiber Vol. (%)	Fiber vol. fraction (%)				Fiber mixture scale	Drop weight (lbs)	Compressive strength (psi/MPa)
			PP	Steel	PVA	Nano			
Control	Control (n/a)-0	0	0	0	0	0	No Fiber	500	6720/46.3
S	Steel (100)-0.75	0.75	0	0.75	0	0	Single Macro	500	7490/51.6
N-300	Nano(n/a)	n/a	0	0	0	1	Single Nano	300	7120/49.1
N	Nano(n/a)	n/a	0	0	0	1	Single Nano	500	6100/42.1
SP50/50-350	Steel/PVA(50/50) -1%	1	0	0.5	0.5	0	Macro + Micro	350	6510/44.9
SP50/50	Steel/PVA(50/50) -1%	1	0	0.5	0.5	0	Macro + Micro	500	6770/46.7
sMIRAC-400 lbs	Steel/PVA(50/50) - 1.0 +Nano(n/a)1 %wt	1	0	0.5	0.5	1	Macro + Micro + Nano	400	
sMIRAC -500 lbs	Steel/PVA(50/50) - 1.0 +Nano(n/a)1 %wt	1	0	0.5	0.5	1	Macro + Micro + Nano	500	6510/44.9

Table 7.2 - Summary of FRC beam specimens for large-scale impact study (Test Group B)

Specimen Designation	Fiber type (Fiber mixing ratio %) - total fiber volume	Total Fiber Vol. (%)	Fiber vol. fraction (%)				Fiber mixture scale	Drop weight (lbs)	Compressive strength (psi/MPa)
			PP	Steel	PVA	Nano			
Control	Control (n/a)-0	0	0	0	0	0	No Fiber	500	6720/46.3
F	PP (100)-1.0	1	1	0	0	0	Single Macro	500	6080/41.9
N-300	Nano(n/a)	n/a	0	0	0	1	Single Nano	300	7120/49.1
N	Nano(n/a)	n/a	0	0	0	1	Single Nano	500	6100/42.1
FP50/50	PP/PVA(50/50)-1.0	1	0.5	0	0.5	0	Macro + Micro	500	6900/47.6
pMIRAC-400	PP/PVA(50/50)-1.0 +Nano(n/a)1%wt	1	0.5	0	0.5	1	Macro + Micro + Nano	400	5620/38.7
pMIRAC	PP/PVA(50/50)-1.0 +Nano(n/a)1%wt	1	0.5	0	0.5	1	Macro + Micro + Nano	500	5290/36.5

7.1.2 Test Setup

All reinforced concrete beam specimens are tested under simply supported conditions with a clear span of 73" (1854 mm). The vertical (upward) movement of the supports is prevented by providing Styrofoam and 2" thick lumber layers and tying down the beam specimen with threaded rods as shown in Fig. 7.3, in order to allow rotations at the supports. The beams are supported by simple support system which allowed the beams to rotate freely at the support location. The floor beams are bolted to the strong floor in order to transfer the reactions.

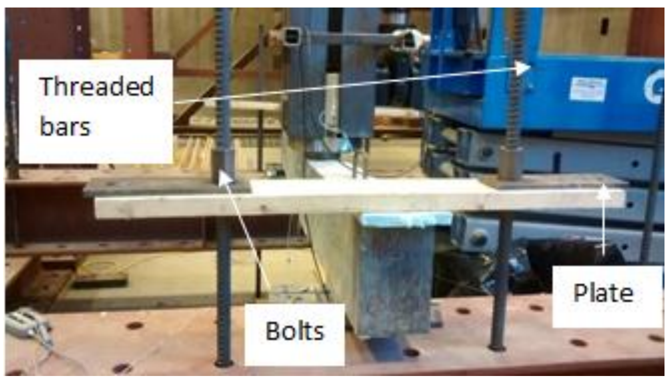

Fig. 7.3 - Impact testing setup with uplift prevention

A well instrumented impact testing setup is constructed at the Instrument Design & Fabrication Shop, UGA. Fig. 7.4 shows the cross section of the guide frame of drop weights and Fig. 7.5 shows an elevation view of the guide frame setup. Fig. 7.6 shows the solid steel impactor or drop weight used to conduct the impact test.

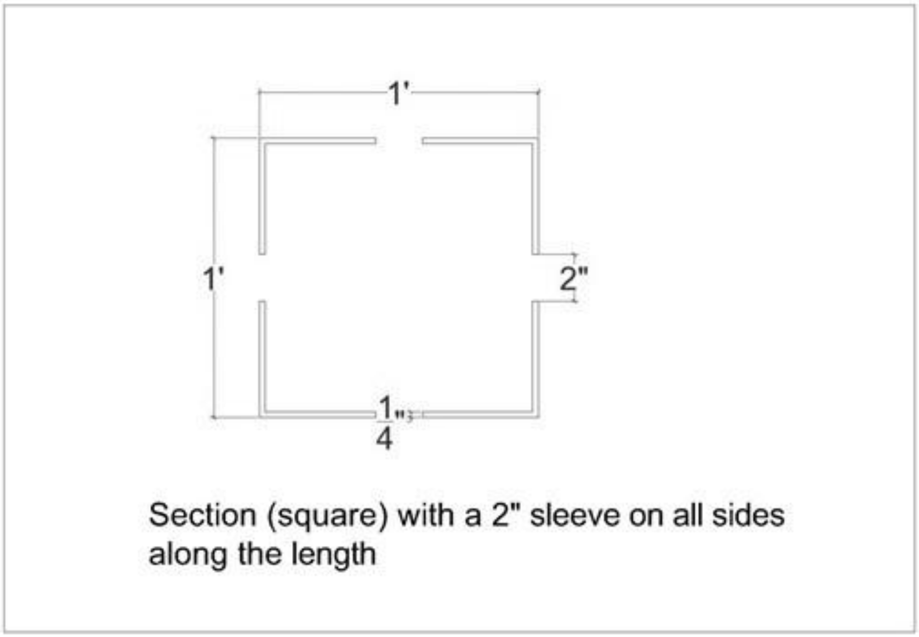

Fig. 7.4 - Cross section of the guide frame for drop weights

Fig. 7.5 - Elevation view of the guide frame for drop weights

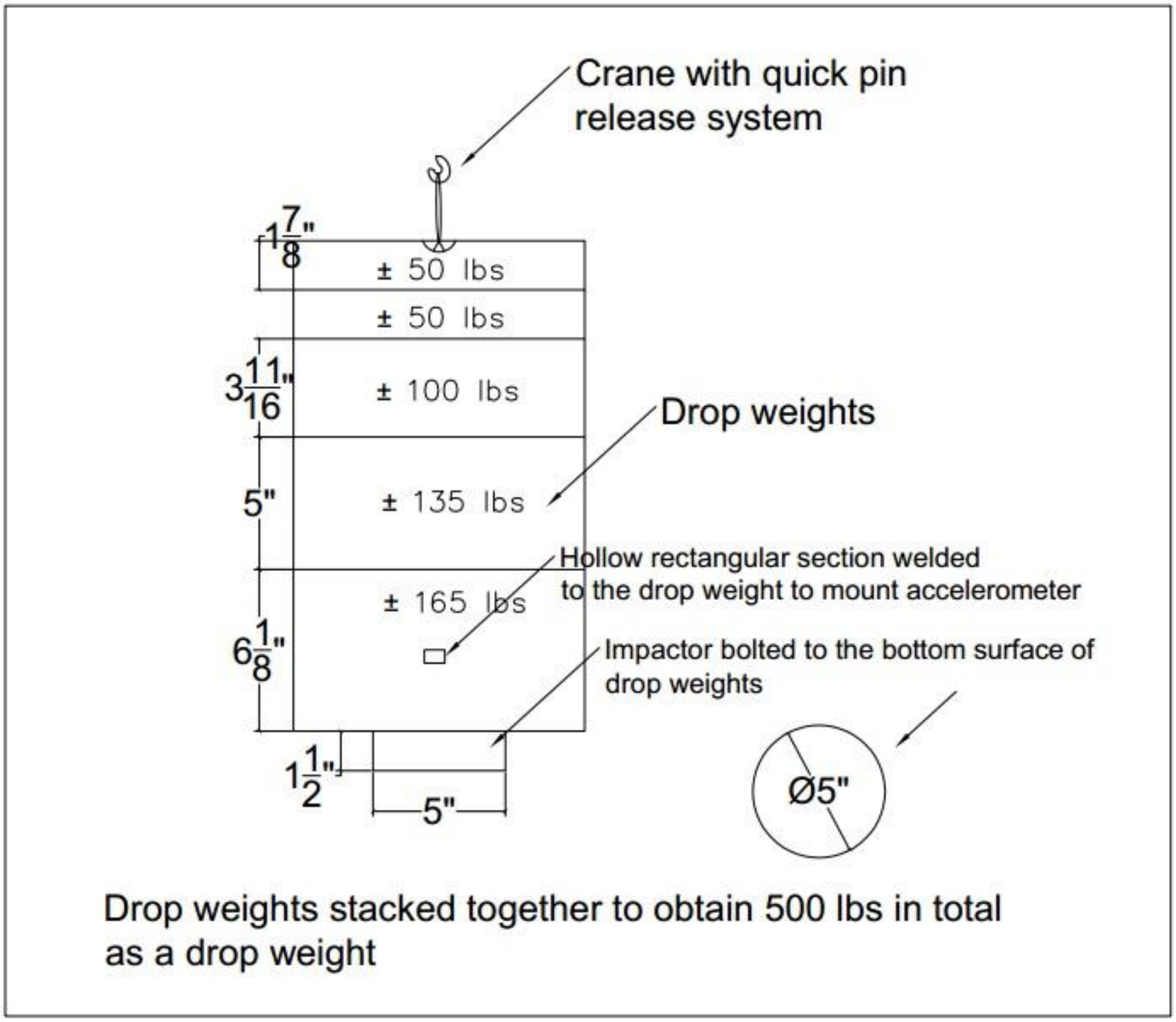

Fig. 7.6 - Drop weights stacked together to obtain a total weight of 500lbs.

7.1.3 Test Procedure

A drop weight impact test setup just before releasing of the solid steel impactor is shown in Fig. 7.7.

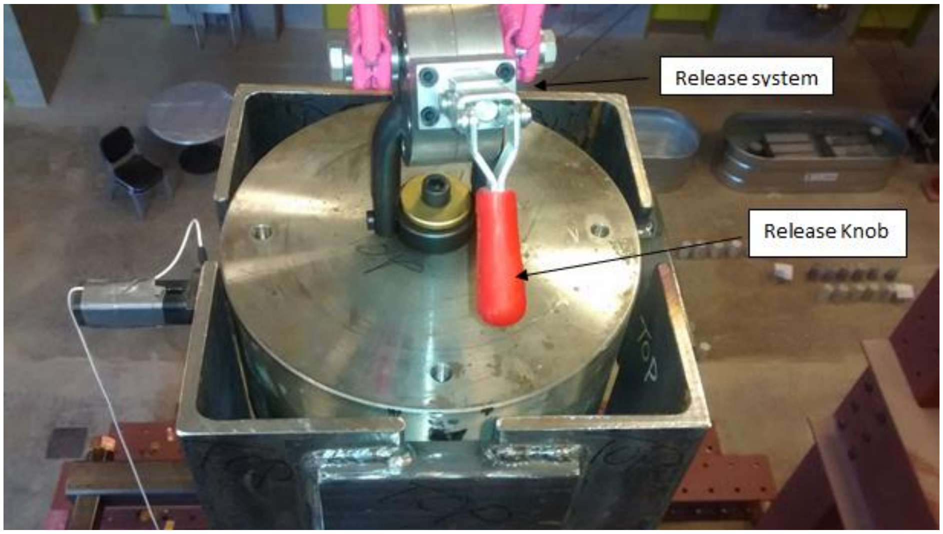

Fig. 7.7 - Drop weight before release.

For each test, the beam displacement-time data is collected using a research-grade motion capture system NDI Optotrak Certus HD, which is typically used for tracking and analyzing kinetics and dynamic motion in real-time (shown in Fig. 7.8), and a string potentiometer (position sensor) is used as a backup measurement system and is shown in Fig. 7.9.

Fig. 7.8 - Motion capture system

Fig. 7.9 - String potentiometer.

The data collected from these two sources are also compared to validate the recorded data. The string potentiometer is mainly used to obtain the deflection at midspan. Due to the high sampling rate (20,000 Hz) used for the potentiometer, more data points per second are recorded. On the other hand, the motion capture system used for the impact tests provides the deflection data for three glued marker locations at 600 Hz.

The drop weight is equipped with an accelerometer [Fig. 7.10] with a measurement range of ± 5000g pk (± 49000 m/s2). The acceleration-time data is collected during the entire test period. The accelerometer is mounted to the drop weight as shown in Fig. 7.11 and is used to get the impact load-time history.

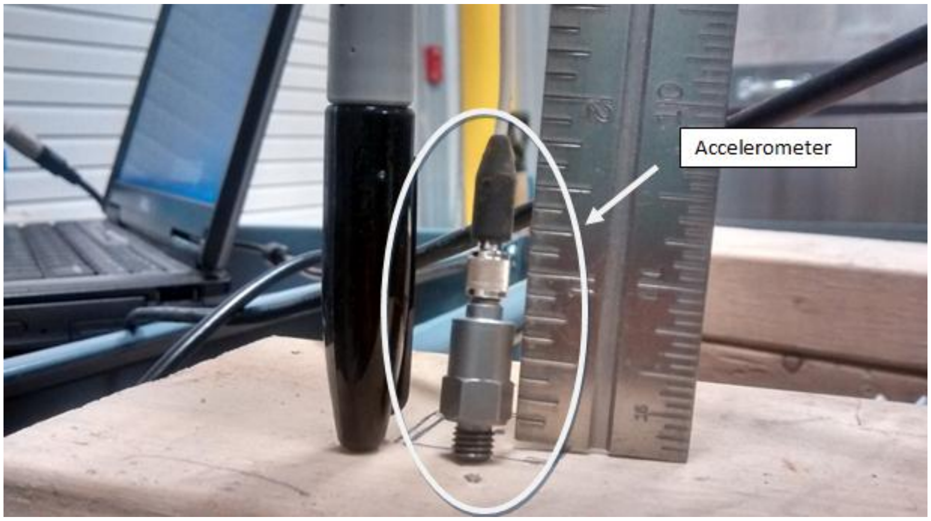

Fig. 7.10 - Accelerometer

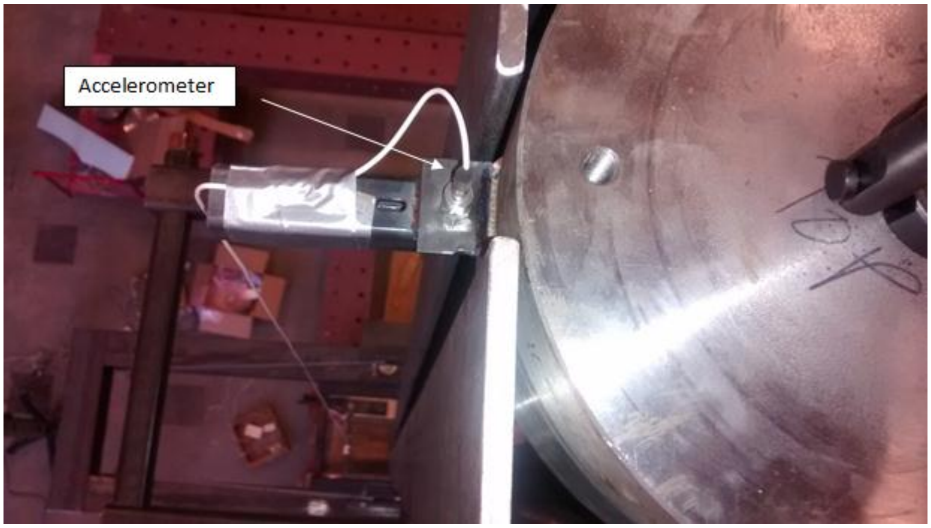

Fig. 7.11 - Mounting configuration of an accelerometer

7.1.4 Data collection

From each drop-weight impact test, two different types of data are collected:

1) Acceleration-time history: An accelerometer is mounted on the drop-weight [Fig. 7.11] while another accelerometer is mounted on the top surface of the beam as shown in Fig. 7.12.

Fig. 7.12 - Position of accelerometer mounted on the top surface of beam.

2) Deflection-time history: The beam deflection is measured using two different methods to ensure that the accurate data is obtained. These two sensors are:

    a. String potentiometer: A string potentiometer is mounted at the midspan of the beam (back face)

    b. Motion capture system: A research capacity motion capture system is used to capture the beam deflection (front face). For each impact test, three sensors are glued to the beam. The arrangement of the three sensors is presented in Fig. 7.13.

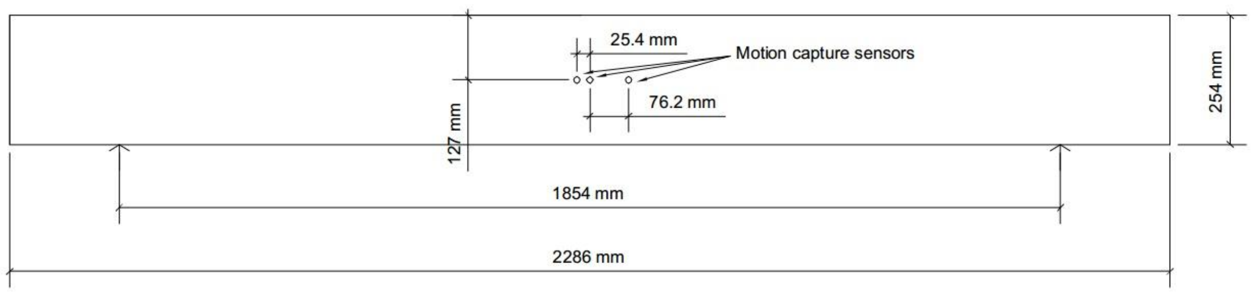

Fig. 7.13 - Location of motion capture sensors/markers

7.2 Static Tests

Three point bending tests are conducted on 3 different fiber reinforced RC beams which are presented in Table 3. The procedures presented in Section 7.1 are used to make the beams.

Table 7.3 - Summary of FRC beam specimens for three-point flexural test.

Specimen Designation	Fiber type (Fiber mixing ratio %) - total fiber volume	Total Fiber Vol. (%)	Fiber vol. fraction (%)				Fiber mixture scale
			PP	Steel	PVA	Nano	
Control	Control (n/a)-0	0	0	0	0	0	No Fiber
SP50/50	Steel/PVA(50/50)-1%	1	0	0.5	0.5	0	Macro + Micro
FP50/50	PP/PVA(50/50)-1.0	1	0.5	0	0.5	0	Macro + Micro

7.2.1 Test setup

Fig. 7.14 shows a three point bending test setup. This test was performed using a hydraulic cylinder and a hydraulic manual pump [Fig. 20]. A load cell is used between the hydraulic cylinder and the RC beam to record the load applied on the beam [Fig. 20]. Similar to the impact tests, a motion capture system and a string potentiometer are used to record the mid-span deflection.

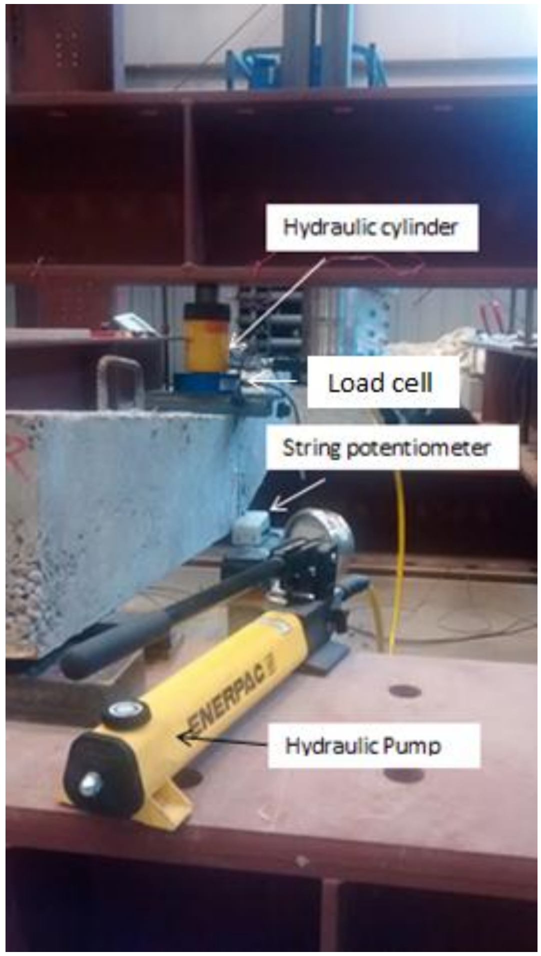

Fig. 7.14 - Three point bending setup.

7.2.2 Test procedure

A manually operated hydraulic pump and a hydraulic cylinder are used to apply load on the beam. The mid-span deflection is recorded using the motion capture system as well as the string potentiometer. Applied load on the beam is measured using a load cell and a data acquisition system.

CHAPTER 8

RESULTS FROM PHASE-II EXPERIMENT

Results from large scale drop weight impact tests and three-point flexural static tests are presented in the following sections.

8.1 Results from static beam tests

The midspan load versus deflection curves obtained from the static beam tests are shown in Fig. 8.1. The Average compressive strength of the specimens, static energy dissipation capacities and linear stiffness are tabulated in Table 8.1. Fig 8.2 shows deflected shapes and crack profiles of the specimens tested under a three-point loading static test. All specimens exhibited a ductile flexural response except the Control beam. In case of the Control beam ductile flexural response was accompanied by crushing of concrete at the load point. As the loads on the beam were approaching the failure load, the steel reinforcement yielded and the concrete failed in compression (crushed).

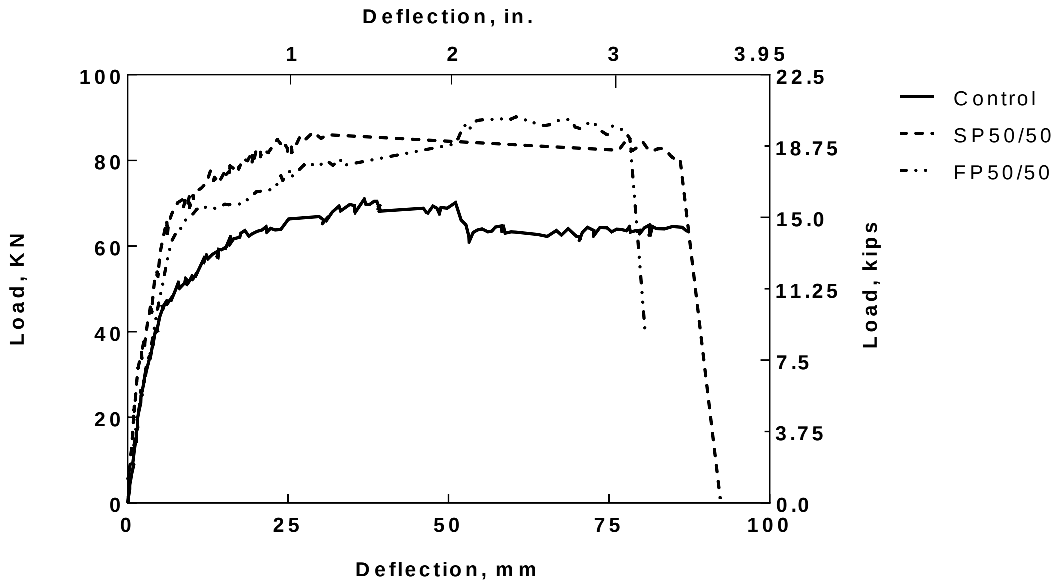

Fig. 8.1 - Load versus deflection curves of beam specimens (of Table 7.3).

Table 8.1 - Static capacities of static test beams.

Specimen Designation	Fiber type (Fiber mixing ratio %) - total fiber volume	Compressive strength, f'c, psi (MPa)	Static energy dissipation capacity, KN-mm	Linear stiffnes, N/m
Control	Control (n/a)-0	7360 (50.7)	5392	11219000
SP50/50	Steel/PVA(50/50)-1%	6240 (43)	7052	2.22E+07
FP50/50	PP/PVA(50/50)-1.0	6770 (46.7)	6160	11219000

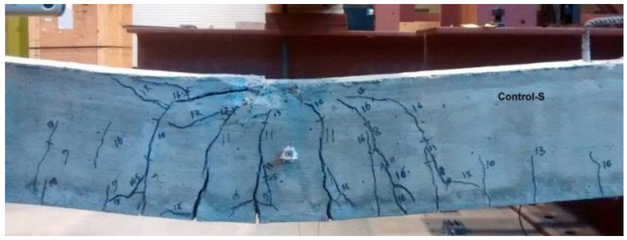

a) Control

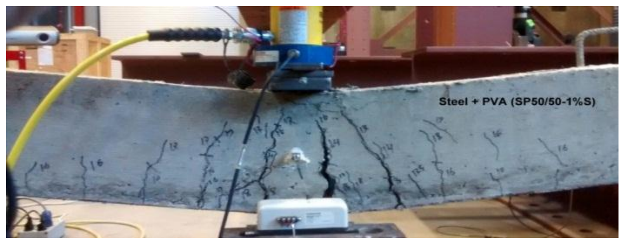

b) SP50/50

c) FP50/50

Fig. 8.2 - Crack profiles and deflected shapes of static test specimens after test.

8.2 Predicted impact weight determined from the static beam test

The impact weight is selected based on the linear stiffness obtained from the static test. The simplified spring-mass model presented in Section 2.4.1 is used to predict the impact force and mid-span displacement for a 227kg (500lb) impactor as shown in Table 8.2. See Appendix A.4 for detailed calculations.

Table 8.2 –Predicted mid-span deflection and impact force

Specimen Designation	Predicted displacement, mm	Predicted Force, N
Control	115.0	551339
SP50/50	161.5	774796
FP50/50	161.3	551339

8.3 Results from Test Group A

The summary of failure modes are presented in Table 8.3 and Figure 8.3.

Table 8.3 –Failure modes of Test Group A

Beam Designation	Failure mode
Control – 500 lbs	Local crushing at contact surface
S – 500 lbs	Flexural, Shear
N-300 lbs	Local crushing at contact surface
N-500 lbs	Local crushing at contact surface
SP50/50-350lbs	Flexural, Shear
SP50/50-500lbs	Flexural, Shear
sMIRAC-400 lbs	To be tested
sMIRAC-500 lbs	Flexural

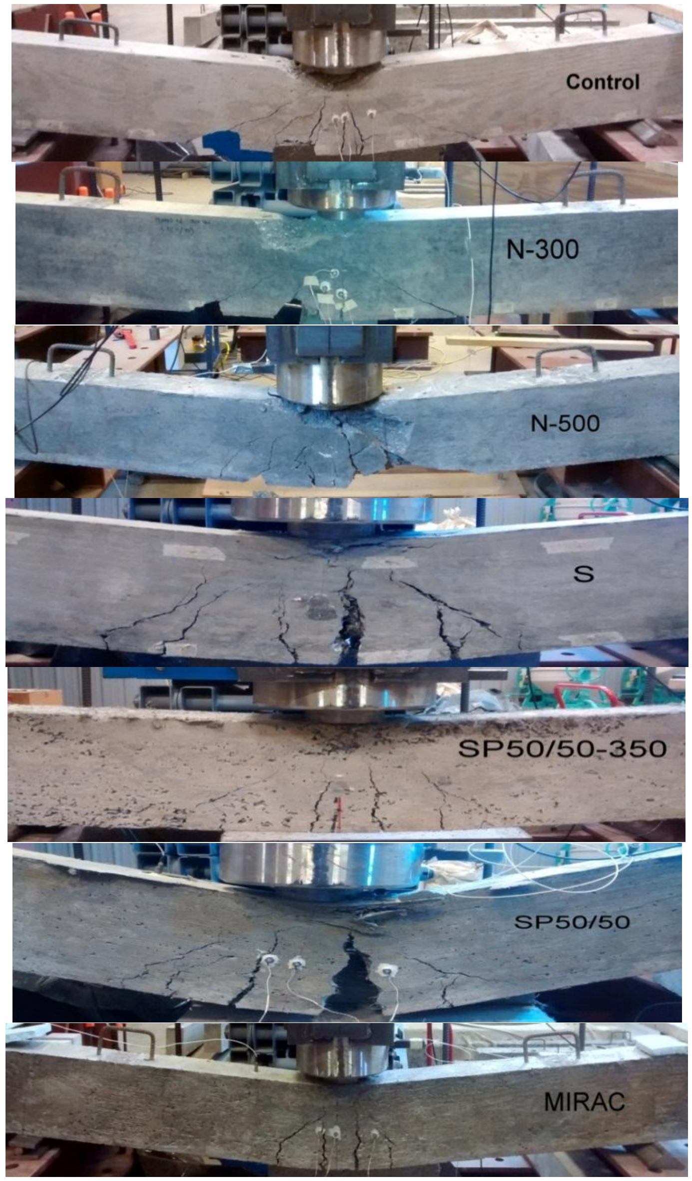

Fig. 8.3 - Crack profiles of composite beams in Group A

The displacement-time history plots of tested beams are presented in Fig. 8.2. The observations made during the impact tests are summarized in the following sections.

1) Control

Due to the impact, several vertical flexural cracks were observed. These flexural cracks started at the bottom of the beam and propagated upward. At the same time, a somewhat less prominent diagonal cracks were observed propagating at an angle of approximately 45 degrees. Severe spalling and scabbing were observed at the impact point and on the distal side of the beam respectively. After the test, the tensile reinforcement was yielded but rupture of the reinforcement was not observed under the impact load.

2) S

When 0.75% by vol. of steel fibers was added, crack profile changed significantly. Although, the crack profile was symmetrical just as the control beam, in this case, vertical flexural cracks were far more prominent. Same behavior was observed in case of diagonal cracks. One major behavior to note was that the tensile reinforcement ruptured under the subjected impact load which is very much different from control beam. Although there was a small amount of spalling, no scabbing was observed.

3) SP50/50

In this case, vertical shear cracks were more prominent than S specimen but crack widths of diagonal cracks were reduced to some extent. As far as the crack profile was concerned, it was almost identical with S beam specimens. But there was hardly any significant spalling and scabbing involved. The tensile reinforcement ruptured under the subjected impact load like S specimen.

4) MIRAC

In case of steel fiber reinforced MIRAC specimens, it could be observed that the propagation of diagonal shear cracks were reduced tremendously compared the previously tested specimens. Again, almost all the cracks were vertical flexural cracks. The tensile reinforcement didn’t rupture unlike other FRC beam specimens. There was hardly any sign of scabbing or spalling in this impact test. One major thing to note was that the drop weight rebounded couple after the first impact before coming to complete rest. This behavior wasn't observed in any other beam tested previously under current study.

8.3.1 Mid-span deflections

The displacement-time history plots of tested beams are presented in Fig. 8.2.

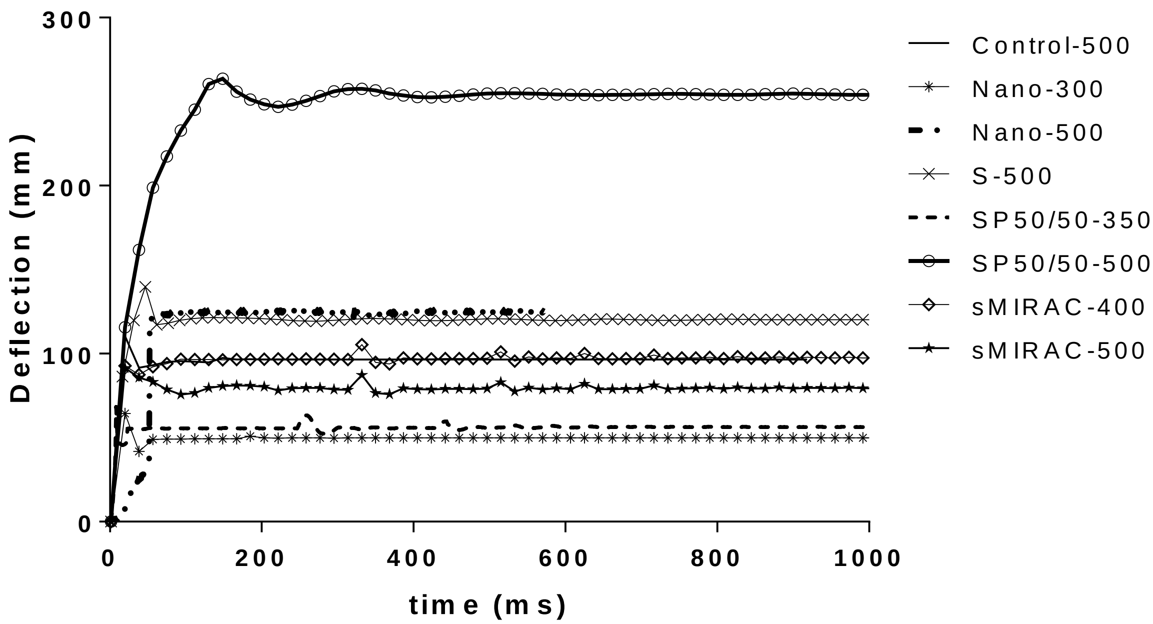

Fig. 8.4 - Deflections of test beams under impact loading (Test Group A).

8.3.2 Impact forces

The impact force-time history (unfiltered) data of the Control, S, N, SP50/50, and MIRAC cases are shown in Fig. 8.5. Appendix A.3.1-A.3.2 includes filtered and unfiltered impact-force time history for the rest of specimens. Table 8.4 summarizes the maximum impact force and mid-span deflection. The methodology used to filter the acceleration data is presented in Appendix A.5.

Table 8.4 –Summary of maximum impact force (unfiltered and filtered) and deflection

Beam Designation	Maximum impact force, unfiltered (KN)	Maximum impact force, filtered (KN)	Impact duration (ms)	Max. Mid-span deflection (mm)	Compressive strength (psi/MPa)
Control – 500 lbs	1893	916	7.86	115.74	6720/46.3
S – 500 lbs	1532	1198	8.0	139.43	7490/51.6
N-500 lbs	1287	721	8.15	125.74	6100/42.1
SP50/50-350lbs	n/a	n/a	n/a	68.39	6510/44.9
SP50/50-500lbs	1372	764	9.35	263.7	6770/46.7
sMIRAC-400 lbs	To be tested	To be tested	To be tested	To be tested	To be tested
sMIRAC-500 lbs	1559	469	12.4	105	6510/44.9

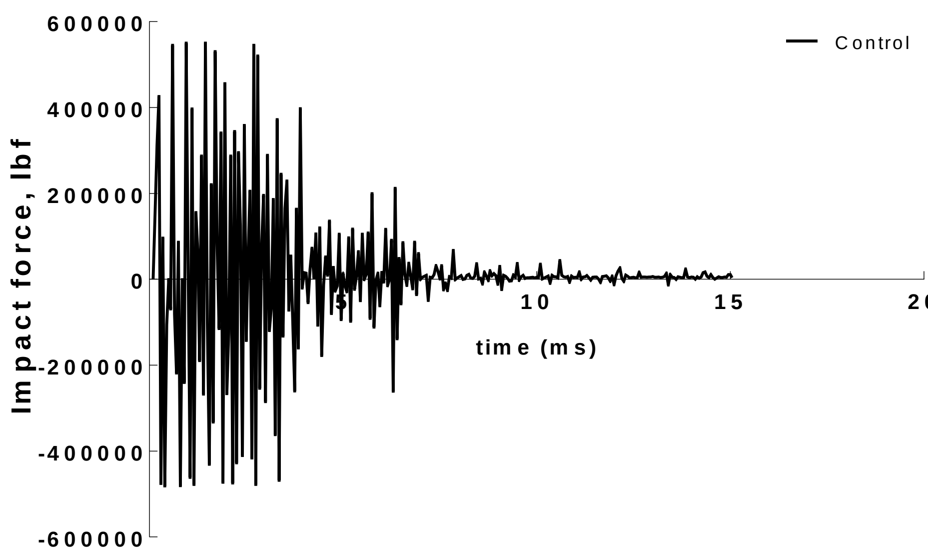

(a) Control Beam

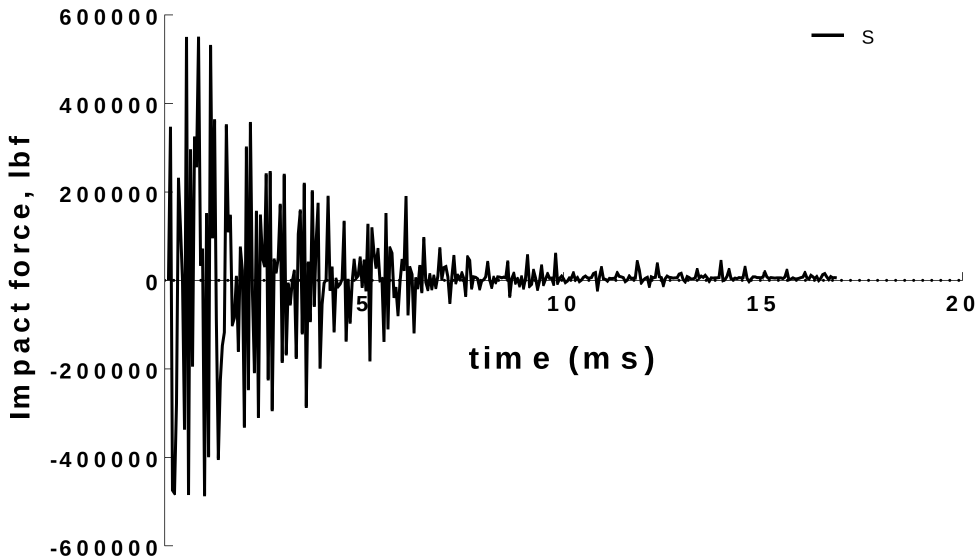

(b) RC Beam singly reinforced with steel fibers

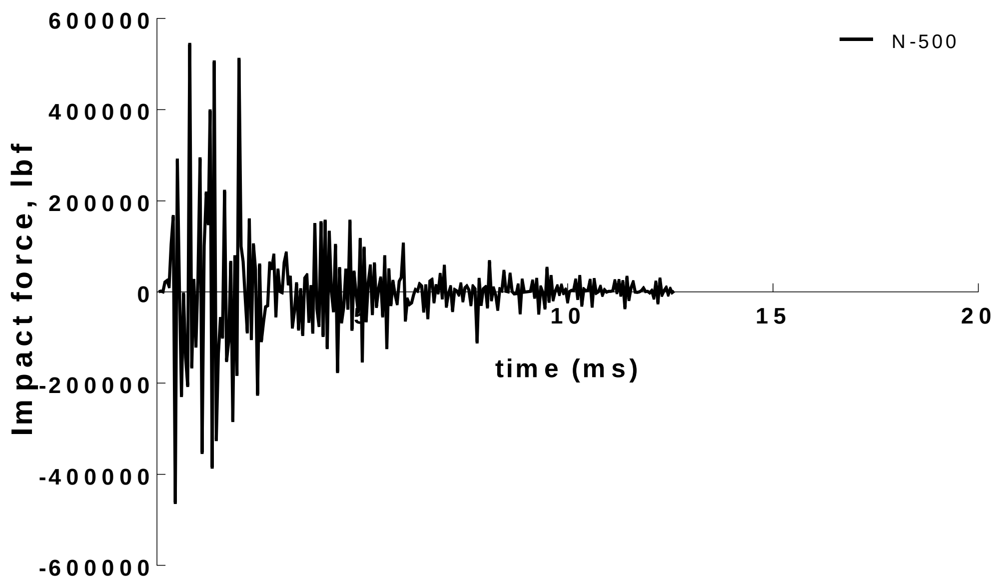

(c) RC Beam singly reinforced with carbon nano fibers

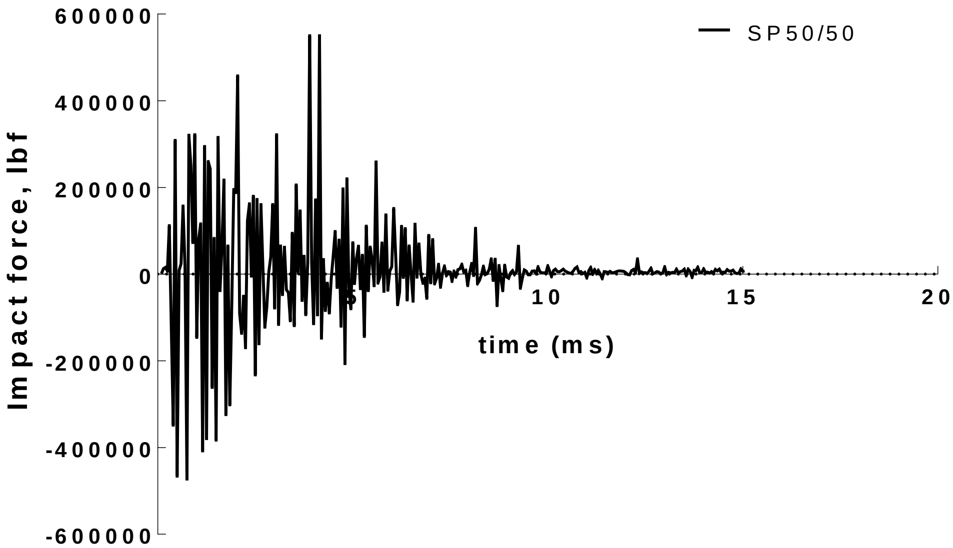

(d) RC Beam reinforced with steel and PVA fibers

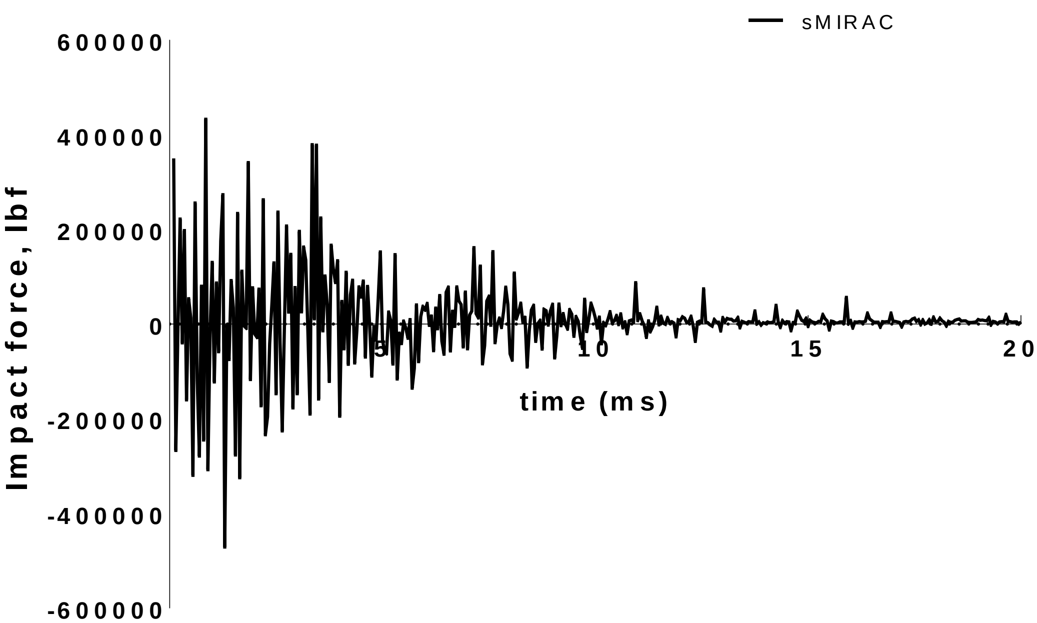

(e) RC Beam reinforced with Steel, PVA, and CNFs

Fig. 8.5 – Impact force time history for specimens in Test Group A.

8.3.3 Discussions (Group A)

The Control beam with no fiber reinforcement is failed by crushing of the impacting surface. The composite beams singly reinforced with CNFs had similar brittle behavior as the Control beam despite the fact that the compressive strength of the beam is relatively lower than other beams. This resulted in brittle delamination of concrete cover along the shear failure surface. On the other hand, the composite beam reinforced with steel fibers yields a larger displacement than the Control beam due to rupture of the flexural steel rebar. When the macro-scale steel fibers are replaced by macro-scale steel fibers and micro-scale PVA fibers (with a 1:1 volume ratio), the beam response changes drastically by doubling the mid-span displacement. This significantly reduces the impact force and slightly increases the impact duration (from 7ms to 9.35ms). By adding CNFs to the macro and micro-scale fiber reinforced composites, the impact force reduces by an additional 38% and the impact duration increases by 50% (from 9.35ms to 12.4ms). Furthermore, the response of the MIRAC beams changes. Instead of dissipating the initial kinetic energy through the beam deformation, the MIRAC composite beams dissipate the energy by rebounding approximately 4-5 times as shown in Fig. 8.4.

8.4 Results from Test Group B

The summary of failure modes are presented in Table 8.5 and Figure 8.6.

Table 8.5 –Failure modes of Test Group B

Beam Designation	Failure mode
F – 500 lbs	Flexural, Shear
FP50/50-500lbs	Flexural, Shear
fMIRAC-400 lbs	Flexural, Shear
fMIRAC-500 lbs	Flexural, Shear

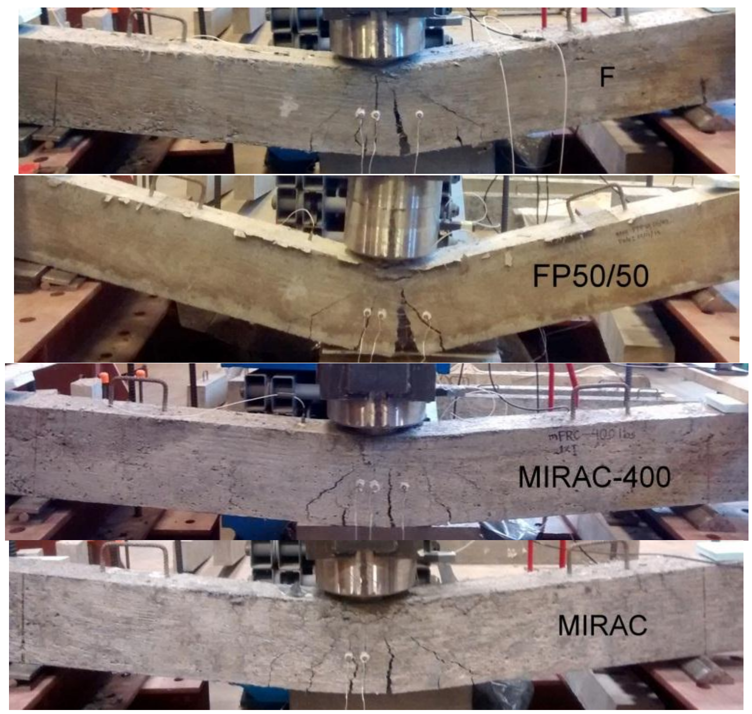

Fig.8.6 - Crack profiles of composite beams in Group B.

8.4.1 Mid-span deflections

The displacement-time history plots of tested beams are presented in Fig. 8.7.

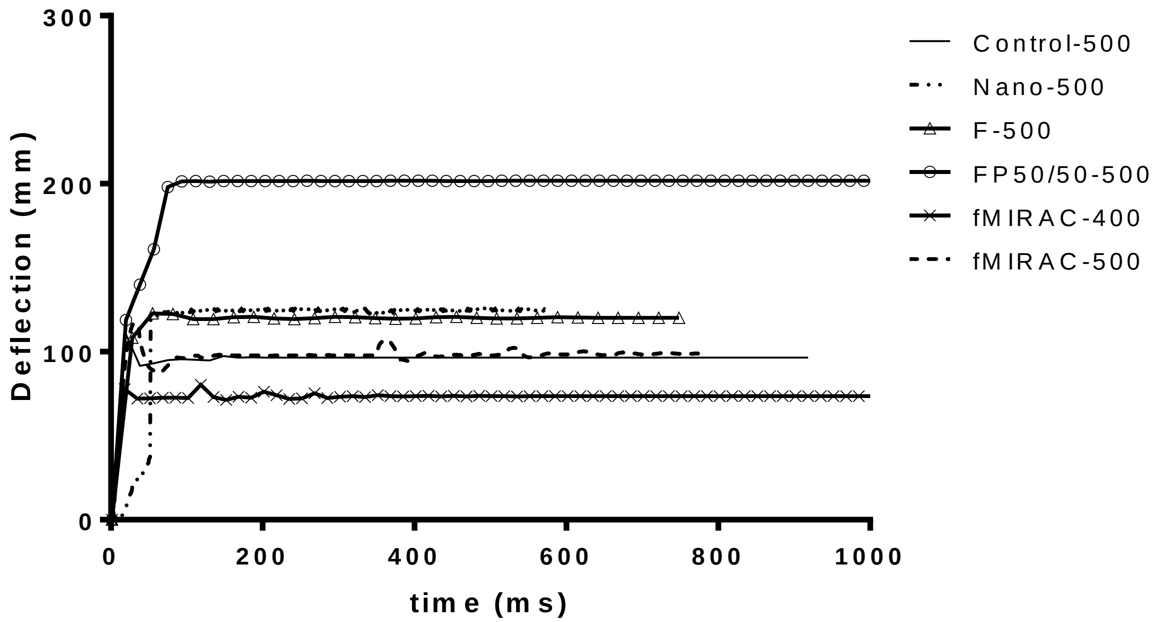

Fig. 8.7 - Deflections of test beams under impact loading (Test Group B).

8.4.2 Impact forces

The impact force-time history (unfiltered) data of the Control, F, FP50/50, and fMIRAC cases are shown in Fig. 8.8. Appendix A.3.5-A.3.6 includes filtered and unfiltered impact-force time history for the rest of specimens. Table 8.6 summarizes the maximum impact force and mid-span deflection. The methodology used to filter the acceleration data is presented in Appendix A.5.

Table 8.6 –Summary of maximum impact force (unfiltered and filtered) and deflection.

Beam Designation	Maximum impact force, unfiltered (KN)	Maximum impact force, filtered (KN)	Impact duration (ms)	Max. Mid-span deflection (mm)	Compressive strength (psi/MPa)
F – 500 lbs	748	492	7.97	123.5	6080/41.9
FP50/50-500lbs	1320	507	12.6	201.7	6900/47.6
fMIRAC-400 lbs	804	220	7.47	80.3	5620/38.7
fMIRAC-500 lbs	1169	352	15.95	117.5	5290/36.5

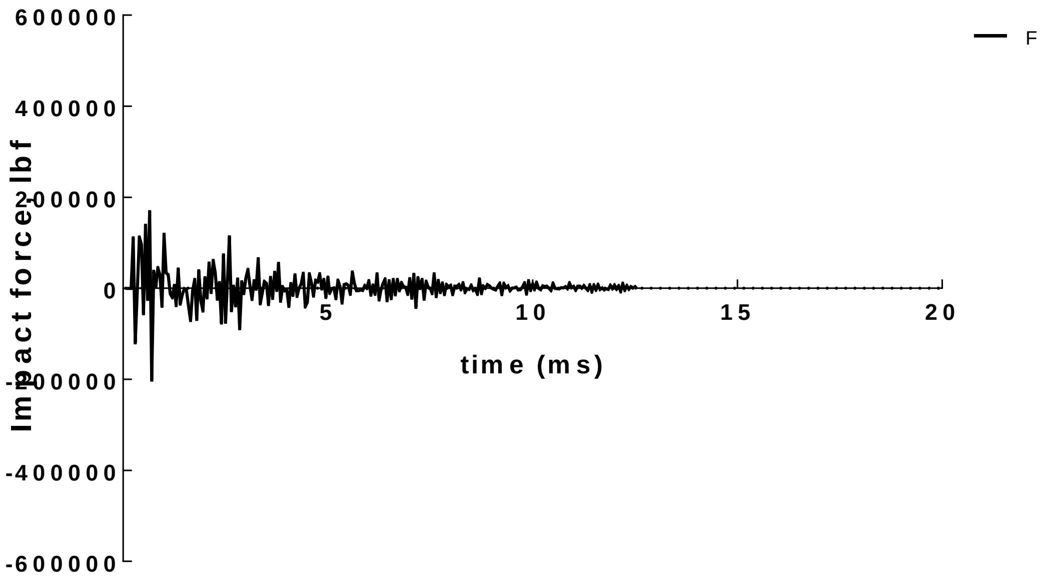

(a) RC Beam singly reinforced with PP fibers

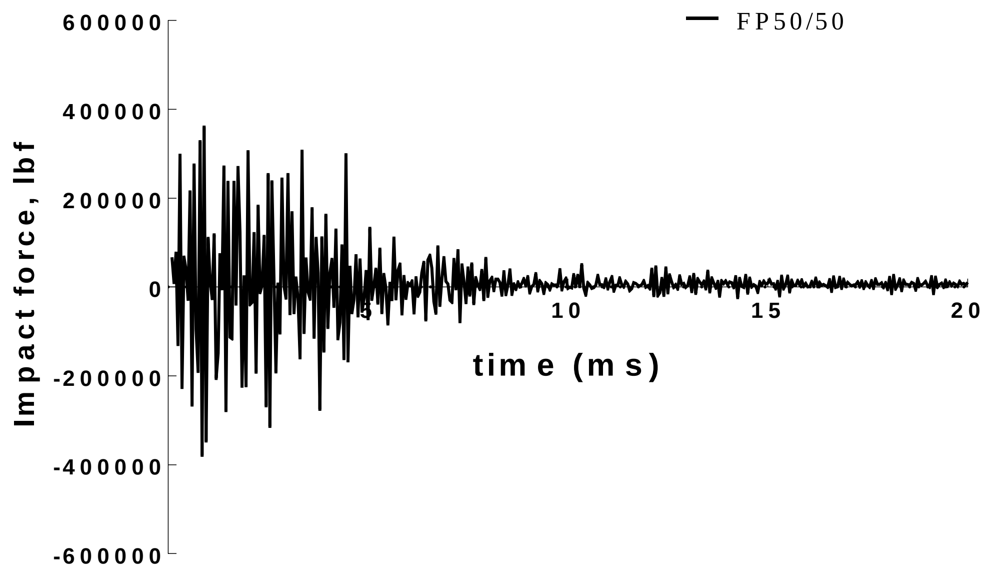

(b) RC Beam reinforced with PP and PVA fibers

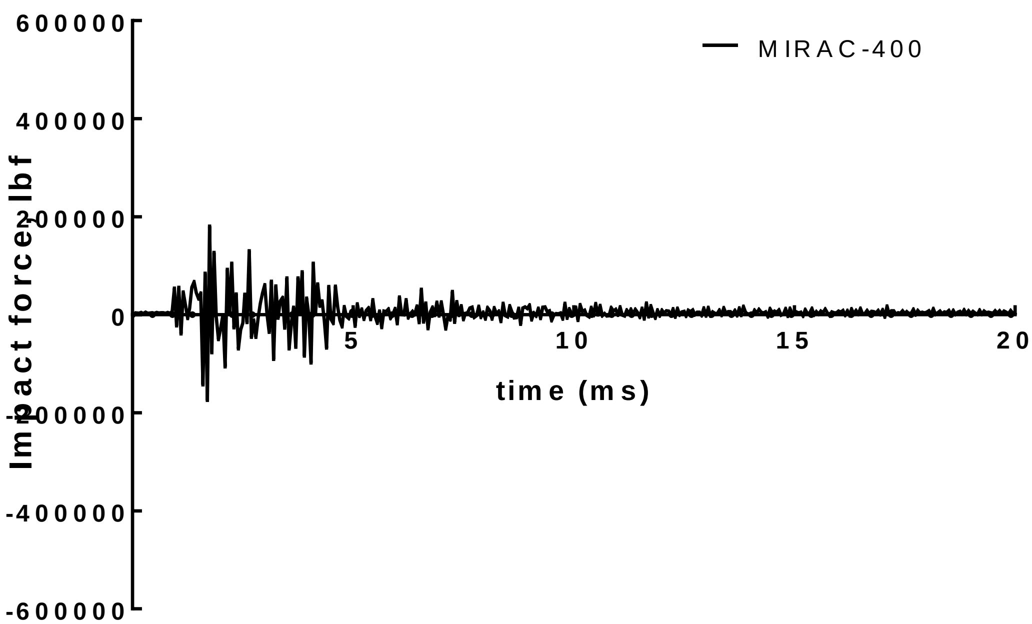

(c) RC Beam reinforced with PP, PVA, and CNFs -400 lbs

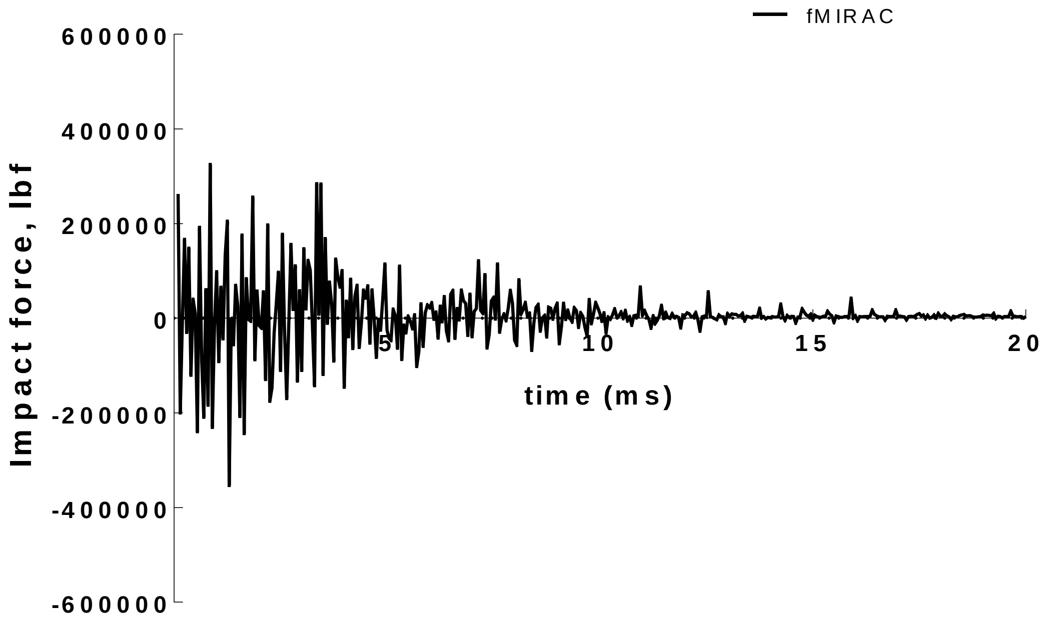

(d) RC Beam reinforced with PP, PVA, and CNFs -500 lbs

Fig. 8.8 – Impact force time history for specimens in Test Group B.

8.4.3 Discussions (Group B)

The Control beam with no fiber reinforcement is failed by crushing of the impacting surface. The composite beams singly reinforced with CNFs had similar brittle behavior as the Control beam despite the fact that the compressive strength of the beam is relatively lower than other beams This resulted in brittle delamination of concrete cover along the shear failure surface. On the other hand, the composite beam reinforced with PP fibers yields a larger displacement than the Control beam due to rupture of the flexural steel rebar. When the macro-scale PP fibers are replaced by macro-scale steel fibers and micro-scale PVA fibers (with a 1:1 volume ratio), the beam response changes drastically by doubling the mid-span displacement. This significantly reduces the impact force and slightly increases the impact duration (from 7.97ms to 12.6ms). By adding CNFs to the macro and micro-scale fiber reinforced composites, the impact force reduces by an additional 11% and the impact duration increases by 50% (from 12.6ms to 15.95ms). Furthermore, the response of the MIRAC beams changes. Instead of dissipating the initial kinetic energy through the beam deformation, the MIRAC composite beams dissipate the energy by rebounding approximately 4-5 times as shown in Fig. 8.7.

8.5 Cost of fiber reinforcement

Approximate cost of different fibers per unit weight used in the current study is tabulated in Table 8.7 and average additional cost of FRC specimens per unit volume over the control mix is also tabulated in Table 8.8.

Table 8.7 – Unit cost of fibers

Fiber type	Cost/lb, $
Steel	0.4-0.7
PP	0.9-1.0
PVA	1.4-1.6
Nano	100

Table 8.8 – Cost of fiber reinforcement

Mix Designation	Fiber contribution/ft^3, lbs.				Average additional cost over control, $
	Steel	PP	PVA	Nano	
S	3.67	x	x	x	2
F	x	0.56	x	x	0.55
N	x	x	x	0.27	27
SP50/50	2.445	x	0.405	x	2
FP50/50	x	0.28	0.405	x	0.9
sMIRAC	2.445	x	0.405	0.27	29
fMIRAC	x	0.28	0.405	0.27	27.9

CHAPTER 9

CONCLUSIONS

Based on the results of this experimental investigation, the following conclusions are drawn:

1. As hypothesized in this study, a combination of fly ash and multi-scale (macro-, micro-, and nano-) fiber reinforcement enhances the macro-level performance (i.e., beam impact resilience) by bridging different scale cracks and preventing the coalescence of cracks in cementitious composites. Therefore, the multi-scale impact resilient smart composites (MIRAC), including nano-scale CNFs, micro-scale PVA, and macro-scale PP or steel fiber reinforcement, are well-suited for impact hazard mitigation;
2. Multi-scale fiber reinforced cementitious composites significantly reduce the impact force due to increased ductility at initial contact;
3. For conventional RC beams with no fiber reinforcement, the impacting projectile crushes the contact surface substantially without rebound, thereby stopping the impacting projectile by fracturing the concrete;
4. For composite beams singly reinforced with polypropylene or steel fibers, the initial impact energy is primarily dissipated by the beam deformation without significantly damaging the contacting surface. The impact force reduces by 19% for steel fibers and 60% for PP fibers;
5. By replacing the macro-scale polypropylene (or steel) fibers with a combination of macro-scale polypropylene (or steel) fibers and micro-scale PVA fibers, the initial impact force reduces by 30% - 40%; and

6. By adding nano-scale carbon nanofibers (by 1% cement weight) to macro- and micro-scale fiber reinforced composites, the kinetic energy developed from a rigid impacting projectile is dissipated by the beam rebounding response as well as the beam deformation. This rebounding behavior dissipates the initial impact energy over a longer period of time without significantly crushing the impacting surface. The MIRAC beams rebound to their initial residual deformation upon recovery. Therefore, the toughness and ductility of MIRACs provide an excellent energy dissipation mechanism.

CHAPTER 10

FUTURE RESEARCH

It is desirable to conduct an impact test of composite beams for varying reinforcing ratios, and efforts should be made to study the effects of reinforcing ratios on the response of multi-scale reinforced composite beams. The results of such studies will directly benefit the design of engineered composites. CNFs reinforced cementitious composites have shown to be durable; however, the durability of MIRAC composites will need to be studied. The MIRAC beams are fairly conductive (resistance ranging between 40 kilo-ohms and 20 mega-ohms), and the conductivity changes under impact loading. However, the monitoring technology needs further improvement.

REFERENCES

[1] Chen, Yi, and Ian M. May. "Reinforced concrete members under drop-weight impacts." Proceedings of the ICE-Structures and Buildings 162.1 (2009): 45-56.

[2] Zineddin, M., and T. Krauthammer. "Dynamic response and behavior of reinforced concrete slabs under impact loading." International Journal of Impact Engineering 34.9 (2007): 1517-1534.

[3] S. Saatci, J.V. Vecchio, “Effect of Shear Mechanisms on Impact Behavior of Reinforced Concrete Beams” ACI Structural Journal, 106 (1) (2009), pp. 78–86

[4] Fujikake, K., Li, B., and Soeun, S. (2009). ”Impact Response of Reinforced Concrete Beam and Its Analytical Evaluation.” J. Struct. Eng., 135(8), 938–950.

[5] Li, Victor C. "On engineered cementitious composites (ECC)." Journal of advanced concrete technology 1.3 (2003): 215-230.

[6] Hughes, G., and Beeby, A. W. (1982). “Investigation of the effect of impact loading on concrete beams.”Struct. Eng., 60B (3), 45–52.

[7] Tang, Taiping, and Hamid Saadatmanesh. "Analytical and experimental studies of fiber-reinforced polymer-strengthened concrete beams under impact loading." ACI structural journal 102.1 (2005).

[8] Websites accessed for Figure 1(Accessed on September30, 2014):

[9] Yang, En-Hua, and Victor C. Li. "Tailoring engineered cementitious composites for impact resistance." Cement and Concrete Research 42.8 (2012): 1066-1071.

[10] F. Sanchez, K. Sobolev, Nanotechnology in Concrete – A Review, Construction and Building Materials, 24 (2010) 2060-2071.

[11] S. Sasmal, B. Bhuvaneshwari, N.R. Iyer, Can Carbon Nanotubes Make Wonders in Civil/Structural Engineering?, Progress in Nanotechnology and Nanomaterials, 2(4) (2013), 117-129.

[12] F. Ren, C. H. Mattus, J. J. Wang, and B. P. DiPaolo, Effect of projectile impact and penetration on the phase composition and microstructure of high performance concretes, Cement and Concrete Composites, 41 (2013) 1-8.

[13] R.N. Howser, H.B. Dhonde, Y.L., Mo, Self-sensing of carbon nanofiber concrete columns subjected to reversed cyclic loadin, Smart Materials and Structures 20(8) (2011) 1-13.

[14] Williamson, Gilbert R. "The effect of steel fibers on the compressive strength of concrete." ACI Special Publication 44 (1974).

[15] Yazıcı, Şemsi, Gözdeİnan, and VolkanTabak. "Effect of aspect ratio and volume fraction of steel fiber on the mechanical properties of SFRC."Construction and Building Materials 21.6 (2007): 1250-1253.

[16] Banthia, Nemkumar, and Sayed Mohamad Soleimani. "Flexural response of hybrid fiber-reinforced cementitious composites." ACI materials journal 102.6 (2005).

[17] Ahmed, Shaikh Faiz Uddin, Mohamed Maalej, and P. Paramasivam. "Flexural responses of hybrid steel–polyethylene fiber reinforced cement composites containing high volume fly ash." Construction and Building Materials 21.5 (2007): 1088-1097.

[18] Soulioti, D. V., et al. "Effects of Fibre Geometry and Volume Fraction on the Flexural Behaviour of Steel-Fibre Reinforced Concrete." Strain 47.s1 (2011): e535-e541.

[19] Uygunoğlu, Tayfun. "Investigation of microstructure and flexural behavior of steel-fiber reinforced concrete." Materials and Structures 41.8 (2008): 1441-1449.

[20] SU, Jun, and Xiang LI. "Analysis on the Mechanical Behavior of the Flexural PVA Fiber-reinforced Concrete Beam." Journal of Hubei University of Technology 2 (2012): 033.

[21] Ayub, Tehmina, Nasir Shafiq, and MuhdFadhilNurudinn. "Analytical Prediction of the Mechanical Properties of High Performance PVA Fiber Reinforced Concrete."Applied Mechanics and Materials.Vol. 567. 2014.

[22] Horiguchi, Takashi, and Kohji Sakai. "Hybrid effects of fiber-reinforced concrete on fracture toughness." ACI Special Publication 172 (1999).

[23] Yanggeunhyeok ." Slump and mechanical properties of hybrid fiber reinforced concrete with steel fiber and PVA . " Concrete Institute Proceedings 22.5 (2010) : 651-658.

[24] Hsie, Machine, ChijenTu, and P. S. Song. "Mechanical properties of polypropylene hybrid fiber-reinforced concrete."Materials Science and Engineering: A 494.1 (2008): 153-157.

[25] Bayasi, Ziad, and Jack Zeng. "Properties of polypropylene fiber reinforced concrete." ACI Materials Journal 90.6 (1993).

[26] Alhozaimy, A. M., P. Soroushian, and F. Mirza. "Mechanical properties of polypropylene fiber reinforced concrete and the effects of pozzolanic materials." Cement and Concrete Composites 18.2 (1996): 85-92.

[27] Yao, Wu, Jie Li, and Keru Wu. "Mechanical properties of hybrid fiber-reinforced concrete at low fiber volume fraction." Cement and Concrete Research 33.1 (2003): 27-30.

[28] Sanchez, Florence, and Chantal Ince. "Microstructure and macroscopic properties of hybrid carbon nanofiber/silica fume cement composites." Composites Science and Technology 69.7 (2009): 1310-1318.

[29] Tyson, Bryan M., et al. "Carbon nanotubes and carbon nanofibers for enhancing the mechanical properties of nanocompositecementitious materials." Journal of Materials in Civil Engineering 23.7 (2011): 1028-1035.

[30] Metaxa Z, Konsta-Gdoutos M, Shah S. “Mechanical properties and nanostructure of cement-based materials reinforced with carbon nanofibers and polyvinyl alcohol (PVA) microfibers.” ACI Special Publication. 2010;270.

[31] Gao, Di, Mariel Sturm, and Y. L. Mo. "Electrical resistance of carbon-nanofiber concrete." Smart Materials and Structures 18.9 (2009): 095039.

[32] Xie, Xiao-Lin, Yiu-Wing Mai, and Xing-Ping Zhou. "Dispersion and alignment of carbon nanotubes in polymer matrix: a review." Materials Science and Engineering: R: Reports 49.4 (2005): 89-112.

[33] Ishikawa, N., Katsuki, S., and Takemoto, K. (2000). “Dynamic analysis of prestressed concrete beams under impact and high speed loadings.” Proc., 6th Int. Conf. on Structures under Shock and Impact, WIT Press, Southampton, 247–256.

[34] Kishi, N., (2003). “Round robin analysis of RC beam subjected to an impact load due to a falling weight.” Proc., 1st Int. Conf. on Design and Analysis of Protective Structure against Impact/Impulsive/Shock Loads, DAPSIL, Tokyo, 305–318.

[35] Habel, Katrin, and Paul Gauvreau. "Behavior of reinforced and posttensioned concrete members with a UHPFRC overlay under impact loading." Journal of structural engineering 135.3 (2009): 292-300.

[36] Farnam, Yaghoob, SoheilMohammadi, and Mohammad Shekarchi. "Experimental and numerical investigations of low velocity impact behavior of high-performance fiber-reinforced cement based composite." International Journal of Impact Engineering 37.2 (2010): 220-229.

[37] L. Daudeville, Y. Malécot. Concrete structures under impact Eur. J. Environ. Civil Eng., 15 (2011), pp. 101–140

[38] Habel, K. "Impact response of post-tensioned and reinforced concrete members with an UHPFRC overlay."

[39] béton Ce-id. Concrete structures under impact and impulsive loading: synthesis report: Comité Euro-International du Béton; 1988.

[40] Abrate, S., Impact on Composite Structures, Cambridge University Press, 1998, 301 pp.

[41] Graff, K. F., Wave Motion in Elastic Solids, Ohio State University Press, Columbus, Ohio, 1975, 649 pp.

[42] Q.M. Li, S.R. Reid, H.M. Wen, A.R. Telford, Local impact effects of hard missiles on concrete targets, International Journal of Impact Engineering, 32 (2005) 224–284.

[43] D. Laurent, M. Yann, Concrete Structures Under Impact, European Journal of Environmental and Civil Engineering,15 (2011)101–140.

[44] F. Ren, C. H. Mattus, J. J. Wang, and B. P. DiPaolo, Effect of projectile impact and penetration on the phase composition and microstructure of high performance concretes, Cement and Concrete Composites, 41 (2013) 1-8.

[45] American Concrete Institute (ACI), Committee 211. The Standard (ACI 211.1-91, Reapproved 2009): Standard practice for selecting proportions for normal, heavyweight and mass concrete. American Concrete Institute, Farmington Hills, MI, USA.

[46] ASTM C150 / C150M-12, Standard Specification for Portland Cement, ASTM International, West Conshohocken, PA, 2012.

[47] ASTM C618-12a, Standard Specification for Coal Fly Ash and Raw or Calcined Natural Pozzolan for Use in Concrete, ASTM International, West Conshohocken, PA, 2012.

[48] ASTM C494 / C494M-13, Standard Specification for Chemical Admixtures for Concrete, ASTM International, West Conshohocken, PA, 2013.

[49] ASTM C143 / C143M-12, Standard Test Method for Slump of Hydraulic-Cement Concrete, ASTM International, West Conshohocken, PA, 2012.

[50] ASTM C511-13, Standard Specification for Mixing Rooms, Moist Cabinets, Moist Rooms, and Water Storage Tanks Used in the Testing of Hydraulic Cements and Concretes, ASTM International, West Conshohocken, PA, 2013.

[51] ASTM C192 / C192M-14, Standard Practice for Making and Curing Concrete Test Specimens in the Laboratory, ASTM International, West Conshohocken, PA, 2014.

[52] ASTM C39 / C39M-14a, Standard Test Method for Compressive Strength of Cylindrical Concrete Specimens, ASTM International, West Conshohocken, PA, 2014.

[53] ASTM C496 / C496M-11, Standard Test Method for Splitting Tensile Strength of Cylindrical Concrete Specimens, ASTM International, West Conshohocken, PA, 2011.

[54] ASTM C78 / C78M-10e1, Standard Test Method for Flexural Strength of Concrete (Using Simple Beam with Third-Point Loading), ASTM International, West Conshohocken, PA, 2010.

[55] ACI Committee 544, Measurements of the properties of fiber reinforced concrete, ACI 544-2R-88American Concrete Institute, Detroit (1988), p. 8.

[56] ASTM D1557-12, Standard Test Methods for Laboratory Compaction Characteristics of Soil Using Modified Effort (56,000 ft-lbf/ft3 (2,700 kN-m/m3)), ASTM International, West Conshohocken, PA, 2012.

APPENDICES

A.1 Equipment and Instruments used for Phase I-II Experiment

A.1.1 Data acquisition

An expandable modular data acquisition system, Instrunetinet 420 was used in this test. The iNET-420 provides 20 single-ended (SE)/10 differential (DI) voltage input channels and 4 universal digital I/O (20 mA sink, -10V to 30V) and requires the iNET-430 A/D module to measure voltages. The iNET- 420 was connected directly to the displacement transducer and potentiometer to obtain strain and deflection respectively.

Expandable modular data acquisition system

Expandable Modular Data Acquisition System

iNET-400 Series

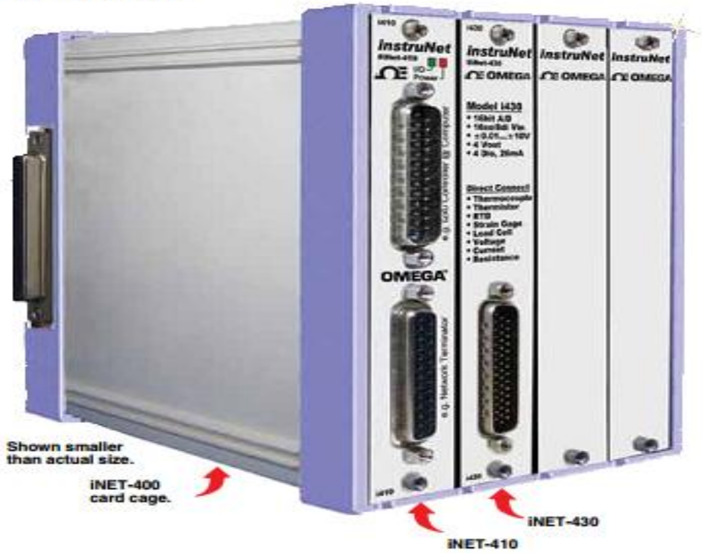

- USB 2.0 High Speed Data Acquisition Hardware for Windows® ≥XP SP2, Vista, 7 or 8 (XP/VS/7/8)
- Analog and Digital Input and Outputs
- Free instruNet World Software
- Directly Connects to Thermocouple, RTD, Thermistor, Strain Gage, Load Cell, Voltage, Current, Resistance and Accelerometer Input's
- Reduce Noise by Placing Boxes Near Sensors and up to 1000' From Noisy Computer
- Digitize Any Combination of Channels at 166,000 Samples Per Second Aggregate
- Each Channel has Independently Programmable Analog Filters, Integration Time, Voltage Range, and Sample Rate; Programmable Digital Filters on All Channels (LP, HP, BP, BS)

The iNET-400 system is a low cost card cage that attaches to Windows computers via USB 2.0. The advantage of a card cage is that you can select which I/O modules to install as needed to build a customized system. The instruNet card cage typically has one A/D measurement module and additional modules provide signal conditioning. The conditioned analog signal is routed to the A/D module via the backplane.

This is dramatically different from comparable systems which place A/D measurement electronics on each module. The advantage of the iNET-400 topology is cost. After the 1st module is installed, additional iNET-400 channels are conditioned at a very low cost per channel.

iNET-400 measurement modules have universal inputs that enable one to directly connect each channel to one of: thermocouple, thermistor, strain gage, load cell, counter/timer, RTD, voltage, current, resistance and accelerometer.

Absolute accuracy for all of these sensor types is specified. In some cases, the end user adds an external shunt resistor. The advantage of universal inputs is cost.

Low Cost 4/8/12/16-Slot Card Cages

The iNET-400 card cage provides 4 slots, and multiple iNET-400's can be bolted together by the end user, side-by-side, to create an 8, 12, or 16 slot system. In many applications, one iNET-400 with 4 slots is sufficient.

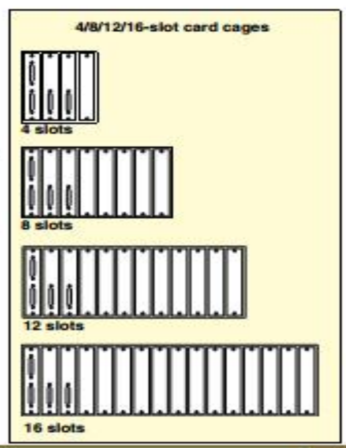

A.1.2 String potentiometer

A position sensor, PT420, manufactured by Measurement Specialties was used to measure the deflection of the test specimens (beams) under the four point bending test The PT420 is capable of full-scale measurement ranging from 2 to 100 inches, providing a 0/4-20 mA feedback signal that is linearly proportional to the position of a traveling stainless-steel extension cable.

String potentiometer

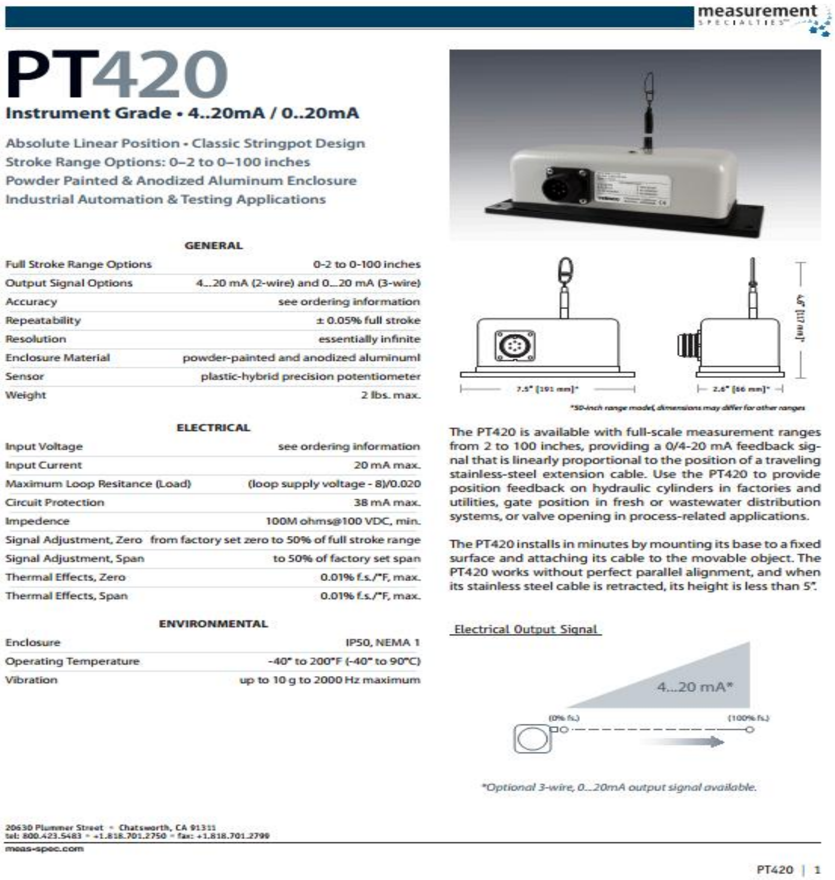

measurement SPECIALTIES

PT420

Instrument Grade • 4..20mA / 0..20mA

Absolute Linear Position • Classic Stringpot Design
Stroke Range Options: 0–2 to 0–100 inches
Powder Painted & Anodized Aluminum Enclosure
Industrial Automation & Testing Applications

GENERAL	
Full Stroke Range Options	0-2 to 0-100 inches
Output Signal Options	4...20 mA (2-wire) and 0...20 mA (3-wire)
Accuracy	see ordering information
Repeatability	± 0.05% full stroke
Resolution	essentially infinite
Enclosure Material	powder-painted and anodized aluminuml
Sensor	plastic-hybrid precision potentiometer
Weight	2 lbs. max.

ELECTRICAL	
Input Voltage	see ordering information
Input Current	20 mA max.
Maximum Loop Resitance (Load)	(loop supply voltage - 8)/0.020
Circuit Protection	38 mA max.
Impedence	100M ohms@100 VDC, min.
Signal Adjustment, Zero	from factory set zero to 50% of full stroke range
Signal Adjustment, Span	to 50% of factory set span
Thermal Effects, Zero	0.01% f.s./°F, max.
Thermal Effects, Span	0.01% f.s./°F, max.

ENVIRONMENTAL	
Enclosure	IP50, NEMA 1
Operating Temperature	-40° to 200°F (-40° to 90°C)
Vibration	up to 10 g to 2000 Hz maximum

7.5" [191 mm]* 2.6" [66 mm]* 4.6" [117 mm]*

*50-inch range model, dimensions may differ for other ranges

The PT420 is available with full-scale measurement ranges from 2 to 100 inches, providing a 0/4-20 mA feedback signal that is linearly proportional to the position of a traveling stainless-steel extension cable. Use the PT420 to provide position feedback on hydraulic cylinders in factories and utilities, gate position in fresh or wastewater distribution systems, or valve opening in process-related applications.

The PT420 installs in minutes by mounting its base to a fixed surface and attaching its cable to the movable object. The PT420 works without perfect parallel alignment, and when its stainless steel cable is retracted, its height is less than 5".

Electrical Output Signal

4...20 mA*

(0% fs.) (100% fs.)

*Optional 3-wire, 0...20mA output signal available.

20630 Plummer Street • Chatsworth, CA 91311
tel: 800.423.5483 • +1.818.701.2750 • fax: +1.818.701.2799
meas-spec.com

PT420 | 1

A.1.3 Displacement transducers

The PI-2-100 displacement transducer manufactured by TML has a simple structure - a combination of strain gauges and an arch-shaped spring plate, the former attached to the latter. This model was designed for gauge length of 100 mm. This transducer was used to measure the crack opening displacement occurring within each gauge length on the surface of concrete beam specimens.

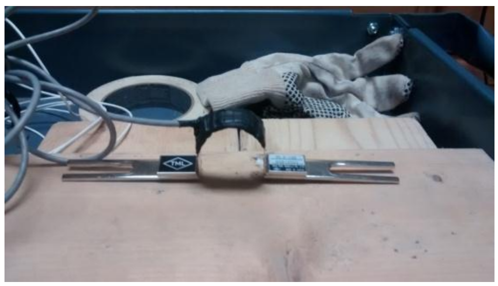

Displacement transducer

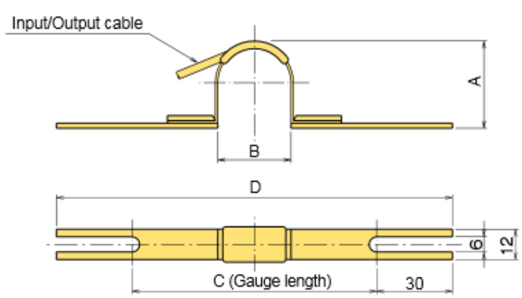

■ Dimensions

TYPE	A	B	C	D	Weight
PI-2-50	35	As per the figure			40
PI-2-100	35	30	100	160	50

Displacement transducer dimensions

PI Displacement Transducer ±2 / ±5mm

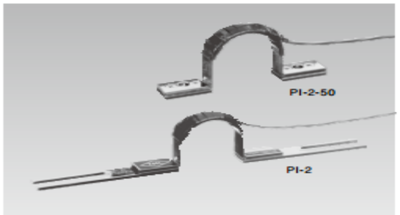

The PI displacement transducer has a simple structure: a combination of strain gauges and an arch-shaped spring plate, the former attached to the latter. Six models designed for gauge lengths of 50 mm to 300 mm are available. This transducer is used to measure the crack opening displacement occurring within each gauge length on the surface of concrete or to measure the displacement of various structures.

Pie-shape type
Surafce measurement use

PI-2-50 / PI-5-50

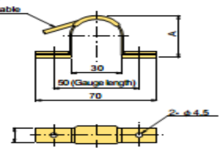

PI-2 / PI-5

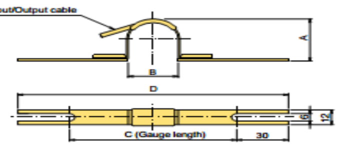

■ Dimensions

TYPE	A	B	C	D	Weight
PI-2-50	35	As per the figure			40
PI-2-100	35	30	100	160	50
PI-2-150	35	30	150	210	60
PI-2-200	35	30	200	260	70
PI-2-250	35	30	250	310	80
PI-2-300	35	30	300	360	90
PI-5-50	50	As per the figure			40
PI-5-100	45	40	100	160	50
PI-5-150	45	40	150	210	60
PI-5-200	45	40	200	260	70
PI-5-250	45	40	250	310	80
PI-5-300	45	40	300	360	90

■ Accessory

TYPE	Dummy plate	Fixing jig
PI-2-50 / PI-5-50	PIF-11-50	PIF-21-50
PI-2-100 / PI-5-100	PIF-11-100	PIF-21-100
PI-2-150 / PI-5-150	PIF-11-150	PIF-21-100
PI-2-200 / PI-5-200	PIF-11-200	PIF-21-100
PI-2-250 / PI-5-250	PIF-11-250	PIF-21-100
PI-2-300 / PI-5-300	PIF-11-300	PIF-21-100

Dummy plate PIF-11
This plate is used to maintain the proper gauge length when mounting the PIF-21 jig to test specimen.

Fixing Jig PIF-21
This Jig is pre-mounted to concrete and other test specimen in order to screw-mount PI displacement transducer.

■ SPECIFICATIONS

TYPE	PI-2	PI-5
Gauge length	50、100、150、200、250、300	
Capacity	±2mm	±5mm
Rated Output	2mV/V(4000×10^{-6} strain)	2.5mV/V(5000×10^{-6} strain)
Sensitivity(x10^{-6} strain)/mm	2000	1000
Non-linearity	0.5%RO	
Allowable temperature range	0 ~ +40°C	
Input/Output resistance	350Ω	
Recommended exciting voltage	Less than 2V	
Allowable exciting voltage	10V	

Input/Output cable : φ3mm 0.09mm^2 4-core vinyl cable 2m

A.1.4 Accelerometers

An accelerometer with a measurement range of ± 5000g pk (± 49000 m/s^2) and a sensitivity of 1.0 mV/g (PCB MODEL: 350B04) was used on the drop weight to measure acceleration due to the impact on the fiber reinforced concrete beams.

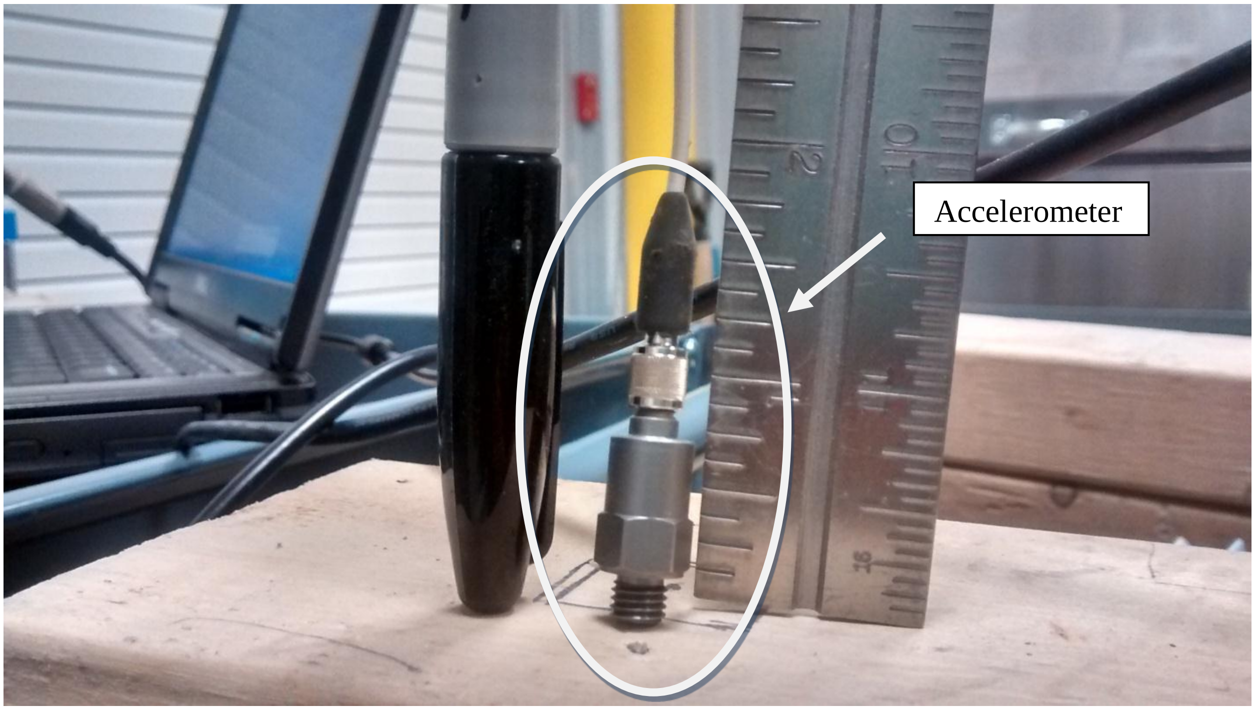

Accelerometer

Model Number 350B04	SHEAR ICP® SHOCK SENSOR	Revision: G ECN #: 42036

Performance	ENGLISH	SI	
Sensitivity(± 30 %)	1.0 mV/g	0.10 mV/(m/s²)	
Measurement Range	± 5000 g pk	± 49,000 m/s² pk	
Frequency Range(± 1 dB)	0.4 to 10,000 Hz	0.4 to 10,000 Hz	
Frequency Range(-3 dB)	0.2 to 25,000 Hz	0.2 to 25,000 Hz	[2]
Electrical Filter Corner Frequency(-3 dB)	13 kHz	13 kHz	[1][3]
Mechanical Filter Resonant Frequency	23 kHz	23 kHz	[1][4]
Resonant Frequency	≥ 100 kHz	≥ 100 kHz	
Broadband Resolution(1 to 10,000 Hz)	0.02 g rms	0.20 m/s² rms	[1]
Non-Linearity	≤ 2.0 %	≤ 2.0 %	
Transverse Sensitivity	≤ 7 %	≤ 7 %	
Environmental			
Overload Limit(Shock)	± 50,000 g pk	± 490,000 m/s² pk	
Temperature Range(Operating)	0 to +150 °F	-18 to +66 °C	
Temperature Range(Storage)	-40 to +200 °F	-40 to +93 °C	
Temperature Response	See Graph	See Graph	
Base Strain Sensitivity	0.002 g/με	0.02 (m/s²)/με	[1]
Electrical			
Excitation Voltage	20 to 30 VDC	20 to 30 VDC	
Constant Current Excitation	2 to 20 mA	2 to 20 mA	
Output Impedance	≤ 200 Ohm	≤ 200 Ohm	
Output Bias Voltage	8 to 14 VDC	8 to 14 VDC	
Discharge Time Constant	1.0 to 2.0 sec	1.0 to 2.0 sec	[1]
Settling Time(within 10% of bias)	<10 sec	<10 sec	
Physical			
Sensing Element	Ceramic	Ceramic	
Sensing Geometry	Shear	Shear	
Housing Material	Titanium	Titanium	
Sealing	Hermetic	Hermetic	
Size (Hex x Height)	0.375 in x 1.02 in	9.5 mm x 25.9 mm	
Weight	0.16 oz	4.5 gm	[1]
Electrical Connector	10-32 Coaxial Jack	10-32 Coaxial Jack	
Electrical Connection Position	Top	Top	
Mounting Thread	1/4-28 Male	1/4-28 Male	

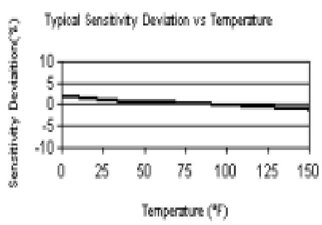

CE [5]

OPTIONAL VERSIONS

Optional versions have identical specifications and accessories as listed for the standard model except where noted below. More than one option may be used.

M - Metric Mount

Mounting Thread	M6 x 0.75 Male	M6 x 0.75 Male

W - Water Resistant Cable

Electrical Connector	Sealed Attached Cable	Sealed Attached Cable

NOTES:

[1] Typical.
[2] Typical corner frequency for coupled electrical and mechanical filters.
[3] Electrical filter is a second order filter.
[4] Amplitude at resonance is +9 dB.
[5] See PCB Declaration of Conformance PS023 for details.

SUPPLIED ACCESSORIES:

Model ACS-14 High G shock accelerometer calibration using Hopkinson bar. (1)
Model ACS-22 NIST Traceable frequency response (100Hz to ±1 dB point) (1)

Entered: AP	Engineer: BAM	Sales: WDC	Approved: BAM	Spec Number:
Date: 9/17/2013	Date: 9/17/2013	Date: 9/17/2013	Date: 9/17/2013	11177

All specifications are at room temperature unless otherwise specified.
In the interest of constant product improvement, we reserve the right to change specifications without notice.

PCB PIEZOTRONICS™
3425 Walden Avenue, Depew, NY 14043
Phone: 716-684-0001
Fax: 716-684-0987
E-Mail: info@pcb.com

A.1.5 Signal Conditioner

A Four-channel, ICP® Sensor Signal Conditioner, Model-482C05, manufactured by PCB PIEZOTRONICS was used for phase II experimental program.

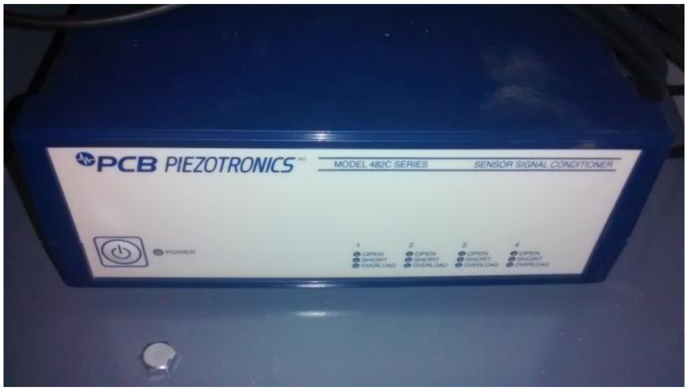

PCB Piezotronics 482C05 signal conditioner

Model Number 482C05

FOUR-CHANNEL, ICP® SENSOR SIGNAL CONDITIONER

Revision: H
ECN #: 40512

Performance	ENGLISH	SI	
Channels	4	4	
Sensor Input Type(s)	ICP®	ICP®	
Voltage Gain(± 1 %)(at 500 Hz)	1:1	1:1	
Output Range(Maximum)	± 10 V	± 10 V	
Low Frequency Response(-5 %)	<0.1 Hz	<0.1 Hz	
High Frequency Response(-5 %)	>1000 kHz	>1000 kHz	
Phase Response(at 1 kHz)	± 1 °	± 1 °	
Cross Talk(maximum)	-72 dB	-72 dB	
Fault/Bias Monitor/Meter(LED)	Open/Short/Overload	Open/Short/Overload	
Environmental			
Temperature Range(Operating)	+32 to +120 °F	0 to +50 °C	
Electrical			
Power Required(for supplied AC power adaptor)	AC Power	AC Power	
Power Required(direct input to unit)	DC power	DC power	
AC Power(47 to 63 Hz)	100 to 240 VAC	100 to 240 VAC	
AC Power	≤ 0.7 amps	≤ 0.7 amps	
Excitation Voltage(± 1 VDC)(To Sensor)	+26 VDC	+26 VDC	
DC Offset	<20 mV	<20 mV	
DC Power	+32 to 38 VDC	+32 to 38 VDC	
DC Power	<0.25 amps	<0.25 amps	
Constant Current Excitation(To Sensor)	2 to 20 mA	2 to 20 mA	[1]
Output Impedance	50 Ohm	50 Ohm	
Overload Threshold(± 1.0 Vpk)	± 10 Vpk	± 10 Vpk	
Broadband Electrical Noise(1 to 10,000 Hz)	3.5 μV rms	3.5 μV rms	[2]
Spectral Noise(1 Hz)	1.30 μV/√Hz	1.30 μV/√Hz	[2]
Spectral Noise(10 Hz)	0.10 μV/√Hz	0.10 μV/√Hz	[2]
Spectral Noise(100 Hz)	0.08 μV/√Hz	0.08 μV/√Hz	[2]
Spectral Noise(1 kHz)	0.07 μV/√Hz	0.07 μV/√Hz	[2]
Spectral Noise(10 kHz)	0.07 μV/√Hz	0.07 μV/√Hz	[2]
Physical			
Electrical Connector(ICP® Sensor Input)	BNC Jack	BNC Jack	
Electrical Connector(Output)	BNC Jack	BNC Jack	
Electrical Connector(DC Power Input)	5-socket DIN (female)	5-socket DIN (female)	
Size (Height x Width x Depth)	3.2 in x 8.0 in x 5.9 in	8.1 cm x 20 cm x 15 cm	
Weight	1.25 lb	567 gm	

CE [3]

All specifications are at room temperature unless otherwise specified.
In the interest of constant product improvement, we reserve the right to change specifications without notice.

ICP® is a registered trademark of PCB Group, Inc.

OPTIONAL VERSIONS

Optional versions have identical specifications and accessories as listed for the standard model except where noted below. More than one option may be used.

NOTES:
[1] User adjustable, factory set at 4 mA (± 0.5 mA). One control adjusts all channels.
[2] Typical.
[3] See PCB Declaration of Conformance PS024 for details.

SUPPLIED ACCESSORIES:
Model 017AXX Power Cord
Model 488B04/NC Power Convertor

Entered: AP	Engineer: AK	Sales: JJM	Approved: JWH	Spec Number:
Date: 2/5/2013	Date: 2/5/2013	Date: 2/5/2013	Date: 2/5/2013	35061

PCB PIEZOTRONICS
3425 Walden Avenue, Depew, NY 14043

Phone: 716-684-0001
Fax: 716-684-0987
E-Mail: info@pcb.com

A.1.6 Motion Capture System

In order to measure the deflection of the RC beams, a research-grade motion capture system NDI OptotrakCertus HD was used. This system is typically used for tracking and analyzing kinetics and dynamic motion in real-time (shown in Fig. 5.31).

Motion capture system

For this system, a maximum frame rate was calculated using the formula given by the manufacturer. The formula is:

Maximum frame rate = $\frac{4600}{N+2}$ Hz

Where, N = no. of markers. In this study, a total of 20 markers were placed on the beams to obtain the deflections rendering 209 Hz of maximum frame rate. This frame rate was sufficient to capture the deflections under the impact load.

A.2 Raw data from Phase I Experiment

A.2.1 Impact toughness of 10 test groups based on the number of drops to observe the first visible crack for fiber reinforced composites consisting of steel, PVA and nano fibers

Control	**P-0.75%**	**S-0.75%**	**S-1%**	**N**	**SP50/50-0.75%**	**SP40/60-0.75%**	**SP50/50-1%**	**SP40/60-1%**	**MIRAC-1%**
16	12	44	97	18	50	24	54	97	159
16	13	42	85	31	27	15	30	107	147
25	15	28	93	32	61	29	115	175	173
28	31	31	99	10	63	23	144	39	250
17	35	34	56	13	28	26	105	84	281
21	30	37	142	24	44	25	57	92	337

A.2.2 Impact toughness of 10 test groups based on the number of drops to observe the ultimate failure for fiber reinforced composites consisting of steel, PVA and nano fibers

Control	**P-0.75%**	**S-0.75%**	**S-1%**	**N**	**SP50/50-0.75%**	**SP40/60-0.75%**	**SP50/50-1%**	**SP40/60-1%**	**MIRAC-1%**
18	21	85	205	19	104	35	125	141	204
22	20	91	237	31	61	53	139	151	188
28	24	62	189	33	90	47	222	256	204
32	44	61	157	11	101	39	256	130	331
19	46	69	145	14	63	45	239	172	350
23	35	68	203	24	95	49	94	137	391

A.2.3 Compressive strength (MPa) of 10 test groups for fiber reinforced composites consisting of steel, PVA and nano fibers

Control	P-0.75%	S-0.75%	S-1%	N	SP50/50-0.75%	SP40/60-0.75%	SP50/50-1%	SP40/60-1%	MIRAC-1%
38.2	29.9	32.9	47.5	42.9	32.8	30.2	37.2	30.9	46.1
36.3	29.5	33.4	46.9	43.4	36	30	38.5	29	48.1
37.1	29.1	37.1	49.8	43.8	32.5	30.3	37.5	29.5	45.6
39.9	28.9	33.4	50.5	43.3	34.5	28.8	38.6	30.1	44.3
37.6	30.2	35.4	50.6	44.6	31.9	28.9	37.8	31.9	47.3
38.5	29.6	35.1	48.7	44.1	33.2	30.5	36.3	29.4	48.8

A.2.4 Splitting tensile strength (MPa) of 10 test groups for fiber reinforced composites consisting of steel, PVA and nano fibers

Control	P-0.75%	S-0.75%	S-1%	N	SP50/50-0.75%	SP40/60-0.75%	SP50/50-1%	SP40/60-1%	MIRAC-1%
2.4	2.7	3.85	5.35	3	3.85	3.05	4.6	4.2	4.9
2.5	2.5	3.95	5.85	3.15	3.3	3.05	4.95	3.85	5.2
2.6	3.15	4.05	6.15	3.5	4.25	2.85	5	4.4	5.55
3.5	2.45	3.5	5.1	3.4	3.95	3.3	4.45	3.95	4.6
3.5	2.3	3.4	4.7	3.65	3.95	3.05	4.3	3.65	5.4
3.6	2.05	3.2	5.3	3.8	3.95	3.45	4.5	3.15	5.05

A.2.4 Modulus of rupture (MPa) of 10 test groups for fiber reinforced composites consisting of steel, PVA and nano fibers

Control	P-0.75%	S-0.75%	S-1%	N	SP50/50-0.75%	SP40/60-0.75%	SP50/50-1%	SP40/60-1%	MIRAC-1%
4.6	4.7	5.05	6.9	4.2	4.7	4.6	5.8	4.95	6.9
4.5	4.95	5	6.9	5.2	4.65	4.7	5.75	4.95	5.75
4.4	4.95	4.75	6.5	4.4	5.15	5.05	6.2	4.9	6.05

A.2.5 Impact toughness of 10 test groups based on the number of drops to observe the first visible crack for fiber reinforced composites consisting of PP, PVA and nano fibers

Control	P-0.75%	S-0.75%	S-1%	N	SP50/50-0.75%	SP40/60-0.75%	SP50/50-1%	SP40/60-1%	mFRC-1%
16	12	13	22	18	37	119	124	81	154
16	13	15	18	31	191	76	109	43	147
25	15	14	25	32	29	33	71	64	155
28	31	15	35	10	136	61	36	174	144
17	35	17	31	13	19	24	64	150	142
21	30	16	24	24	32	46	96	78	139

A.2.6 Impact toughness of 10 test groups based on the number of drops to observe the ultimate failure for fiber reinforced composites consisting of PP, PVA and nano fibers

Control	P-0.75%	S-0.75%	S-1%	N	SP50/50-0.75%	SP40/60-0.75%	SP50/50-1%	SP40/60-1%	mFRC-1%
18	21	44	31	19	51	172	198	120	181
22	20	48	74	31	208	107	177	81	165
28	24	49	37	33	37	55	111	93	240
32	44	59	82	11	154	93	97	219	252
19	46	31	46	14	32	35	91	207	162
23	35	42	57	24	54	87	147	124	186

A.2.7 Compressive strength (MPa) of 10 test groups for fiber reinforced composites consisting of PP, PVA and nano fibers

Control	P-0.75%	S-0.75%	S-1%	N	SP50/50-0.75%	SP40/60-0.75%	SP50/50-1%	SP40/60-1%	mFRC-1%
38.2	29.9	36.5	31.6	42.9	40.4	43.2	32.7	41.4	34.7
36.3	29.5	36.2	37.9	43.4	41.7	43.8	42.1	36.8	35.7
37.1	29.1	36.7	28.9	53.4	41.9	42.8	31.9	35.2	38
39.9	28.9	37.1	27.9	43.3	41.1	43.6	41	33.5	35.7
37.6	30.2	37.3	32.3	44.6	40	38.2	33.4	33.4	42.3
38.5	29.6	36.7	31.1	44.1	41.3	43.1	44.5	35.6	37.4

A.2.8 Splitting tensile strength (MPa) of 10 test groups for fiber reinforced composites consisting of PP, PVA and nano fibers

Control	P-0.75%	S-0.75%	S-1%	N	SP50/50-0.75%	SP40/60-0.75%	SP50/50-1%	SP40/60-1%	mFRC-1%
2.4	2.7	2.25	3.95	3	3	3.85	3.4	3.6	3.9
2.5	2.5	2.75	3.4	3.15	3.3	4.05	3.3	3.2	4.05
2.6	3.15	2.75	3.2	3.5	3.85	3.7	3.6	3.9	4.35
3.5	2.45	2.7	3.55	3.4	3.3	4.05	4.4	3.9	4.25
3.5	2.3	3.05	3.35	3.65	3.35	3.3	4.1	3.4	3.3
3.6	2.05	2.9	3.45	3.8	3.05	4.35	3.6	3.4	4.15

A.2.9 Modulus of rupture (MPa) of 10 test groups for fiber reinforced composites consisting of PP, PVA and nano fibers

Control	P-0.75%	S-0.75%	S-1%	N	SP50/50-0.75%	SP40/60-0.75%	SP50/50-1%	SP40/60-1%	mFRC-1%
4.6	4.7	4.35	4.15	4.2	5.05	4.95	4.75	5.85	5.8
4.5	4.95	4.8	4.7	5.2	5.45	5.15	5.7	6.15	6.9
4.4	4.95	4.5	4.4	4.4	5.25	5.05	5.35	6	6.25

A.3 Raw data and images from Phase II Experiment

A.3.1 Unfiltered acceleration obtained from large scale impact tests (Test Group A)

Control:

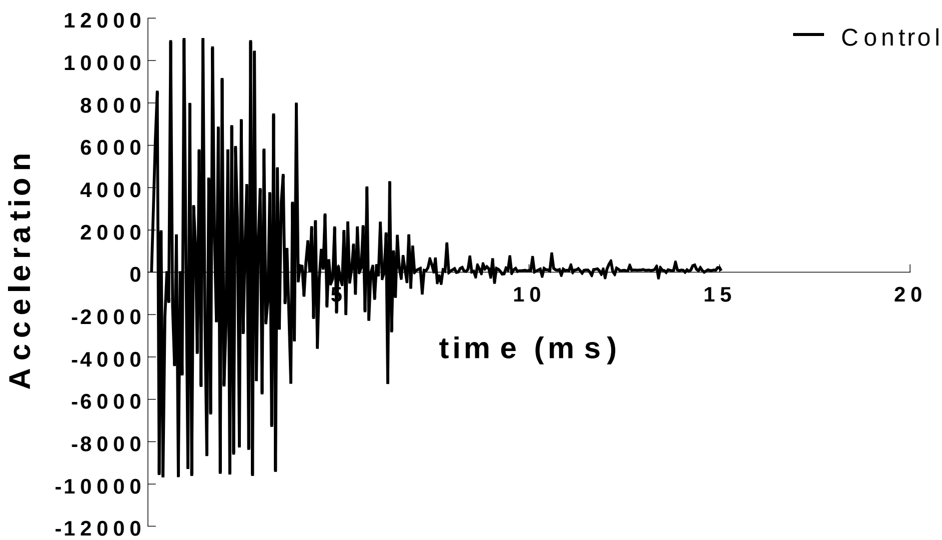

S-0.75%:

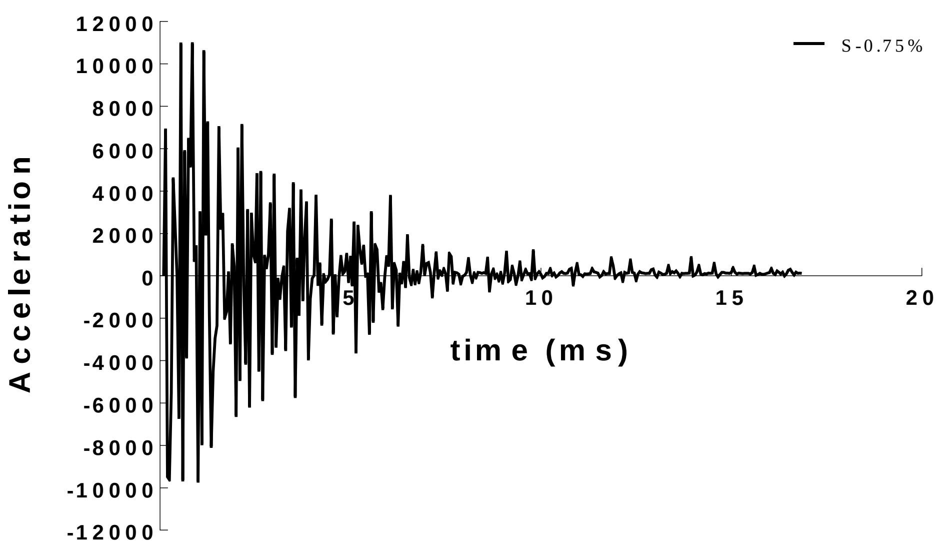

SP50/50-1%:

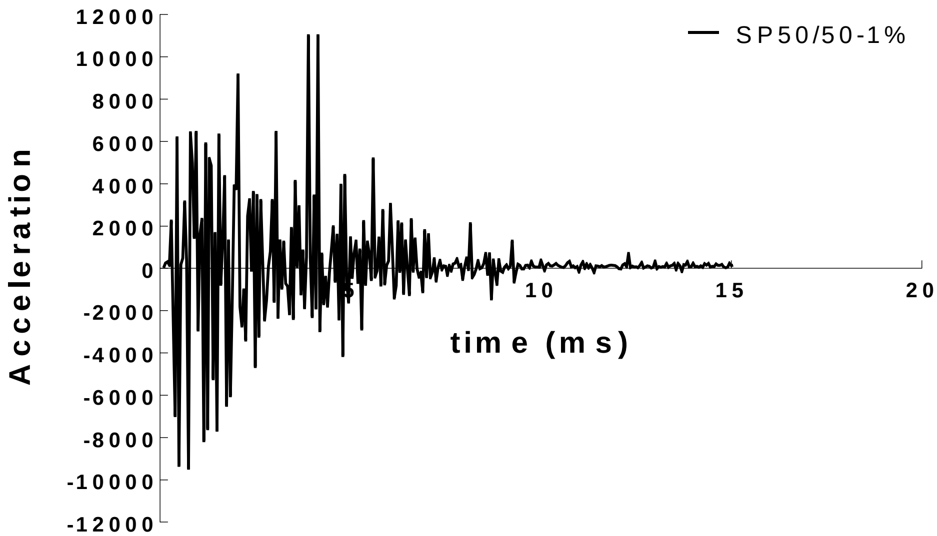

PP50/50-1%:

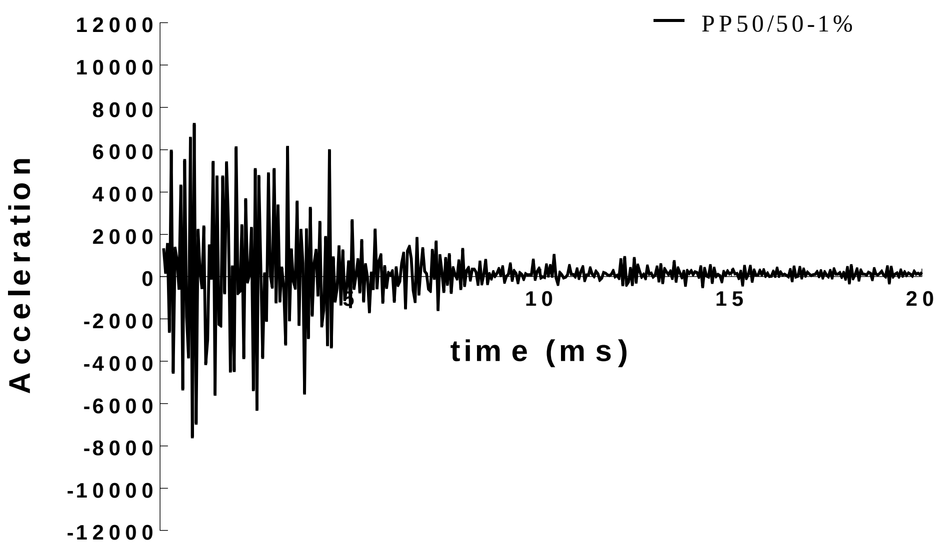

Nano:

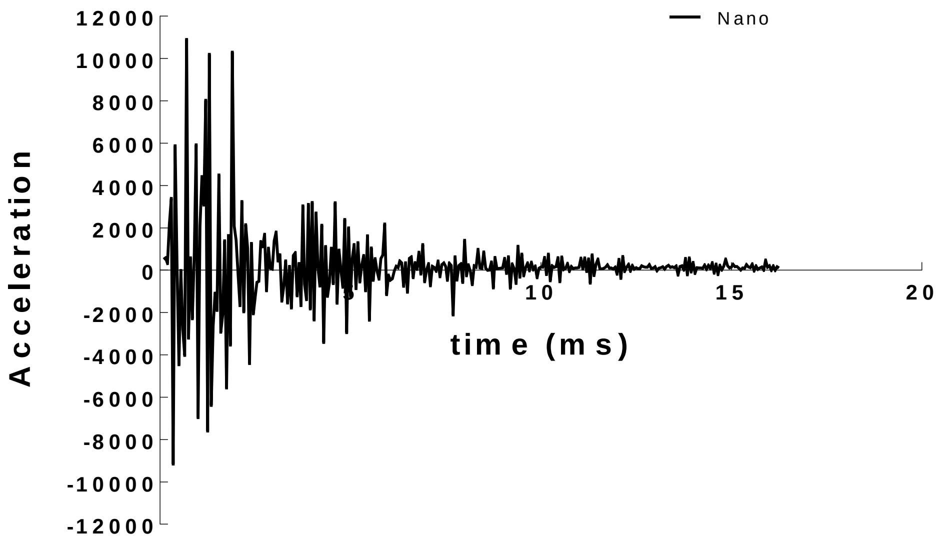

Nano
12000
10000
8000
6000
4000
2000
0
-2000
-4000
-6000
-8000
-10000
-12000
Acceleration
5
10
15
20
time (ms)

MIRAC-1%:

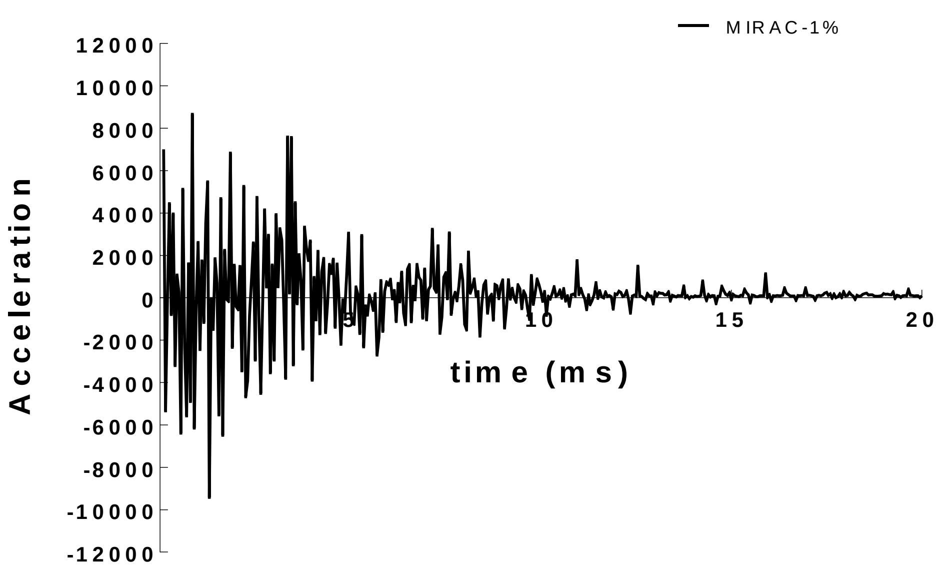

MIRAC-1%
12000
10000
8000
6000
4000
2000
0
-2000
-4000
-6000
-8000
-10000
-12000
Acceleration
5
10
15
20
time (ms)

A.3.2 Filtered acceleration obtained from large scale impact tests (Test Group A)

Control:

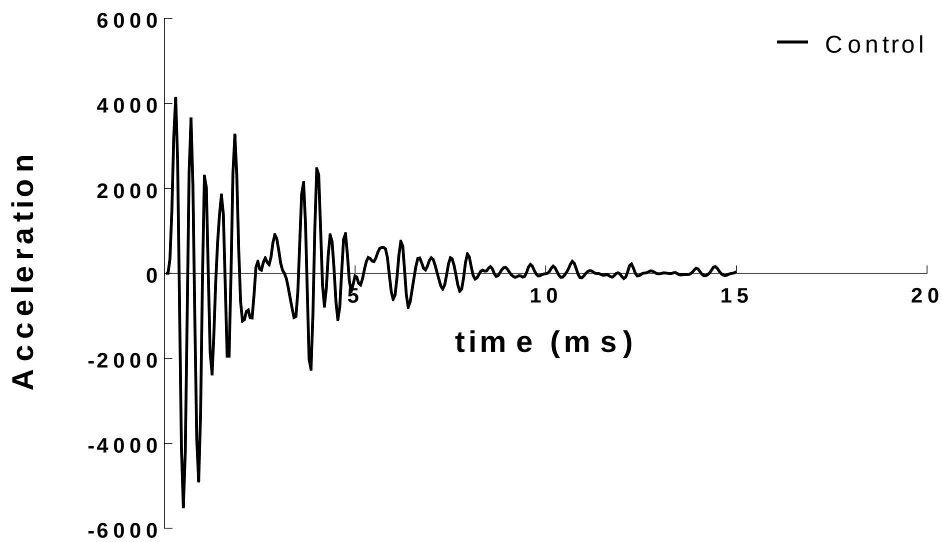

S-0.75%:

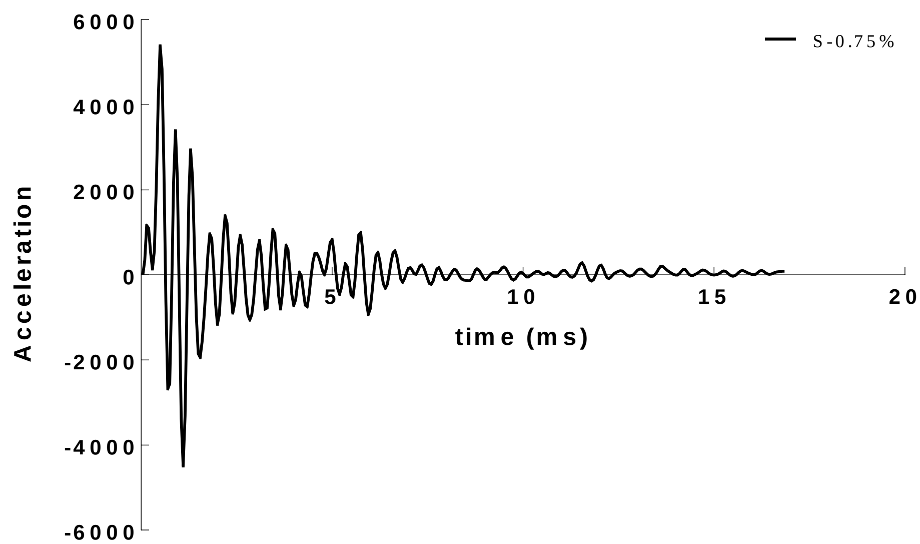

SP50/50-1%:

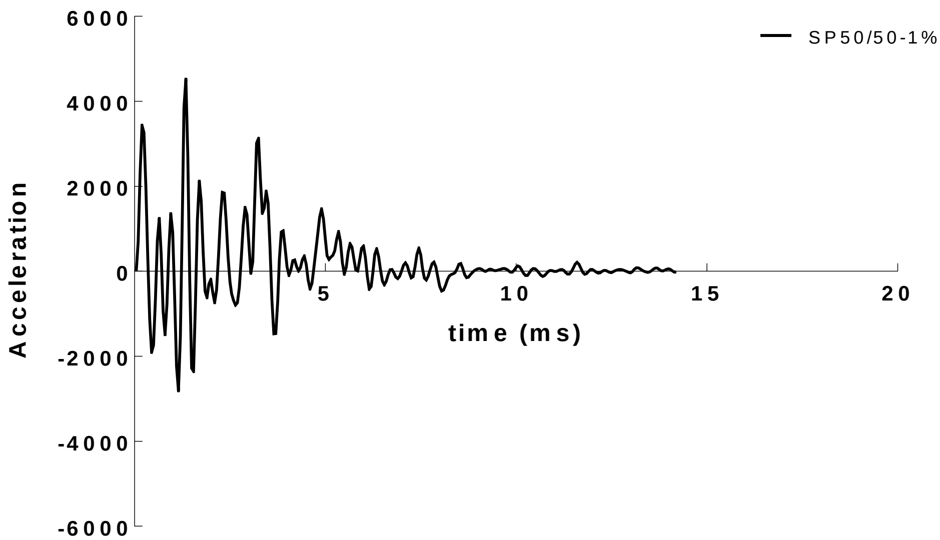

PP50/50-1%:

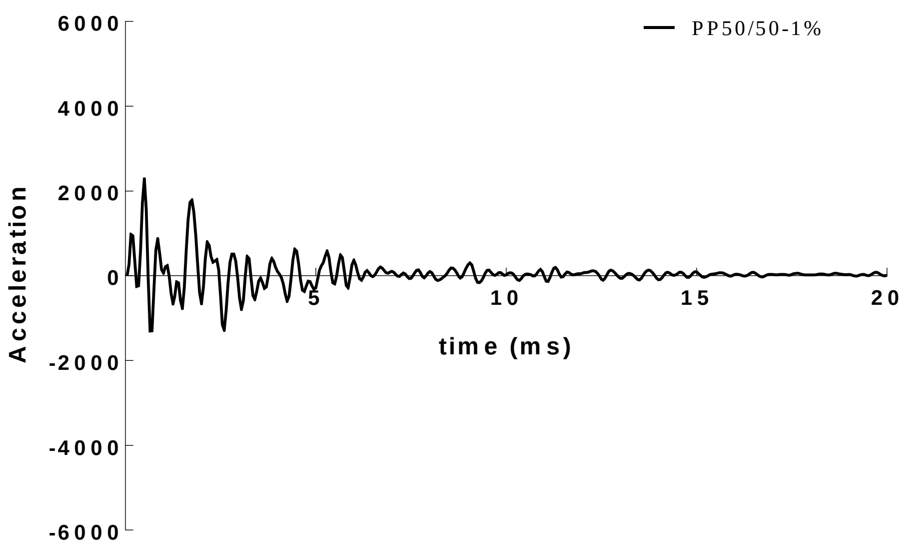

Nano:

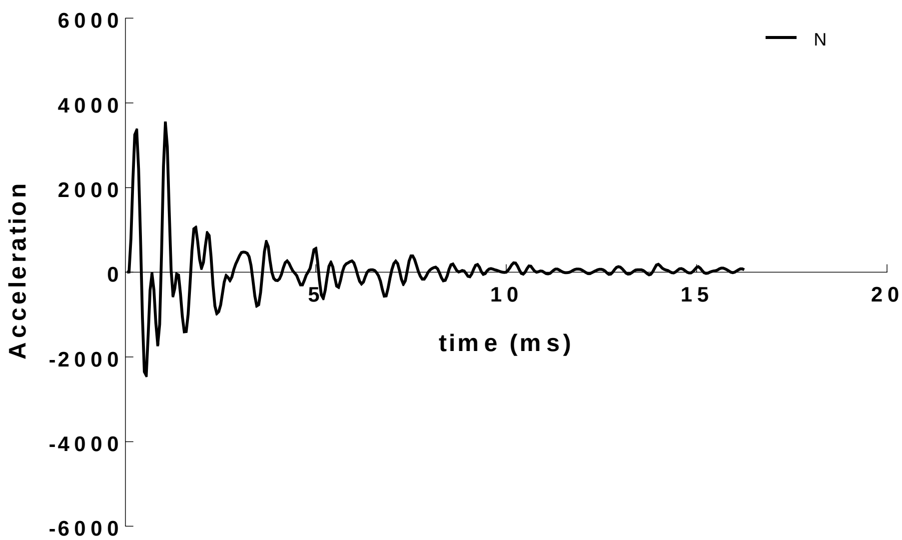

N
6000
4000
2000
0
-2000
-4000
-6000
Acceleration
5
10
15
20
time (ms)

MIRAC-1%:

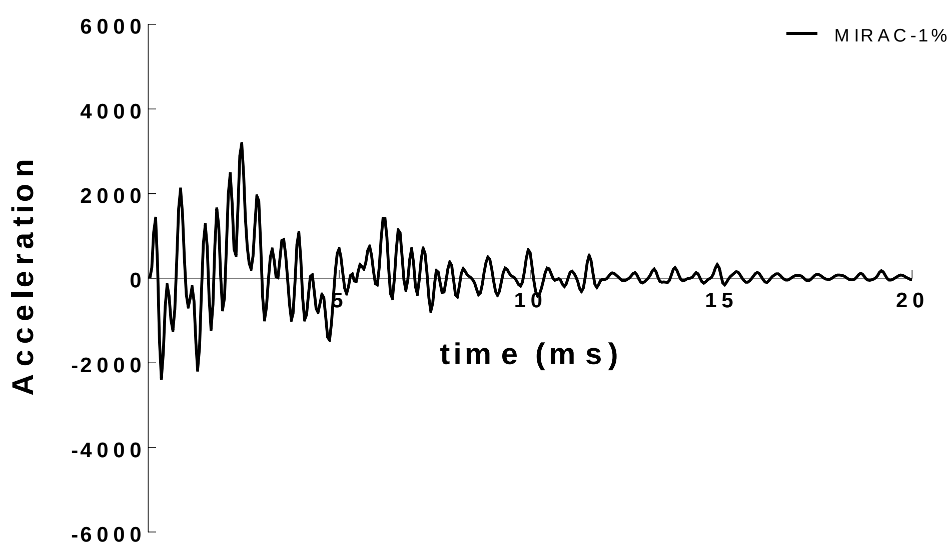

MIRAC-1%
6000
4000
2000
0
-2000
-4000
-6000
Acceleration
5
10
15
20
time (ms)

A.3.3 Mid-span deflections (Test Group A)

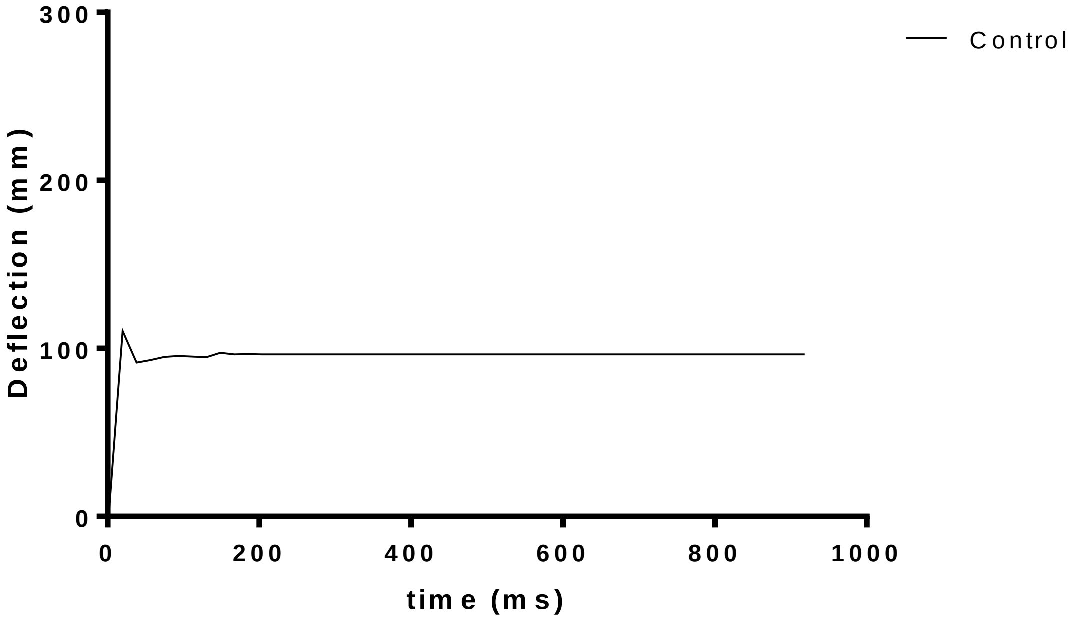

a)

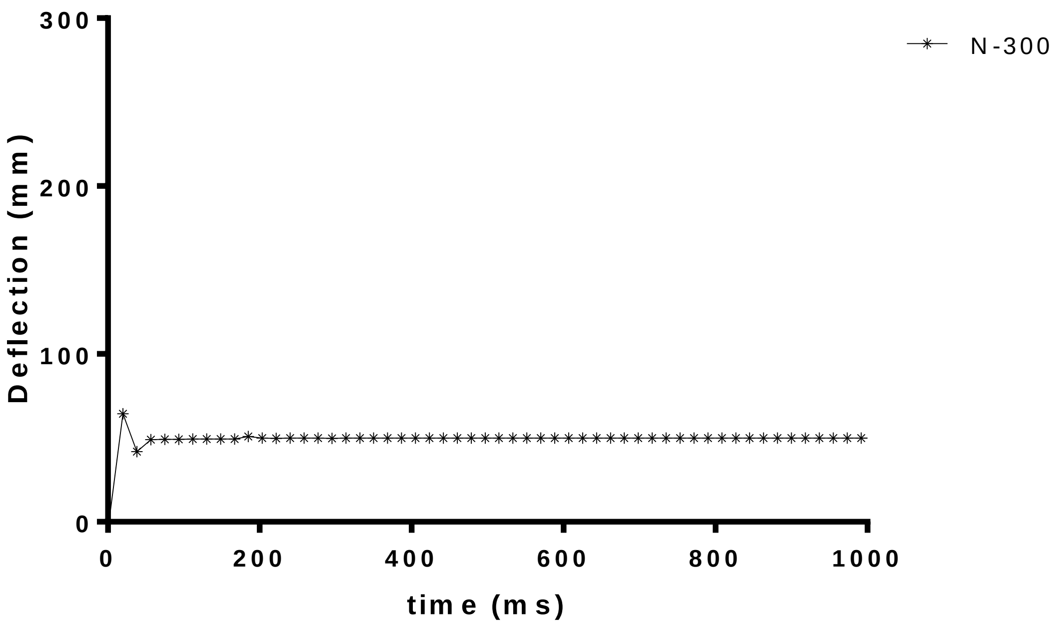

b)

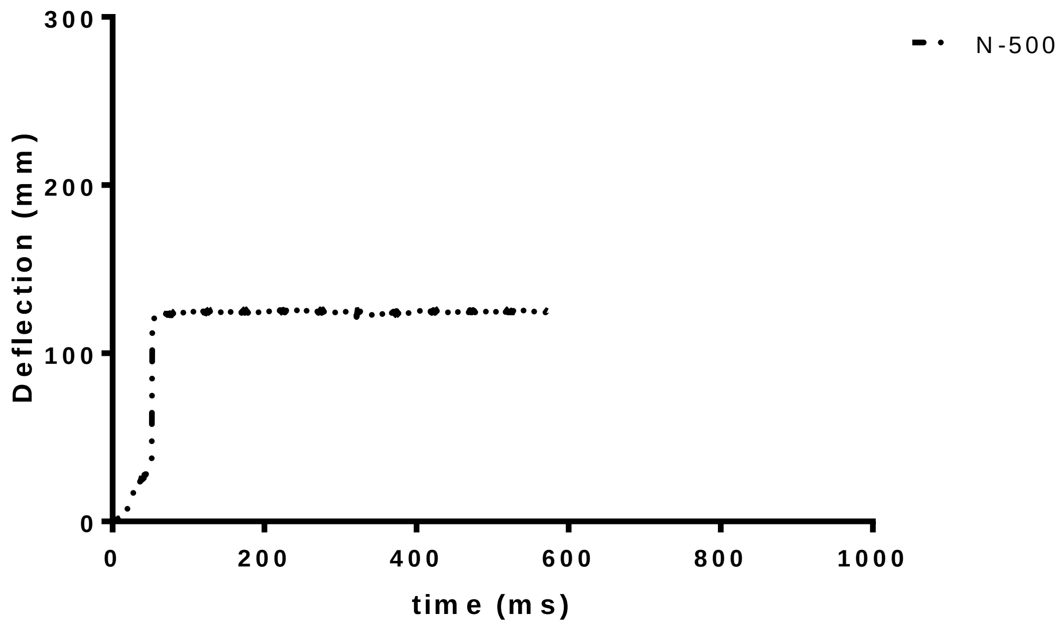

N-500
300
200
100
0
Deflection (mm)
0
200
400
600
800
1000
time (ms)

c)

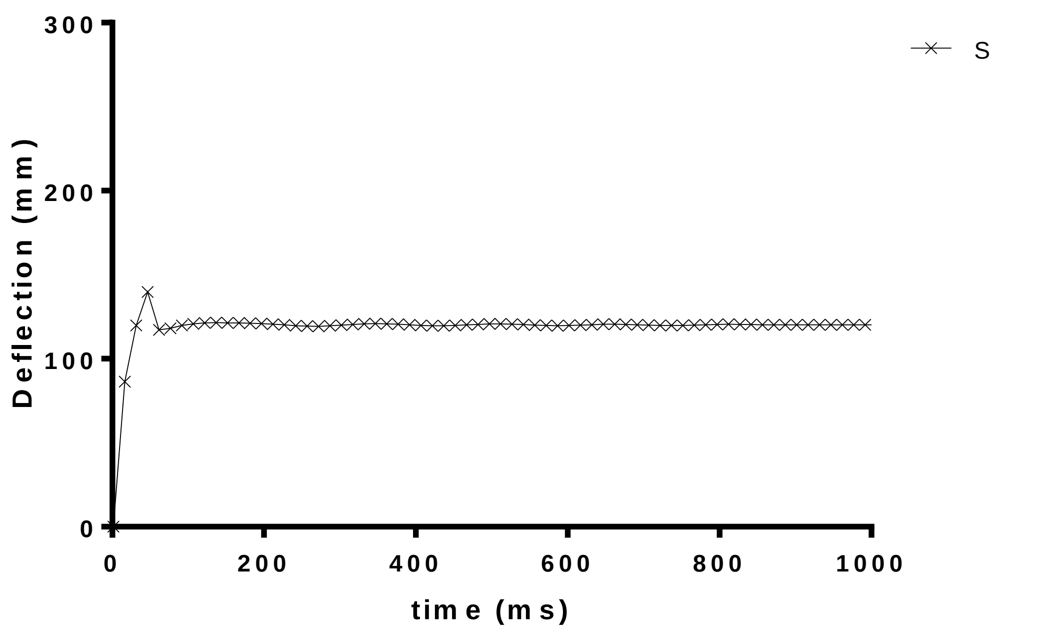

S
300
200
100
0
Deflection (mm)
0
200
400
600
800
1000
time (ms)

d)

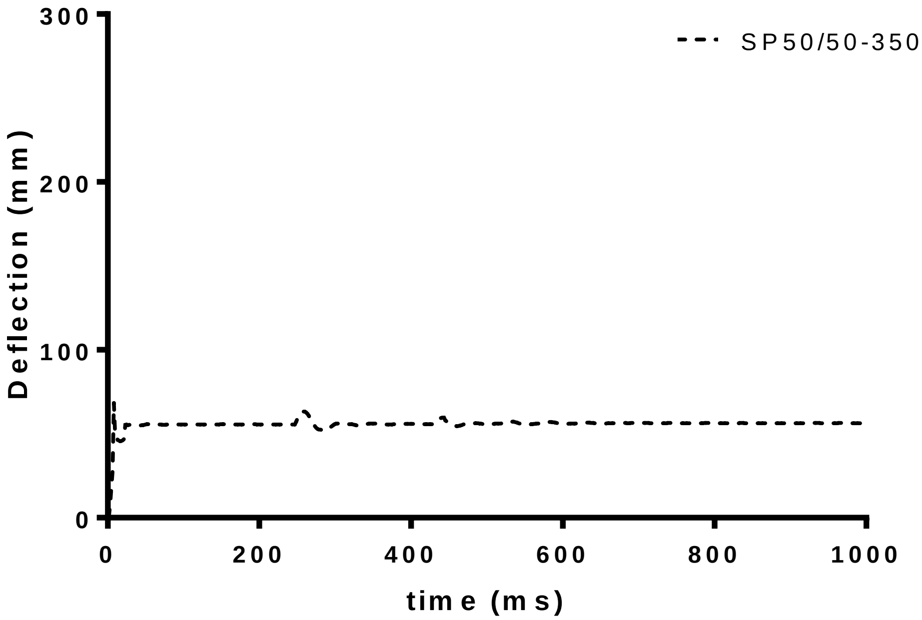
SP50/50-350
Deflection (mm)
time (ms)
0
100
200
300
0
200
400
600
800
1000

e)

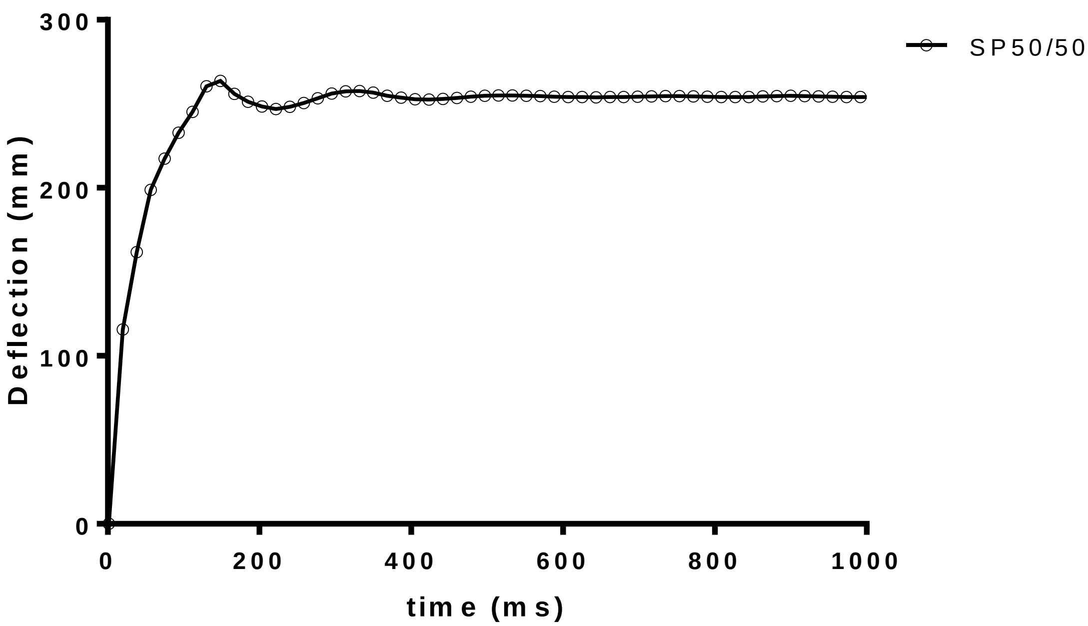
SP50/50
Deflection (mm)
time (ms)
0
100
200
300
0
200
400
600
800
1000

f)

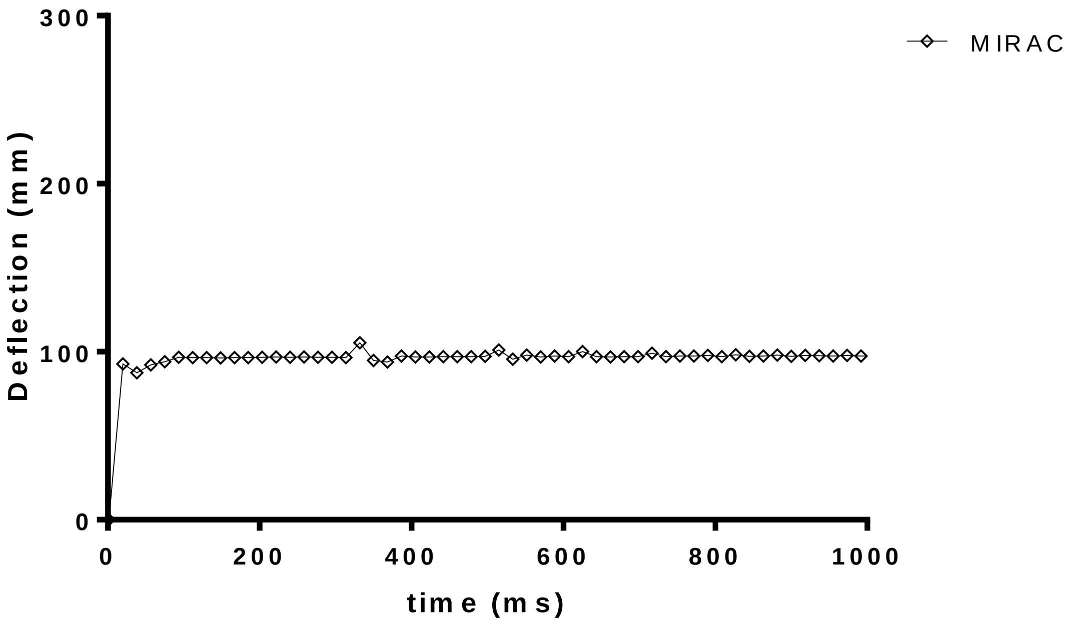

g)

Individual deflection versus time plots of the specimens of test group -1 a) Control b) N-300 c) N-500 d) S e) SP50/50-350 f) SP50/50 g) MIRAC

A.3.4 Crack profiles and deflected shapes (Test Group A)

a)

b)

c)

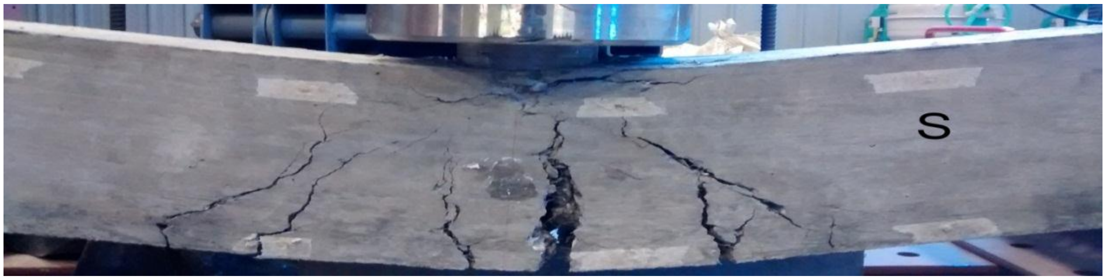

d)

e)

f)

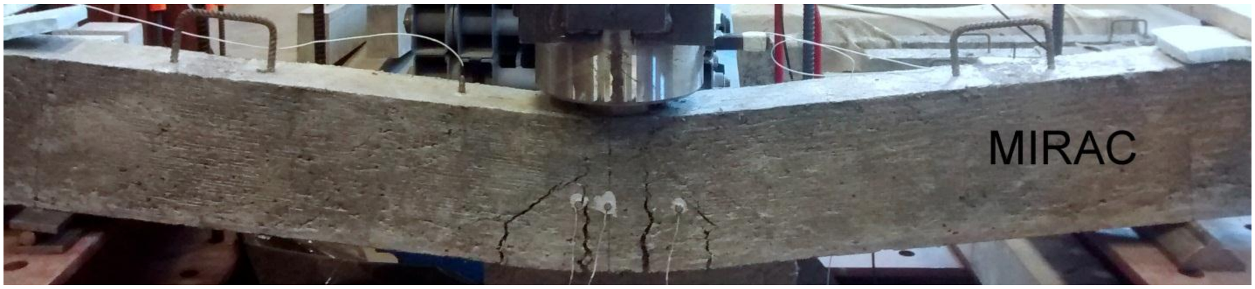

g)

Crack profiles of specimens of Test group-1 a) Control b) N-300 c) N-500 d) S e) SP50/50-350 f) SP50/50 g) MIRAC

A.3.5 Unfiltered acceleration obtained from large scale impact tests (Test Group B)

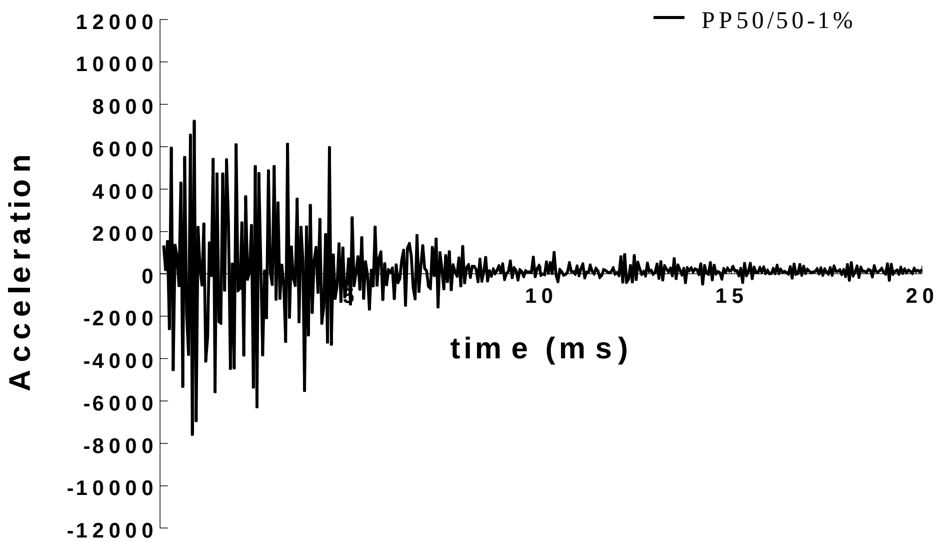

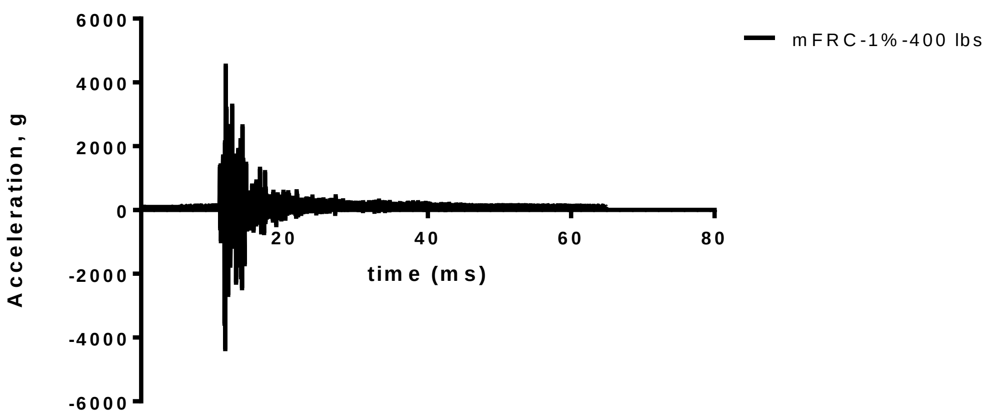

A.3.6 Filtered acceleration obtained from large scale impact tests (Test Group B)

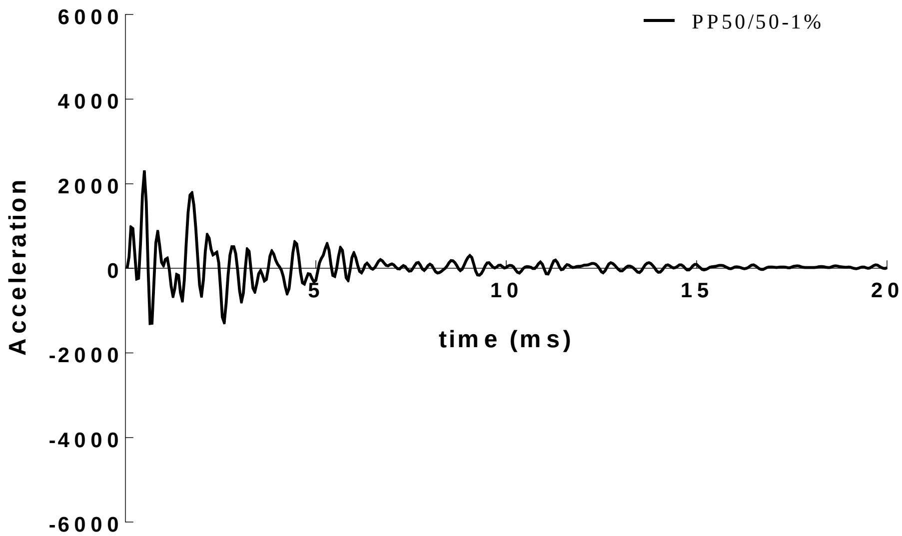

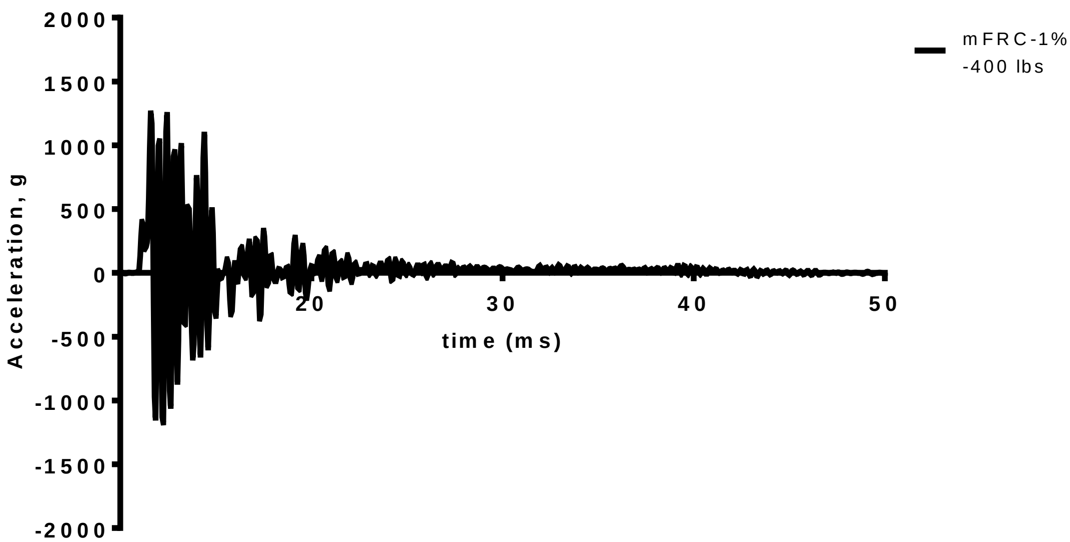

A.3.7 Mid-span deflections (Test Group B)

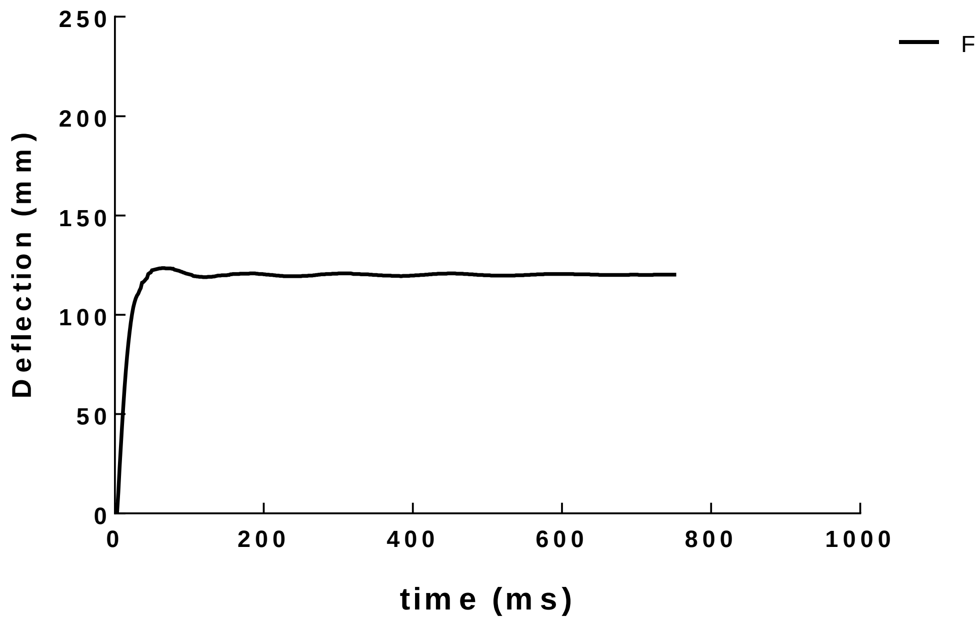

a)

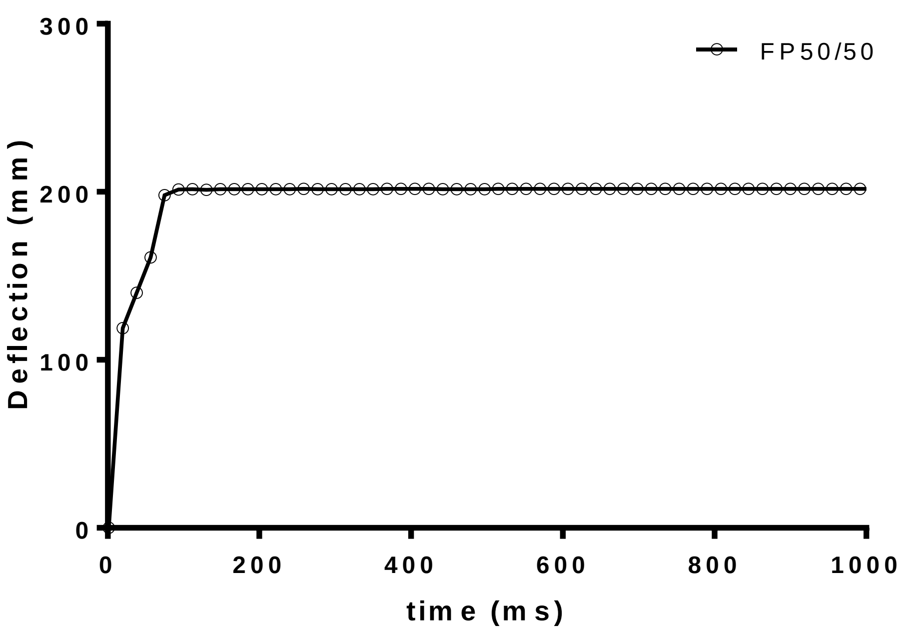

b)

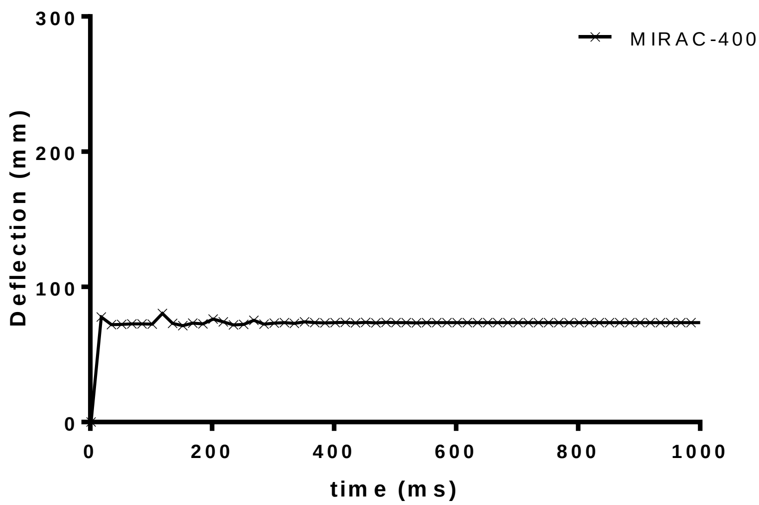

c)

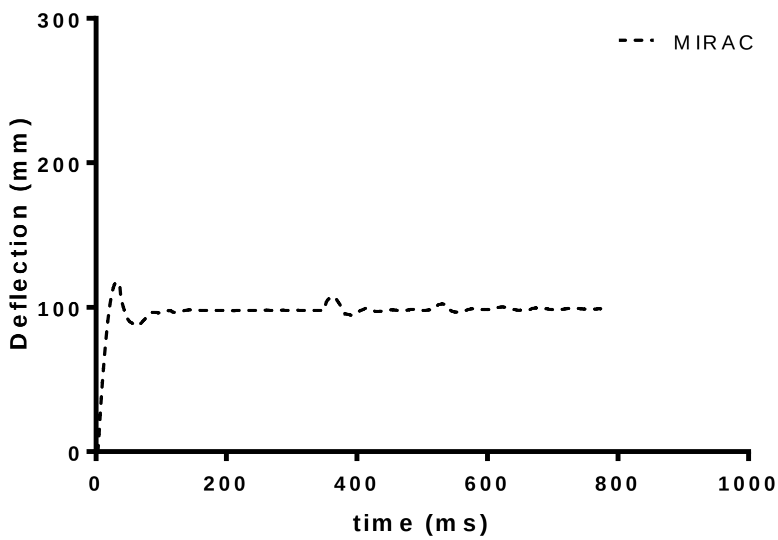

d)

Individual deflection versus time plots of the specimens of test group -2 a) F b) FP50/50 c) MIRAC-400 d) MIRAC

A.3.8 Crack profiles and deflected shapes (Test Group B)

a)

b)

c)

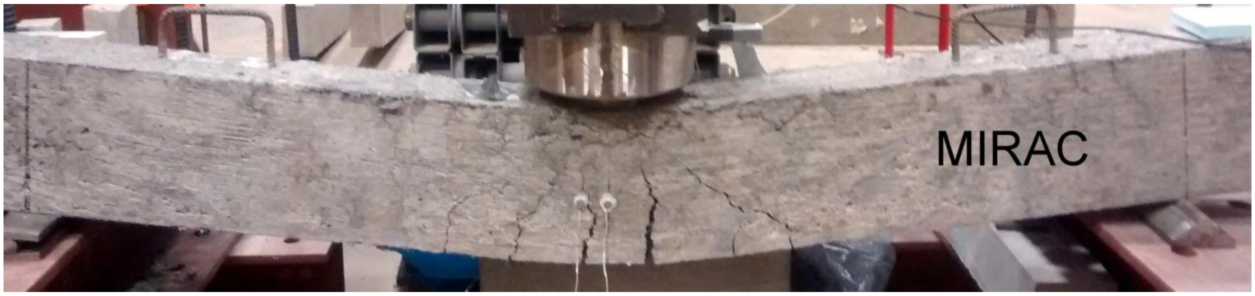

d)

Crack profiles of specimens of Test group-1 a) F b) FP50/50 c) MIRAC-400 d) MIRAC

A.4 Calculation of impact force and deflections

A.4.1 Calculation of impact force and comparison with measured impact force

Contact force history,

$$F = K_{bs}y = V(K_{bs}m_1)^{1/2}\sin\omega t \qquad (1)$$

Considering reduced stiffness, Eq. (1) is modified as,

$$F = K_{bs}y = \frac{V(K_{bs}m_1)^{1/2}}{\gamma}\sin\omega t \qquad (2)$$

Data:

Velocity of the impactor, $V = 10.66\ \mathrm{ms}^{-1}$

Mass of impactor, $m_1 = 226.8$ kg

Linear stiffness, $K_{bs} = 11219000$ N/m

Measured force from acceleration of impact for Control beam, $F = 915480$ N

Calculated average $\gamma = 1.18$

Calculation:

$$\omega = \sqrt{\frac{K_{bs}}{m_1}} = \sqrt{\frac{11219000}{226.8}} = 222.41$$

From Eq. (2), $F = \frac{10.66(11219000x226.8)^{1/2}}{1.18} = 455694.5$ N

Modified F/Measured $F = \frac{455694.5}{915480} = 0.498$

A.4.2 Calculation of maximum deflection and comparison with maximum measured deflection

Displacement, $y(x,t) = \frac{2P}{\rho Al}\sum_{n=1,3,5}^{\infty}\frac{(-1)^{(n-1)/2}\sin\beta_n x_0 \sin\omega_n t}{w_n}$ (3)

Data:

Area of beam, $A = 0.0387096\ m^2$

Span of beam, $l = 1.854$ m

Density of beam, $\rho = 2400\ kg/m^3$

Calculated force from Eq. (2), $P = F = 455694.5$ N

Bending stiffness, $EI = 1629735\ N - m$

Measured deflection, $\delta = 115.74$ mm

$n = 1,3,5,7,9$

$\beta_n = \frac{n\pi}{l}$

$\beta_n x_0 = \frac{n\pi}{2}$

$a = \frac{EI}{A\rho}$

$\omega_n = a{\beta_n}^2$

Calculation:

$a = \frac{EI}{A\rho} = 17542.3$

n	β_n	$\beta_n x_0$	$\sin\beta_n x_0$	ω_n	δ_i, m (using Eq. (3))
1	1.694498382	1.5708	1	50369.70696	0.105049293
3	5.083495146	4.7124	-1	453327.3627	-0.011672144
5	8.472491909	7.854	1	1259242.674	0.004201972
7	11.86148867	10.9956	-1	2468115.641	-0.002143863
9	15.25048544	14.1372	0.999999999	4079946.264	0.001296905

Total calculated, $\delta_c = \sum \delta_i = 0.096732163 \text{ m} = 96.732 \text{ mm}$

Measured deflection, $\delta = 115.74 \text{ mm}$

A.5 Filtration of data

From large-scale drop-weight impact test, acceleration of the impact was obtained at 20000 Hz sampling rate. Due to this high sampling rate, a lot of noise was observed in the acceleration response. In order to get rid of these noises, a 4th order Butterworth low-pass filter was used. A cut-off frequency of 3050 Hz was used in general. In order to determine the cut-off frequency of the low-pass filter, Fast Fourier Theorem (FFT) was used.

Fourier Transform – MATLAB CODE:

```
[X,TXT,RAW] = xlsread('steel.75%.xlsx');
xdft = fft(X(:,2));
% sampling interval -- as we did equal sampling all throughout
  DT = X(2,1)-X(1,1); % time period
  Fs = 1/DT;% sampling frequency (f = 1/T)
  DF = Fs/size(X,1);%frequency/data point
  freq = 0:DF:Fs/2;
  xdft = xdft(1:length(xdft)/2+1);
  plot(freq,abs(xdft));
 title('Fourier transform of acceleration data - Steel .75% beam')
 ylabel ('amplitude')
 xlabel('frequency (Hz)')
```

Butterworth filter – MATLAB CODE:

```
filename = ('Nano500tbf.xlsx');
x = xlsread (filename); %reading acceleration values from excel
%plot(x(:,1),x(:,2));
[b,a]=butter(4,.305); % For a cutoff frequency of 3050 Hz
y=filter(b,a,x(:,2));
plot(x(:,1),y);
dlmwrite('nano500_filter_final.txt',y)
title('nano500 beam - Butterworth')
ylabel ('Acceleration')
xlabel('time (sec)')
```

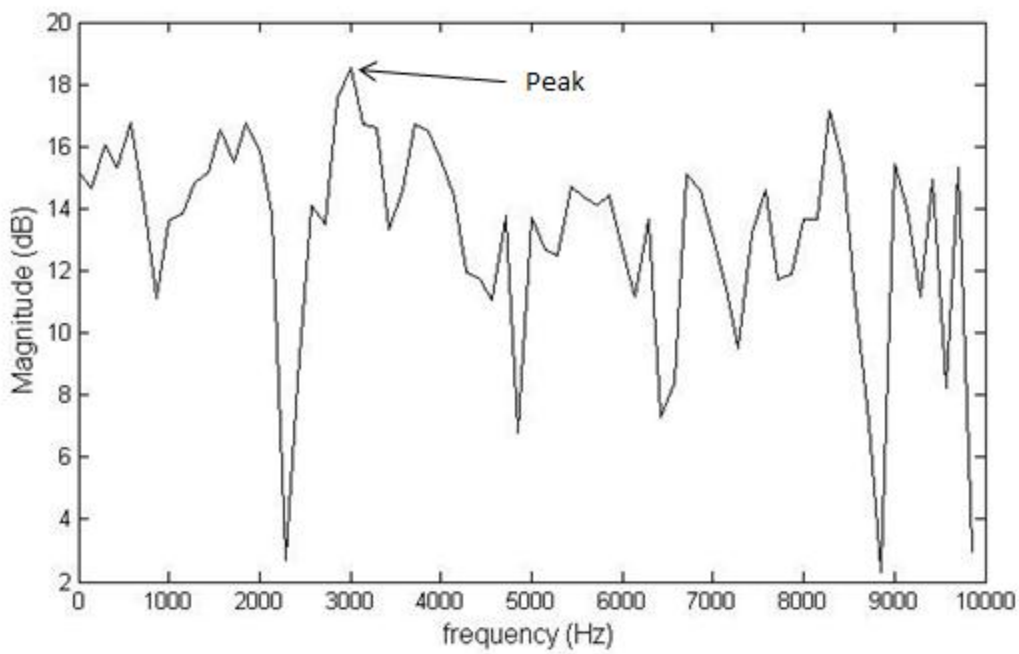

Power spectrum of acceleration response for Control beam.

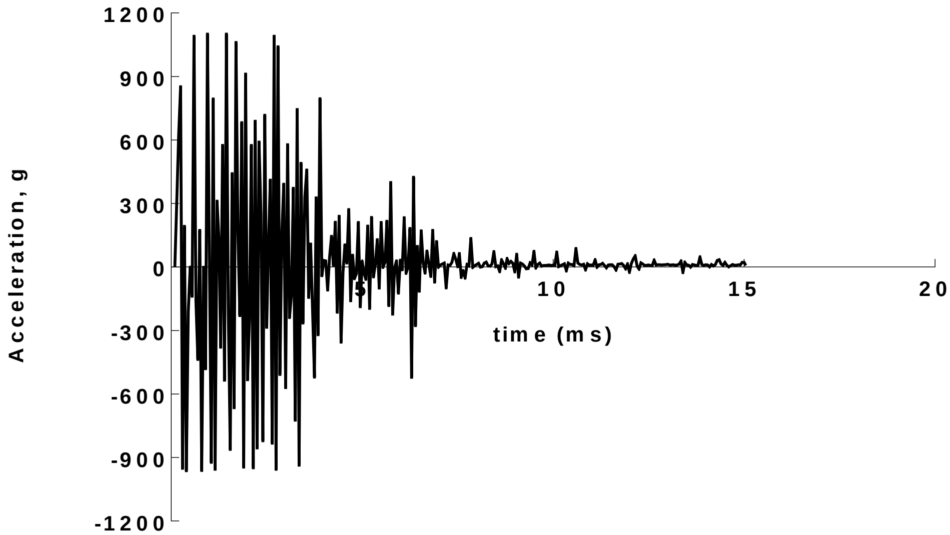

Unfiltered acceleration due to impact on Control beam.

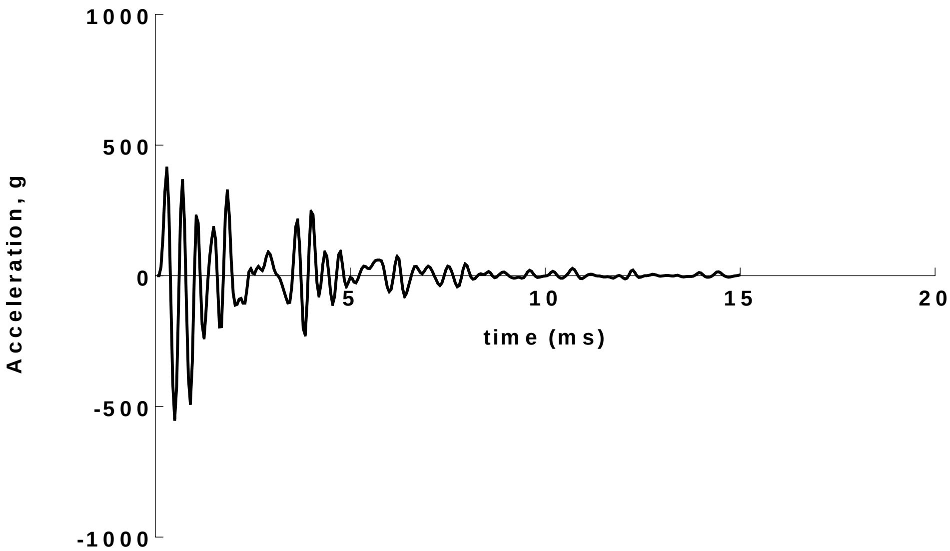

Filtered acceleration due to impact on Control beam.